UNIVERSITY OF HAWAII
LIBRARY
MAR 14 '60

# The
# Philosophical Magazine

FIRST PUBLISHED IN 1798

## A Journal of Theoretical Experimental and Applied Physics

Vol. 4 November 1959 No. 47
*Eighth Series*

25s. 0d., plus postage
Annual Subscription £13 10s. 0d., payable in advance

ALERE FLAMMAM

*Printed and Published by*
TAYLOR & FRANCIS LTD
RED LION COURT, FLEET STREET, LONDON, E.C.4

# THE PHILOSOPHICAL MAGAZINE

*Editor*

Professor N. F. Mott, M.A., D.Sc., F.R.S.

*Editorial Board*

Sir Lawrence Bragg, O.B.E., M.C., M.A., D.Sc., F.R.S.
Sir George Thomson, M.A., D.Sc., F.R.S.
Professor A. M. Tyndall, C.B.E., D.Sc., F.R.S.

Authors wishing to submit papers for publication in the Journal should send manuscripts directly to the Publishers.

Manuscripts should be typed in *double* spacing on one side of quarto (8 × 10 in.) paper, and authors are urged to aim at absolute clarity of meaning and an attractive presentation of their texts.

References should be listed at the end in alphabetical order of authors and should be cited in the text in terms of author's name and date. Diagrams should normally be in Indian ink on white card, with lettering in soft pencil, the captions being typed on a separate sheet.

A leaflet giving detailed instructions to authors on the preparation of papers is available on request from the Publishers.

Authors are entitled to receive 25 offprints of a paper in the Journal free of charge, and additional offprints can be obtained from the Publishers.

The *Philosophical Magazine* and its companion journal, *Advances in Physics*, will accept papers for publication in experimental and theoretical physics. The *Philosophical Magazine* publishes contributions describing new results, letters to the editor and book reviews. *Advances in Physics* publishes articles surveying the present state of knowledge in any branch of the science in which recent progress has been made. The editors welcome contributions from overseas as well as from the United Kingdom, and papers may be published in English, French and German.

# Permeation of Hydrogen through Metals†

By R. Ash and R. M. Barrer
Physical Chemistry Laboratories, Chemistry Department, Imperial College, London, S.W.7

[Received June 1, 1959]

## Abstract

The theory of permeation of hydrogen through certain transition metals has been further developed. It has been shown that this theory, in which certain slow phase-boundary processes couple with diffusion to produce the permeation phenomena, can in rather simple ways predict the observed behaviour. In particular, ' threshold pressures ' for permeation can be understood; and also permeation velocities which depend on the ingoing pressure, $p_1$, according to $p_1^n$ where $0 \leqslant n \leqslant 1$, and upon membrane thickness $l$ according to $l^m$ where $-1 \leqslant m \leqslant 0$.

## § 1. Introduction

It is some time since the adsorption of hydrogen was first considered as a modifying influence in the permeation of this gas through metals (Smithells and Ransley 1935). The rôle of slow phase-boundary processes in permeation was considered quantitatively by Wang (1936) and by Barrer (1939, 1940). The latter of these authors was able to demonstrate the presence of slow processes for diffusion of hydrogen through hollow Pd cathodes, and to show that in successive experiments with a freshly activated Pd surface phase-boundary reactions increasingly dominated the tempo of permeation (Barrer 1940). Subsequently Wahlin and Naumann (1953) found that the rate of permeation did not vary as $1/l$, where $l$ is the thickness of the metal membrane. Recently it has been found (Silberg and Bachman 1958) that in diffusion of hydrogen through Pd discs between 200 and 600°c the permeation rate did not vary either as $1/l$ or as $p^{1/2}$, the latter being the pressure variation expected in the simplest cases, as shown by various experiments (Barrer 1951, Toda 1958). It was then suggested that no current theory of permeation through metals could explain these experimental results (Silberg and Bachman 1958). It is the purpose of the present paper further to develop the analyses of Smithells and Ransley, Wang, and Barrer, and thus to show how far the theory of phase boundary processes coupled with diffusion is able to explain experimental observations on permeation so far made.

---

† Communicated by the Authors.

## § 2. FORMULATION OF THE PROBLEM

We consider a plate of metal bounded by planes $x=0$ and $x=l$, the pressures $p_1$ and $p_2$ being maintained at the faces $x=0$ and $l$ respectively. The hydrogen undergoes chemisorption as atoms to give localized monolayers which at equilibrium follow Langmuir's isotherm. Absorption into, and diffusion within, the metal occurs as atoms. The fractions of the surface covered by adsorbed hydrogen at $x=0$ and $l$ are $\theta_1$ and $\theta_2$, while the concentrations of dissolved hydrogen just inside the metal at $x=0$ and $l$ are $u_0$ and $u_l$ respectively.

Then the following processes of adsorption, desorption, and penetration may be considered as typical, in all cases for unit area:

(*a*) A gas molecule strikes the surfaces, dissociates and is adsorbed as atoms:

$$\text{Rate}=k_1 p(1-\theta)^2.$$

(*b*) A pair of adsorbed atoms combines and evaporates as a molecule:

$$\text{Rate}=k_2\theta^2.$$

(*c*) An adsorbed atom passes into the metal:

$$\text{Rate}=k_3\theta[1-(u/u_s)],$$

where $u_s$ denotes the saturation concentration of hydrogen atoms in the metal.

(*d*) An atom in the metal enters the surface:

$$\text{Rate}=k_4 u(1-\theta).$$

(*e*) A molecule strikes the surface and dissociates, one atom staying on the surface and the other entering the metal:

$$\text{Rate}=k_5 p(1-\theta)[1-(u/u_s)].$$

(*f*) An atom in the metal enters the surface, combines with another adsorbed atom and evaporates as a molecule:

$$\text{Rate}=k_6 u\theta.$$

In the above processes the $k$'s denote transmission coefficients for transport of atoms across the relevant interface, per unit area per unit time. In addition, within the metal there is a diffusion flux, $J$ per unit area of membrane normal to the direction of flow, which may be written

$$J=D\frac{(u_0-u_l)}{l}. \qquad (1)$$

This diffusion flux in the steady state equals the net transport across any chosen interface, such as that between gas phase and adsorbed layer or that between the adsorbed layer and the metal surface. Then the following equations must be valid in addition to and simultaneously with eqn. (1):

$$J=k_1p_1(1-\theta_1)^2-k_2\theta_1^2+2k_5p_1(1-\theta_1)[1-(u_0/u_s)]-2k_6\theta_1u_0, \qquad (2)$$

$$J=k_3\theta_1[1-(u_0/u_s)]-k_4u_0(1-\theta_1)+k_5p_1(1-\theta_1)[1-(u_0/u_s)]-k_6\theta_1u_0, \qquad (3)$$

$$J=k_4u_l(1-\theta_2)-k_3\theta_2[1-(u_l/u_s)]+k_6\theta_2u_l-k_5p_2(1-\theta_2)[1-(u_l/u_s)], \qquad (4)$$

$$J=k_2\theta_2^2+2k_6\theta_2u_l-k_1p_2(1-\theta_2)^2-2k_5p_2(1-\theta_2)[1-(u_l/u_s)]. \qquad (5)$$

$J$ is in all cases expressed as the net number of atoms transferred across the relevant interface, per unit time per unit area. Processes ($e$) and ($f$) give rise to a factor of 2 in terms containing $k_5$ and $k_6$ in eqns. (2) and (5), since for every atom crossing the interface between the adsorbed layer and the metal, two atoms cross the corresponding interface between the gas-phase and the adsorbed layer. This factor of 2 has been omitted from earlier formulations of equations analogous to (2) and (5) above (Wang 1936, Barrer 1939) without, however, invalidating the conclusions reached, giving:

$$J'=k_1p_1(1-\theta_1)^2-k_2\theta_1^2+k_5p_1(1-\theta_1)[1-(u_0/u_s)]-k_6\theta_1u_0, \quad . \quad . \quad . \quad (2a)$$

$$J'=k_2\theta_2^2+k_6\theta_2u_l-k_1p_2(1-\theta_2)^2-k_5p_2(1-\theta_2)[1-(u_l/u_s)], \quad . \quad . \quad . \quad (5a)$$

where $J'$ was then identified with $J$. For the eqns. ($2a$), (3), (4), ($5a$) to be internally consistent however, $J'$ is to be regarded as the net flux of diatomic molecules across the interface between the gas-phase and the adsorbed layer, with $k_1$ and $k_2$ transmission coefficients for transport of diatomic molecules. Thus, $J'=J/2$.

From these equations by suitable rearrangement one may eliminate $u_0$ and $u_l$ and obtain three relationships involving $J$, $p_1$ and $p_2$, the $\theta$'s, $u_s$, $D$ and the various rate constants. For example, from eqns. (1), (3) and (4) one obtains

$$J\left[\frac{l}{D}+\frac{1}{\dfrac{k_3\theta_1}{u_s}+k_4(1-\theta_1)+k_5p_1\dfrac{(1-\theta_1)}{u_s}+k_6\theta_1}+\frac{1}{\dfrac{k_3\theta_2}{u_s}+k_4(1-\theta_2)+\dfrac{k_5p_2(1-\theta_2)}{u_s}+k_6\theta_2}\right]$$
$$=\frac{k_3\theta_1+k_5p_1(1-\theta_1)}{\dfrac{k_3\theta_1}{u_s}+k_4(1-\theta_1)+\dfrac{k_5p_1(1-\theta_1)}{u_s}+k_6\theta_1}-\frac{k_3\theta_2+k_5p_2(1-\theta_2)}{\dfrac{k_3\theta_2}{u_s}+k_4(1-\theta_2)+\dfrac{k_5p_2(1-\theta_2)}{u_s}+k_6\theta_2}. \quad . \quad . \quad (6)$$

Thus, from eqn. (6), we may write

$$J=\frac{F_1(p_1,p_2,\theta_1,\theta_2)}{(l/D)+F_2(p_1,p_2,\theta_1,\theta_2)}, \quad . \quad . \quad . \quad . \quad . \quad . \quad (7)$$

where $F_1$ and $F_2$ are the functions of $p$ and $\theta$ defined by eqn. (6). If $F_2\gg(l/D)$ then $J$ depend on $l$ and $D$ only in so far as $\theta_1$ and $\theta_2$ depend on $l$ and $D$ (eqns. (1) to (5)), while if $F_2\ll(l/D)$ then

$$J=(D/l)\,.\,F_1 \quad . \quad . \quad . \quad . \quad . \quad . \quad . \quad . \quad . \quad (8)$$

and $J$ tends to have the normal dependence on $D$ and $l$, with a moderating influence due to $F_1$.

$\theta_1$ and $\theta_2$ are functions *inter alia* of $p_1$ and $p_2$, and so $J$ may not vary directly as $\surd p$. Since there is a net flux in the $x$-direction, $\theta_1$ and $\theta_2$ will not have values corresponding to the equilibria for pressures $p_1$ and $p_2$ respectively in static systems. If, however, we approximate to $\theta_1$ and $\theta_2$ by assuming $k_1, k_2 \gg k_3, k_4, k_5$ or $k_6$ we would normally have on the basis of ideal localized adsorption (Fowler and Guggenheim 1939)

$$\theta_1 \sim \frac{a\surd(p_1)}{1+a\surd(p_1)}; \quad \theta_2 \sim \frac{a\surd(p_2)}{1+a\surd(p_2)} \quad \text{where } a=\sqrt{\left(\frac{k_1}{k_2}\right)}. \quad . \quad . \quad (9)$$

We may now consider limiting cases based on eqns. (9) and (6) and see what dependences of $J$ upon $l$, $p$ and $D$ could be anticipated.

## § 3. LIMITING CASES BASED ON EQNS. 6 AND 9

In order to simplify eqn. (6) we will throughout assume $p_2$ and $\theta_2$ to be very small. Then from eqns. (9) and (6),

$$J=\frac{k_3a\surd(p_1)+k_5p_1}{\left(\frac{l}{D}+\frac{1}{k_4}\right)\left[\frac{k_3a\surd(p_1)}{u_s}+k_4+\frac{k_5p_1}{u_s}+k_6a\surd(p_1)\right]+(1+a\surd(p_1))}. \quad (10)$$

This expression can lead to various limiting cases, according to the relative magnitudes of the terms in it. Several of these are given in table 1 for the case when *D is sufficiently small.* In all instances given, the flux, $J$, is inversely proportional to thickness and proportional to the diffusion coefficient. $J$ may however depend variously upon the rate constants $k_3$, $k_4$, $k_5$ and $k_6$ and upon $p_1$, being independent of pressure in one extreme and proportional to pressure in the other. The $\surd p$ pressure dependence of case (v) of the table is not uncommon. Cases (viii) and (ix) arise when either one or other of the two mechanisms by which hydrogen atoms can pass into and out of the metal is absent. Other limiting cases can also readily be seen, such as those arising when the term $(1+a\surd(p_1))$ is much greater than the other terms in the denominator of eqn. (10). This can give fluxes such as

$$J=\frac{k_3\,.\,a\surd(p_1)+k_5p_1}{1+a\surd(p_1)}, \quad . \quad . \quad . \quad . \quad . \quad . \quad (11)$$

which are independent either of $D$ or of $l$, while still giving pressure dependences in which the exponent lies *between zero and unity,* according to the relative magnitudes of the several terms of eqn. (11).

A third group of limiting cases arises when $D$ is sufficiently large. Typical examples are summarized in table 2, in all of which *the flux is independent both of D and of thickness l,* and so the rate-controlling processes are always at the phase-boundaries. The flux may vary with pressure, however, *the exponent of pressure lying between* 0 *and* 1 *according to circumstances.* The examples given in tables 1 and 2, and in eqn. (11) are extremes: under appropriate conditions the terms $l/D$ and $1/k_4$ in eqn. (10) may be comparable (see Discussion) and, there will then be partial dependence of the flux upon diffusion coefficient and thickness of membrane.

Table 1. Limiting Values for $J$ when $p_2$ and $\theta_2$ are Very Small

| Main condition | Subsidiary conditions | Value of $J$ |
|---|---|---|
| $D$ small enough | (i) $[1+a\sqrt{(p_1)} \ll l\left[\frac{k_3a\sqrt{(p_1)}}{u_s}+k_4+\frac{k_5p_1}{u_s}+k_6a\sqrt{(p_1)}\right]$ | $J=\frac{D[k_3a\sqrt{(p_1)}+k_5p_1]}{l\left[\frac{k_3a\sqrt{(p_1)}}{u_s}+k_4+\frac{k_5p_1}{u_s}+k_6a\sqrt{(p_1)}\right]}$ |
| | (ii) As for (i), and also $p_1$ made small enough | $J=\frac{D}{l}\cdot\frac{1}{k_4}\cdot(k_3a\sqrt{(p_1)}+k_5p_1)$ |
| | (iii) As for (i), and $k_3a\sqrt{(p_1)} \gg k_5p_1$ | $J=\frac{D[u_sk_3a\sqrt{(p_1)}]}{l[u_sk_4+(k_3+u_sk_6)a\sqrt{(p_1)}]}$ |
| | (iv) As for (iii), with $p_1$ large enough | $J=\frac{Du_sk_3}{l[k_3+u_sk_6]}$ |
| | (v) As for (iii), with $p_1$ small enough | $J=\frac{Dk_3a\sqrt{(p_1)}}{lk_4}$ |
| | (vi) As for (i), and with $k_3a\sqrt{(p_1)} \ll k_5p_1$ | $J=\frac{Dk_5p_1}{l\left[k_4+\frac{k_5p_1}{u_s}+k_6a\sqrt{(p_1)}\right]}$ |
| | (vii) As for (vi), and $p_1$ sufficiently small | $J=\frac{Dk_5p_1}{lk_4}$ |
| | (viii) As for (i), but with $k_5$ and $k_6$ zero | $J=\frac{Dk_3a\sqrt{(p_1)}}{l\left[\frac{k_3a\sqrt{(p_1)}}{u_s}+k_4\right]}$ |
| | (ix) As for (i), but with $k_3$ and $k_4$ zero | $J=\frac{Dk_5\sqrt{(p_1)}}{l\left[\frac{k_5\sqrt{(p_1)}}{u_s}+k_6a\right]}$ |

Table 2. Additional Limiting Values for $J$ when $p_2$ and $\theta_2$ are Very Small

| Main condition | Subsidiary conditions | Value of $J$ |
|---|---|---|
| $D$ large enough | (i) None | $J=\dfrac{[k_3a\surd(p_1)+k_5p_1]}{\left[\dfrac{k_3a\surd(p_1)}{k_4u_s}+1+\dfrac{k_5p_1}{k_4u_s}+\dfrac{k_6a\surd(p_1)}{k_4}\right]+[1+a\surd(p_1)]}$ |
| | (ii) $p_1$ made sufficiently small | $J=\dfrac{k_3a\surd(p_1)+k_5p_1}{2}$ |
| | (iii) As for (ii), and $k_3a\surd(p_1)\ll k_5p_1$ | $J=\dfrac{k_5p_1}{2}$ |
| | (iv) As for (ii), and $k_3a\surd(p_1)\gg k_5p_1$ | $J=\dfrac{k_3a\surd(p_1)}{2}$ |
| | (v) $k_5$ and $k_6$ are zero | $J=\dfrac{k_3a\surd(p_1)}{\dfrac{k_3a\surd(p_1)}{k_4u_s}+a\surd(p_1)+2}$ |
| | (vi) As for (v), with $p_1$ small enough | $J=\dfrac{k_3a\surd(p_1)}{2}$ |
| | (vii) As for (v), with $p_1$ large enough | $J=\dfrac{k_3k_4u_s}{k_3+k_4u_s}$ |

## § 4. DISCUSSION

In order to see the ways in which pressure and membrane thickness may influence the flux, $J$, through the metal we will consider quantitatively a small number of the possibilities. Table 1, case (ii).

$$\left\{J=\frac{D}{l}\frac{k_3a}{k_4}\sqrt{(p_1)}\left[1+\frac{k_5}{k_3a}\sqrt{(p_1)}\right]\right\}$$

and table 2, case (ii),

$$\left\{J=\frac{k_3a}{2}\sqrt{(p_1)}\left[1+\frac{k_5}{k_3a}\sqrt{(p_1)}\right]\right\}$$

Fig. 1

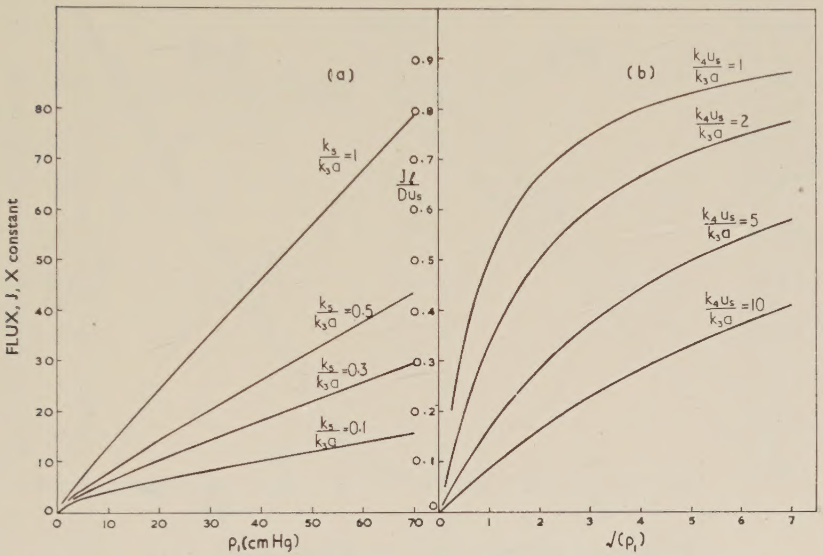

Some possible pressure dependences of the permeation rates. (*a*) The flux, $J$, as a function of pressure for table 1, case (ii), and for table 2, case (ii). The constant multiplying $J$ is $lk_4/Dk_3a$ in the former instance and $2/k_3a$ in the latter. (*b*) Pressure dependence of the flux for table 1, case (viii).

both give the same kind of pressure dependence, which is seen in fig. 1(*a*). In this figure $J(lk_4/Dk_3a)$ or $J(2/k_3a)$, respectively, are shown as functions of $p_1$, when $(k_5/k_3a)=1$, 0·5, 0·3 and 0·1. The flux at low pressure is proportional to $\sqrt{(p_1)}$, but at larger pressures becomes proportional to $p_1$. Another kind of pressure dependence is shown by the flux according to table 1, case (viii),

$$\left[J=\frac{Du_s}{l}\cdot\frac{\sqrt{(p_1)}}{\frac{k_4u_s}{k_3a}+\sqrt{(p_1)}}\right].$$

Figure 1(*b*) shows $Jl/Du_s$ as a function of $\sqrt{(p_1)}$, taking $(k_4u_s/k_3a)=1$, 2, 5 and 10 respectively. The limiting value of the flux as $p_1 \to \infty$ is $Du_s/l$.

As a third example of the ways in which $J$ may vary with the pressure we may consider eqn. (11):

$$\left\{ J = k_5 \cdot \sqrt{(p_1)} \frac{\left[\frac{k_3a}{k_5} + \sqrt{(p)_1}\right]}{1 + a\sqrt{(p_1)}} \right\}.$$

Fig. 2

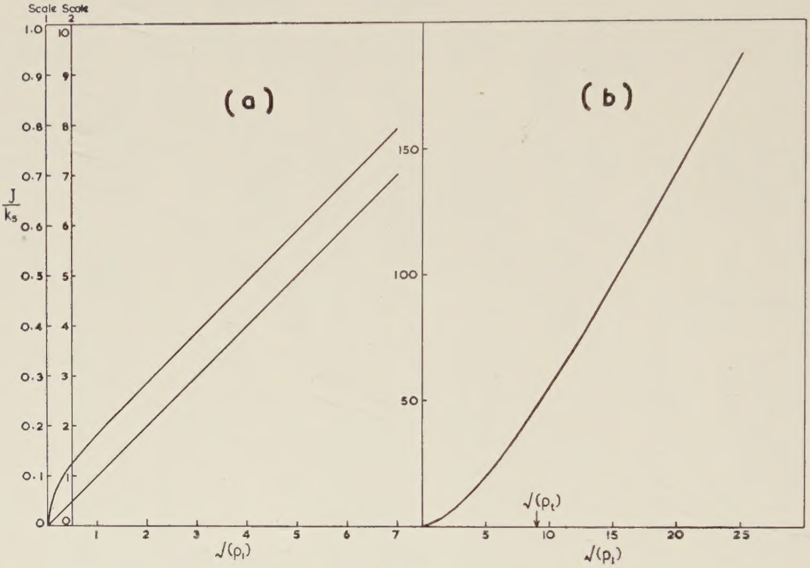

Pressure dependence of $J$ according to eqn. (11).
(*a*) Upper curve: $k_3/k_5=0{\cdot}1$; $a=10$ (scale 1).
Lower curve: $k_3/k_5=1$; $a=1$ (scale 2).
(*b*) $k_3/k_5=10$; $a=0{\cdot}1$.

When $J/k_5$ is plotted against $\sqrt{(p_1)}$ curves are obtained which may initially be concave towards the axis of $J/k_5$ or towards that of $\sqrt{(p_1)}$. However at higher pressures $J/k_5$ always becomes proportional to $\sqrt{(p_1)}$, (fig. 2(*a*) and 2(*b*)). The flux is also initially proportional to $\sqrt{(p_1)}$, the slope $dJ/d\sqrt{(p_1)}$ being $k_3a$ when $p_1 \to 0$. On the other hand the final slope $dJ/d\sqrt{(p_1)} = k_5/a$ when $p_1 \to \infty$. The curve of $J/k_5$ vs $\sqrt{(p_1)}$ is thus convex towards the axis of $J/k_5$ if $a > \sqrt{[(k_5/k_3)]}$ and convex towards the axis of $\sqrt{(p_1)}$ if $a < \sqrt{[(k_5/k_3)]}$. This latter condition leads to the idea of a 'threshold pressure', $p_t$, shown in fig. 2(*b*), which is the intercept made by the asymptotic curve upon the axis of $\sqrt{(p_1)}$. Such threshold pressures have been observed in various experiments where hydrogen diffuses through metals (Barrer 1951, Toda 1958, Borelius and Lindblom 1927), but one notes that under the conditions giving rise to eqn. (11) negative intercepts on the axis of $\sqrt{(p_1)}$ are also possible. The flux $J$ in eqn. (11) can be written as

$$J=\frac{k_5}{a}\sqrt{(p_1)}\left\{1+\frac{\left(\dfrac{k_3a^2}{k_5}-1\right)}{[1+a\sqrt{(p_1)}]}\right\} \quad . \; . \; . \; . \; . \; . \quad (12)$$

which, when $p_1 \to \infty$, approaches the asymptote

$$J=\frac{k_5}{a}\left\{\sqrt{(p_1)}-\frac{\left(1-\dfrac{k_3a^2}{k_5}\right)}{a}\right\} \quad . \; . \; . \; . \; . \; . \quad (13)$$

Fig. 3

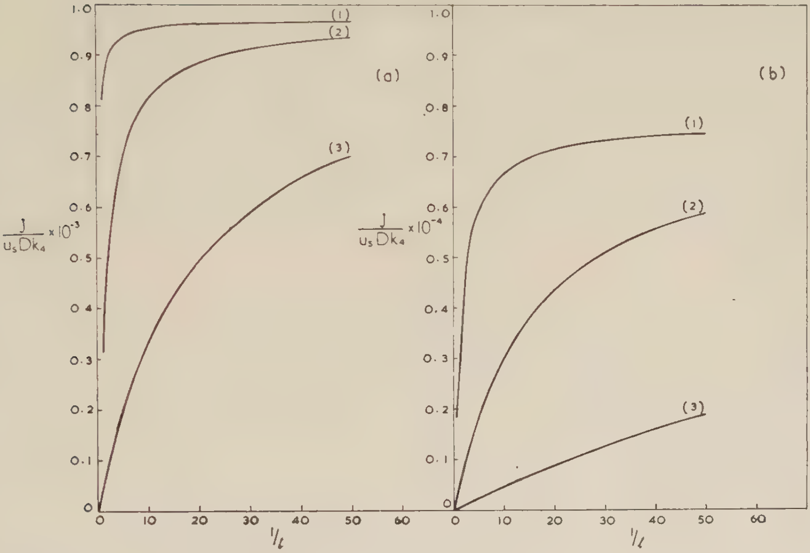

Dependence of $J$ upon thickness of membrane, according to eqn. (10), but assuming that $k_5$ and $k_6$ tend to zero.

(*a*) For all curves, $D=10^{-5}$ cm$^2$ sec$^{-1}$; $a=10$; $\sqrt{p}=10$; $u_sk_4/ak_3=10$; and for curves 1, 2 and 3 respectively, $k_4=10^{-4}$, $10^{-3}$ and $10^{-2}$.

(*b*) For all curves, $D=10^{-5}$ cm$^2$ sec$^{-1}$; $a=1$; $\sqrt{p}=10$; $u_sk_4/ak_3=10$; and for curves 1, 2 and 3 respectively, $k_4=10^{-4}$, $10^{-3}$ and $10^{-2}$.

Thus the 'threshold pressure' is given by

$$\sqrt{(p_t)}=\frac{1-\dfrac{k_3a^2}{k_5}}{a} \quad . \; . \; . \; . \; . \; . \; . \quad (14)$$

and $\sqrt{(p_t)}$ may have positive or negative values according as

$a$ is $<\sqrt{[(k_5/k_3)]}$ or $a>\sqrt{[(k_5/k_3)]}$ respectively.

The effect of thickness of membrane upon the flux was examined using eqn. (10) as a starting point. For simplicity we will assume that $k_5$ and $k_6$ tend to zero. When $l/D$ and $1/k_4$ are comparable in magnitude the flux can then be written in the form

$$\frac{J}{u_s D k_4} = \frac{\surd(p_1)}{(lk_4+D)\left\{\surd(p_1)+\dfrac{u_s k_4}{ak_3}\right\}+\dfrac{u_s D k_4}{ak_3}[1+a\surd(p_1)]}. \quad . \quad (15)$$

Figures 3($a$) and 3($b$) show $J/u_s D k_4$ as a function of $1/l$ at a fixed pressure $p_1$. For all curves $D$ was taken as $10^{-5}\,\text{cm}^2\,\text{sec}^{-1}$, $\surd(p_1)$ as 10 and $u_s k_4/ak_3$ as 10. The three curves in fig. 3($a$) then refer in order to $k_4 = 10^{-4}$, $10^{-3}$ and $10^{-2}$ respectively, for $a = 10$. Those in fig. 3($b$) have the same values of $k_4$, but $a = 1{\cdot}0$. In all cases, as the membrane becomes thinner, $J$ tends to become independent of thickness, although in fig. 3($b$), curve 3, $J$ is initially almost a linear function of $1/l$.

It is thus seen that the theory of coupled diffusion and phase-boundary processes can offer simple explanations of $H_2$-metal permeabilities which vary with membrane thickness $l$ or with ingoing pressure $p_1$ between $l^0$ to $l^{-1}$ and $p^0$ to $p^1$ (where 0, $-1$, 1, are exponents) as well as providing an explanation of the 'threshold pressure' effect sometimes observed in permeation studies, The number of limiting possibilities is large, but the theory seems ready for quantitative application, and phenomena so far recorded in the study of hydrogen flow through metals appear to be within its compass.

## REFERENCES

Barrer, R. M., 1939, *Phil. Mag.*, **28**, 353; 1940, *Trans. Faraday Soc.*, **36**, 1235; 1951, *Diffusion in and through Solids*, Chap. 4 (Cambridge: University Press).
Borelius, G., and Lindblom, S., 1927, *Ann. Phys., Lpz.*, **82**, 201.
Fowler, R. H., and Guggenheim, E. A., 1939, *Statistical Thermodynamics*, Chap. 10 (Cambridge: University Press).
Silberg, P. A., and Bachman, C. H., 1958, *J. chem. Phys.*, **29**, 777.
Smithells, C., and Ransley, C. E., 1935, *Proc. roy. Soc.* A, **150**, 172.
Toda, G., 1958, *J. Res. Inst. Catalysis*, **6**, 13.
Wahlin, H. B., and Naumann, V. O., 1953, *J. appl. Phys.*, **24**, 42.
Wang, J. S., 1936, *Proc. Camb. phil. Soc.*, **32**, 657.

# Pressure Dependence of the Critical Field in Indium Single Crystals†

By H. Rohrer
Institut für Kalorische Apparate und Kältetechnik
Eidgenössische Technische Hochschule, Zürich

[Received July 15, 1959]

## Abstract

The pressure dependence of the critical magnetic field in single crystals of indium has been calculated from measurements of length changes at the transition. We find

$$\partial H_c/\partial p_{\|} = -[(3{\cdot}4 \pm 0{\cdot}2) + (2{\cdot}8 \pm 0{\cdot}2)t^2] \,.\, 10^{-9} \text{ oe dyn}^{-1}\text{ cm}^2$$

and

$$\partial H_c/\partial p_{\perp} = -[(0{\cdot}2 \pm 0{\cdot}1) + (0{\cdot}1 \pm 0{\cdot}1)t^2] \,.\, 10^{-9} \text{ oe dyn}^{-1}\text{ cm}^2$$

where $t = T/T_c$ and $p_{\|}$ and $p_{\perp}$ are uniaxial pressures parallel and perpendicular to the tetragonal axis. The anisotropy disappears when the effect of equal length changes rather than equal pressures in different directions is considered.

## § 1. Introduction

Experiments to determine the change of critical magnetic field with pressure have by now been carried out either directly (vide e.g. Muench 1955), or by means of observations of the volume change at the superconducting transition (Olsen and Rohrer 1957, Cody 1958), on polycrystalline specimens of most superconductors with transition points above 2°K. The most important information obtained from such measurements is the volume dependence of the density of states, $N(0)$ at the Fermi surface, and of the interaction constant, $V$, in Bardeen, Cooper and Schrieffer's (1957) theory of superconductivity. In the polycrystalline case theoretical work on the volume dependence by Morel (1958, 1959) is in partial agreement with the experimental data.

Very little work has been done on single crystals, and only for tin have accurate measurements on the effect of uniaxial tension on single crystals been made by Grenier (1955, 1956), who also made preliminary investigations on mercury. Measurements on single crystals are, however, of additional interest because conclusions may be drawn about possible anisotropies in the behaviour of the electronic level density under pressure. We have therefore examined single crystals of indium even though such work provides relatively little information about anisotropies in the electron–electron interaction causing superconductivity.

---

† Communicated by the Author.

## § 2. EXPERIMENTAL

To determine the pressure coefficient of the critical magnetic field, $H_c$, we measured the change of length of indium single crystals on destruction of superconductivity by a magnetic field. From this change of length, we may calculate the pressure change of $H_c$ using the following thermodynamical relation (Shoenberg 1952, Grenier 1956):

$$(l_{n\theta}-l_{s\theta})/l_{s\theta}=H_c/4\pi\times\partial H_c/\partial p_\theta+H_c^2/8\pi\times\partial l_\theta/l_{\theta s}\partial p_\theta \quad . \quad . \quad (1)$$

where $p_\theta$ is a uniaxial pressure in the direction $\theta$ and $l_{n\theta}$ and $l_{s\theta}$ are the lengths of the specimen in direction $\theta$ in the normal and superconducting state respectively.

This indirect method is considerably more accurate than a direct measurement of the effect of pressure on the critical field. This is partly due to the inherent accuracy of the technique used, and partly due to the small change in critical field at the yield stress of pure single crystals (a tension of *ca.* 1000 kg cm$^{-2}$ is required to shift the critical field by 1 oersted, while indium single crystals are damaged by a tension of about 10 kg cm$^{-2}$).

The apparatus used has been described previously (Olsen and Rohrer 1957). It was however necessary to reduce the stiffness of the mechanical part to avoid the single crystals being deformed during the measurements. This causes a slight reduction of sensitivity compared to our previous work, though changes in length of $10^{-8}$ cm in our 10 cm long specimens could still be detected.

The single crystals were made in the usual way by zone melting. Their orientation was determined using an optical goniometer method, and by measuring the electrical resistance. The anisotropy of the electrical resistance is small ($\rho_\perp/\rho_\parallel=1{\cdot}05$), and its determination gives only a rough approximation of the orientation. It is however useful for finding the tetragonal axis. To be sure that the single crystals were not damaged by the rather complicated mounting procedure, we measured the orientation both before and after the experiment.

## § 3. RESULTS

Measurements of the length change on destruction of superconductivity were made in the temperature range down to 1·4°K, and the values of $\partial H_c/\partial p_\theta$ obtained were found to be reliable between 1·4°K, and *ca.* 3°K. At higher temperatures the length changes become small, so that even small absolute errors in the observations can cause large relative errors in $l_{n\theta}-l_{s\theta}$ and $\partial H_c/\partial p_\theta$.

It has been shown previously (Olsen and Rohrer 1957), that $\partial H_c/\partial p_\theta$ will have the form $\partial H_c/\partial p_\theta=a+b(T/T_c)^2$ if the critical field curve is parabolic. We find that our measurements in the range 1·4–3°K obey this relation to within the limits of experimental error. For pressures $p_\parallel$ parallel and $p_\perp$ perpendicular to the tetragonal axis of the crystal, the observed temperature dependence is given by

$$\partial H_c/\partial p_\parallel=-[(3{\cdot}4\pm0{\cdot}2)+(2{\cdot}8\pm0{\cdot}2)t^2]\,.\,10^{-9}\,\mathrm{oe\,dyn^{-1}\,cm^2},$$
$$\partial H_c/\partial p_\perp=-[(0{\cdot}2\pm0{\cdot}1)+(0{\cdot}1\pm0{\cdot}1)t^2]\,.\,10^{-9}\,\mathrm{oe\,dyn^{-1}\,cm^2},$$

In the figure we have plotted values of $\partial H_c/\partial p_\theta$ at $T=0$°K and $T=T_c$ for all single crystals investigated against $\sin^2\theta$, where $\theta$ is the angle between the tetragonal axis and the sample axis. These values are, of course, extrapolated from values of $(\partial H_c/\partial p_\theta)_T$ measured in the temperature range between 1·4 and 3·0°K. For a certain orientation we expect

$$(\partial H_c/\partial p_\theta)_T = (\partial H_c/\partial p_{\parallel})_T \cos^2\theta + (\partial H_c/\partial p_{\perp})_T \sin^2\theta \quad . \quad . \quad . \quad (2)$$

and it will be seen that our points obey such a relation quite well.

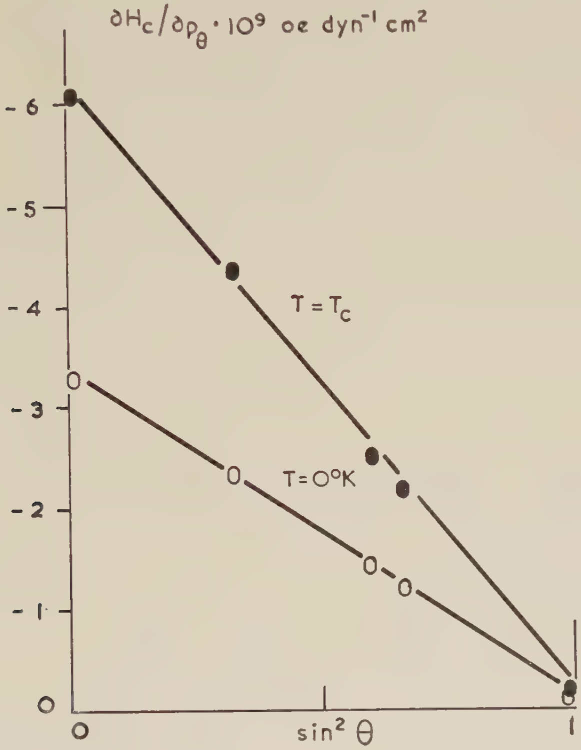

By adding the effects of three uniaxial pressures in mutually perpendicular directions, we obtain the critical field change for hydrostatic pressure $p$:

$$(\partial H_c/\partial p) = \partial H_c/\partial p_{\parallel} + 2(\partial H_c/\partial p_{\perp}). \quad . \quad . \quad . \quad . \quad (3)$$

Under certain assumptions, this value is equal to that for polycrystalline samples under hydrostatic pressure and can be compared with previous measurements on polycrystalline indium.

The meaning of these results is best seen if we use the temperature dependence of $\partial H_c/\partial p$ to calculate the rates of change with volume, $v$, of $T_c$, the critical temperature, of $H_0$, the critical field at the absolute zero, and of $\gamma^*$, the electronic specific heat constant per unit volume in the normal state. This is proportional to the density of states, $N^*(0)$, at the Fermi surface. These rates of change may conveniently be described by the following dimensionless quantities:

$$g^* = \frac{\partial \log \gamma^*}{\partial \log v} = \frac{\partial \log N^*(0)}{\partial \log v}, \qquad (4a)$$

$$h = \frac{\partial \log H_0}{\partial \log v}, \qquad (4b)$$

$$s = \frac{\partial \log T_c}{\partial \log v}. \qquad (4c)$$

A relation between these quantities is easily calculated if we make use of the fact true for any given shape of critical field curve that

$$\gamma^* = \text{const.} \times H_0^2/T_c^2. \qquad (5)$$

This implies

$$g^* = 2(h - s) \qquad (6)$$

while $h$ and $s$ are given by

$$h = \frac{v}{H_0}\left(\frac{\partial p}{\partial v}\right)\left(\frac{\partial H_0}{\partial p}\right), \qquad (7)$$

$$s = \frac{v}{T_c}\left(\frac{\partial p}{\partial v}\right)\left(\frac{\partial T_c}{\partial p}\right) = -\frac{v}{T_c}\left(\frac{\partial p}{\partial v}\right)\left(\frac{\partial H_c}{\partial p}\right)_{T=T_c}\Big/\left(\frac{\partial H_c}{\partial T}\right)_{T=T_c}. \qquad (8)$$

So far we have not specified the sort of volume variation we wish to consider in (4), (7) and (8). For polycrystals it is natural to consider changes of volume under hydrostatic pressure. In a single crystal we have various possibilities: We may consider a change caused by uniaxial pressure. This case is easily calculated, because eqn. (1) yields information for just this case. We denote the volume variabilities so calculated by $g^*$, $h$ and $s$ in the table, and we have listed their values for directions parallel and perpendicular to the symmetry axis in the columns marked ‖ and ⊥ respectively. In the column marked ~ the value for hydrostatic pressure is given. Unfortunately, however, the volume changes implied in the above calculations are rather complicated, and the significance of the anisotropy shown is not obvious.

A much clearer picture is obtained if we consider uniaxial deformations rather than pressures. The logarithmic derivatives obtained using such uniaxial volume changes are denoted by $g^{*\prime}$, $h'$ and $s'$ in the table. In this case the metal must be considered to be exposed to a system of stresses so that it changes its linear dimensions in a given direction while remaining undeformed in directions at right angles. These $g^{*\prime}$, $h'$ and $s'$ can, however, only be calculated for directions parallel or perpendicular to the symmetry axis, since a calculation for any other direction requires a knowledge of the effect of shear stresses on $H_c$. Such measurements are only available for polycrystalline tin (Olsen 1955).

In the column marked ~ we show the effect of a stress system which gives rise to a uniform expansion or contraction of the crystal. Except in the case of elastically highly anisotropic crystals, the two sets of values $g^*, s, h$ and $g^{*\prime}, s', h'$ in the ~ column should be nearly equal.

It will be seen from the values given in the table that for indium the anisotropy in the logarithmic derivatives is completely removed by going from $g^*$, $h$ and $s$ to $g^{*\prime}$, $h'$ and $s'$. This is really quite remarkable in view of the anisotropy of so many other properties of indium. For comparison we also show values for tin in the table. These have been calculated from Grenier's (1956) measurements. In tin the anisotropy is also less when $g^{*\prime}$, $h'$ and $s'$ are examined rather than $g^{*\prime}$, $h$ and $s$, although the anisotropy does not disappear completely.

| | | In | | | Sn | | |
|---|---|---|---|---|---|---|---|
| | | ∥ | ⊥ | ~ | ∥ | ⊥ | ~ |
| $\rho(T=293°\text{K})$ | $10^{-6}$ Ω cm | 8·65 | 9·05 | 8·92 | 14·3 | 9·90 | 11·4 |
| $\dfrac{1}{l_\theta}\dfrac{\partial l_\theta}{\partial p}$ | $10^{-12}$ c.g.s. | 0·64 | 0·94 | 0·83 | 0·68 | 0·61 | 0·63 |
| $g^*$ | | 0 | 0 | 0 | 2·1 | 0·1 | 0·7 |
| $s$ | | 20 | 0·5 | 5·4 | 18·3 | 1·0 | 6·6 |
| $h$ | | 20 | 0·5 | 5·4 | 19·3 | 1·0 | 6·9 |
| $\phi$ | | — | — | 2·0 | — | — | 2·0 |
| $g^{*\prime}$ | | 0 | 0 | 0 | 2·8 | 1·2 | 1·7 |
| $s'$ | | 5·3 | 5·0 | 5·1 | 12·3 | 5·0 | 6·7 |
| $h'$ | | 5·3 | 5·0 | 5·1 | 13·7 | 5·6 | 7·5 |
| $\phi'$ | | — | — | 2·0 | — | — | 2·0 |
| $(\partial H_c/\partial T)_{T_c}$ | oe/°K | 146 | | | 150 | | |

$g^*$ and $g^{*\prime}$ are rather sensitive to the value of $(\partial H_c/\partial T)_{T=T_c}$ used in the calculations, but we may say with confidence that $|g'| < 0{\cdot}5$ for all directions in indium. It is thus close to the free electron value of $-\frac{1}{3}$.

It is interesting to compare this very normal result with recent indications that $g^*$ may be of the order of 100 in aluminium (Olsen 1959). Both metals are trivalent, aluminium is face centred cubic, while indium is tetragonal face centered (with axial ratio of 1·08). Perhaps the aluminium results may be explained in terms of strongly pressure dependent pockets in higher Brillouin Zones (Heine 1957, Harrison 1959). It appears possible that the slight distortion of the cubic lattice to form the tetragonal structure of indium removes these pockets.

For completeness the table also contains the values of $\phi$ given by

$$\phi = \frac{\partial \log V}{\partial \log v} = (s-c)\,N(0)\,.\,V - g$$

where $V$ is the interaction constant occurring in the Bardeen, Cooper and Schrieffer (1957) theory of superconductivity, and $c$ is the Grüneisen constant.

## ACKNOWLEDGMENTS

I am very grateful to Professor Dr. P. Grassmann, the director of the institute, for his kind support and specially to Dr. J. L. Olsen for helpful advice and useful discussions. The work was supported financially by a credit from the 'Arbeitsbeschaffungsfond des Bundes'.

## REFERENCES

BARDEEN, J., COOPER, L. N., and SCHRIEFFER, J. R., 1957, *Phys. Rev.*, **108,** 1175.
CODY, G. D., 1958, *Phys. Rev.*, **111,** 1078.
GRENIER, C., 1955, *Comptes rendus*, **240,** 2302 ; 1956, *Thesis*, Paris.
HARRISON, W. A., 1959 (in the press).
HEINE, V., 1957, *Proc. roy. Soc.* A, **240,** 340.
MOREL, P., 1958, *Phys. Rev.*, **1**, 244 ; 1959, *J. phys. Chem. Solids*, **10,** 277.
MUENCH, N., 1955, *Phys. Rev.*, **99,** 1814.
OLSEN, J. L., 1955, *Nature, Lond.*, **173,** 37 ; 1959, *Helv. phys. acta*, **32,** 310.
OLSEN, J. L., and ROHRER, H., 1957, *Helv. phys. acta*, **30,** 49.
SHOENBERG, D., 1952, *Superconductivity* (Cambridge : University Press).

# Quenching Defects in Binary Aluminium Alloys†

By G. THOMAS‡
Metallurgy Department, University of Cambridge

[Received July 16, 1959]

## ABSTRACT

Thin foils of binary aluminium alloys containing various amounts of copper, silver, zinc and magnesium in solid solution have been prepared from quenched specimens and examined by transmission electron microscopy. In all the alloys closed loops of dislocation line and complex dislocation networks were observed. The dislocation loops did not show any stacking fault contrast so they are glissile dislocations of prismatic $\frac{1}{2}\langle 110\rangle$ type. These loops are formed by the condensation of vacancies into collapsed discs and the results indicate that this often occurs during the quench. The vacancy concentrations required to produce the defects were calculated from the density and size of the loops and varied from $10^{-3}$ to $10^{-6}$ as the quenching temperature was decreased from 600°c to 500°c and as the solute content was increased when quenching from the same temperature. This result led to the conclusion that most of the vacancies remain ' quenched in ' in the concentrated alloys, i.e. the supersaturation of vacancies decreases with increasing alloy content. The magnitude of this effect decreases in the order copper, silver, magnesium, zinc. This is also the order of increasing mobility of these elements in aluminium. At composition above 0·9 at % Cu, 1·3 at % Ag, 8 at % Mg and >15 at % Zn most of the vacancies may be retained in solution after quenching the alloys from 550°c. The precipitation of vacancies in the Al–Cu, Al–Ag and Al–Zn alloys is thought to be accompanied by clustering of solute atoms. The annealing process in Al–Mg alloys is complicated and there is no evidence for clustering of magnesium atoms. Dislocations and grain boundaries have been shown to be sinks for vacancies and the possibilities that these defects are also collectors for solute atoms is discussed. Helical dislocations were observed in quenched alloys only when the quenching temperature was close to the limit of solid solubility.

## § 1. INTRODUCTION

IT is now well established that when metals are quenched rapidly from high temperatures, excess concentrations of vacancies may be introduced. Several mechanisms have been proposed to account for the way in which these vacancies subsequently anneal out, e.g. by the formation of cavities along dislocations (Coulomb and Friedel 1957) the condensation of vacancies into collapsed discs to form loops of dislocation line (Frank 1950, Kuhlmann-Wilsdorf 1958, Kimura *et al.* 1958 a, b, 1959, Maddin *et al.* 1958, Kuhlmann-Wilsdorf *et al.* 1958) and the condensation of vacancies on dislocations causing climb (Seitz 1952, Cottrell 1957).

---

† Communicated by the Author.

‡ Now at Department of Mineral Technology, University of California, Berkeley, U.S.A.

Recently, direct electron microscope evidence in favour of the formation of collapsed discs of vacancies has been obtained by Hirsch *et al.* (1958) who observed small dislocation loops with the expected properties in quenched aluminium and tetrahedra in quenched gold. These workers confirmed the predictions of Kuhlmann-Wilsdorf (1958) who drew attention to the fact that differences in loop properties should be expected in metals of different stacking fault energies. Hirsch *et al.* (1958) and Silcox and Hirsch (1959) estimated the initial concentration of vacancies required to produce the observed defects to be $10^{-4}$ in aluminium and $6\times10^{-5}$ in gold.

Microscopic evidence for climb of dislocations in fluorite crystals has been obtained using decoration techniques (Bontinck and Amelinckx 1957, Amelinckx *et al.* 1957, Bontinck 1957). These workers observed helical dislocations about $10\,\mu$ diameter as expected for the climb of screw dislocations. Similar effects in germanium have been observed by Dash (1958) and by Tweet (1958). Recently helical dislocations have been observed in quenched aluminium 4% copper alloys by Thomas and Whelan (1959) who showed that the formation of loops by condensation of vacancies did not readily occur but that most of the vacancies condensed on screw dislocations producing helices which varied in radius and pitch from about 250 Å to more than 1500 Å. The vacancy concentration to produce the observed climb was estimated to be about $3\times10^{-5}$. Smallmann *et al.* (1958) and Nicholson (private communication) have observed helical dislocations in quenched and aged aluminium–20% silver alloys. In more complex alloys, e.g. aluminium–zinc–magnesium, Thomas (1959) showed that few dislocation loops or helices formed after quenching and ageing, which indicated that most of the vacancies remained ‘quenched in’.

Recently, considerable attention has been paid to the decomposition of supersaturated solid solutions of binary aluminium alloys containing copper, silver and zinc, e.g. Panseri *et al.* (1958), Federighi (1958), De Sorbo *et al.* (1958), De Sorbo and Turnbull (1959), Rosenbaum and Turnbull (1958), Turnbull *et al.* (to be published) and Panseri and Federighi (to be published). In these alloys the solute atoms segregate at comparatively low temperatures into very small solute-rich clusters which by resistivity measurements were shown to form at rates very much faster than would be expected from the extrapolated values at the diffusion coefficients measured at high temperatures. This result was explained by considering that a high vacancy concentration was retained in the alloys by quenching and these excess vacancies assisted in the diffusion process. In view of this the present investigation was undertaken to try to obtain direct evidence in favour of the quenched-in vacancy hypothesis and to find out what would be the effect of varying the concentration of solute atoms in alloys quenched from the same temperature. The presence of alloying elements may change the activation energy to form a vacancy in pure metals. Thus, although the vacancy concentration in aluminium alloys may be different from that in pure aluminium at equivalent temperatures, it will be assumed in this paper that the total number of vacancies is not altered appreciably by increasing the solute concentration.

## § 2. EXPERIMENTAL

The alloys used in this investigation were high purity aluminium containing 1 and 2% copper, 1 and 5% silver, 10 and 30% zinc, and 1, 3, 5 and 7% magnesium. In all cases the total impurity content did not exceed 0·005%. Foils 100 $\mu$ thick were prepared from thicker sections by several stages of cold rolling with intermediate anneals. The specimens were then solution treated at 530°C for 15 hours and water-quenched. The quenching experiments were subsequently carried out by dropping specimens directly into iced brine from a vertical furnace after holding for 3 hours at temperatures between 500°C and 600°C. Some of the specimens were then aged at 100°C and 160°C. Thin foils suitable for transmission electron microscopy were prepared by electro polishing in a phosphoric-chromic acid bath (Nicholson *et al.* 1958), or in ethyl alcohol-perchloric acid.

The specimens were examined in a Siemens Elmiskop I electron microscope operating at 100kv at instrumental magnifications of ×20 000 and ×40 000. Specimens were mounted in a stereo holder so that the foils could be tilted to obtain maximum dislocation contrast. Selected area diffraction patterns were also taken to establish crystallographic orientations.

## § 3. THE PHASE DIAGRAMS

Figures 1–4 show the equilibrium phase diagrams for the alloys used in this investigation. It can be seen that in all cases the compositions of the alloys used were within the limits of solid solubility at the quenching temperature. Figure 5 shows the solubility curve for vacancies in aluminium as calculated from Bradshaw and Pearson's results (1957).

The effect of the alloying elements on the lattice parameter of aluminium is that copper and zinc produce a contraction, magnesium an expansion, whilst silver has little effect.

## § 4. RESULTS

### 4.1. *The Al–Cu Alloys*

Both the 1% and 2% copper alloys were quenched from 540°C and 600°C respectively. In all cases contrast effects were observed which were interpreted in terms of closed loops of dislocation lines and complex dislocation lines. The density of dislocation loops increased and their diameter decreased with increasing quenching temperature and decreasing solute concentration, e.g. in fig. 6 (Pl. 139) the loop density is $10^{16}/\mathrm{cm}^3$ and the loop diameters vary from 100–300 Å after quenching the 1% copper alloy from 600°C, whilst in fig. 7, (Pl. 140), which shows the structure after quenching from 540°C, the diameters vary from 250 Å to about 4000 Å

Fig. 1

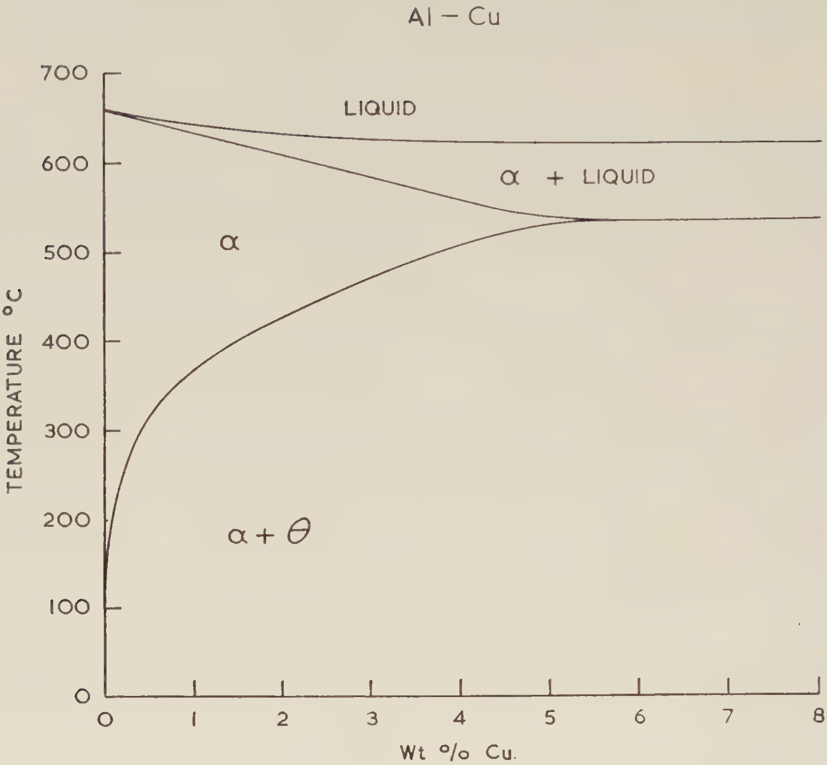

The equilibrium phase diagram for the system Al–Cu.

Fig. 2

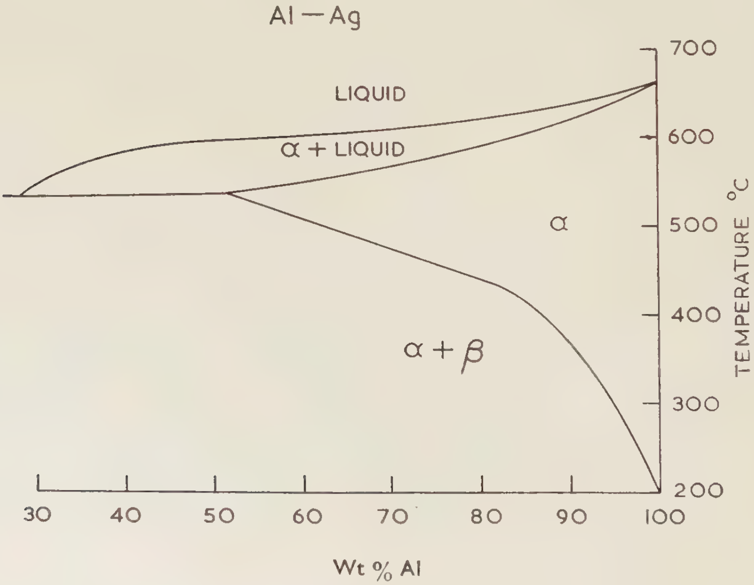

The equilibrium phase diagram for the system Al–Ag.

Fig. 3

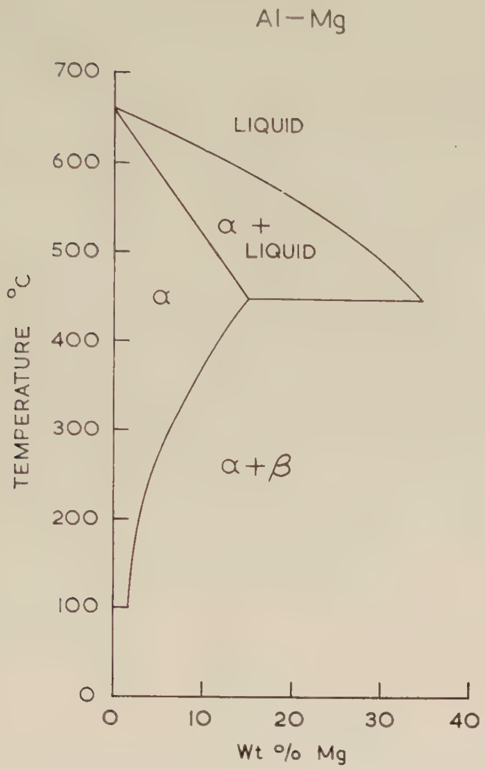

The equilibrium phase diagram for the system Al–Mg.

Fig. 4

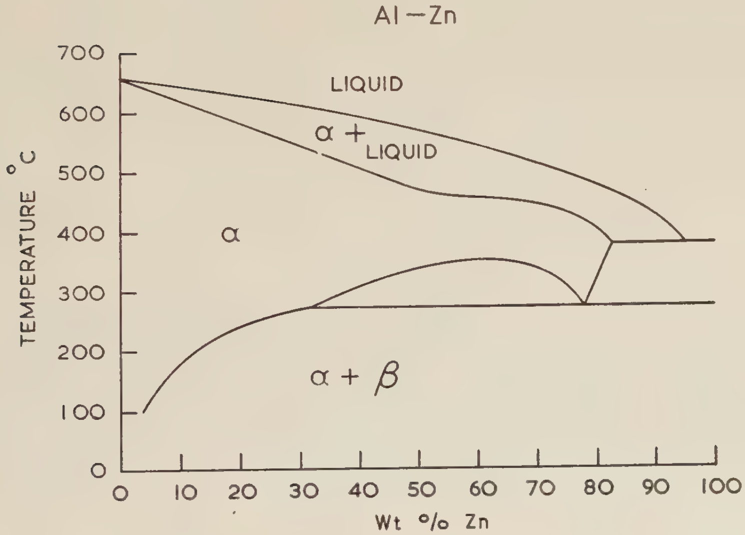

The equilibrium phase diagram for the system Al–Zn.

in the elongated loop at B. The maximum density of dislocation loops was about $10^{13}$ after the 540°c quench. Elongated loops are always found after quenching from the lower temperature. In fig. 7 the orientation of the foil is (001) so that the loops appear to be extended in [110]. This probably means that some loops are actually formed at high temperatures or during quenching since they can only glide in [110] under the action of quenching stresses. When the copper content is increased to 2%, quenching from 600°c produces a slightly smaller density of loops. The mean loop diameter is slightly greater than in the 1% alloy quenched from the same temperature. A remarkable difference in structure between the two alloys is found after the 540°c quench. For example, in fig. 8 (Pl. 140), only one or two loops are visible but at A a helical dislocation is observed. This is to be compared with fig. 7. The general picture of the 2% copper alloy after the 540°c quench is one of a tangle of dislocations with very few loops (less than $10^{13}/\text{cm}^3$). Dislocation loops were not observed in either alloy near dislocation lines and grain boundaries.

Fig. 5

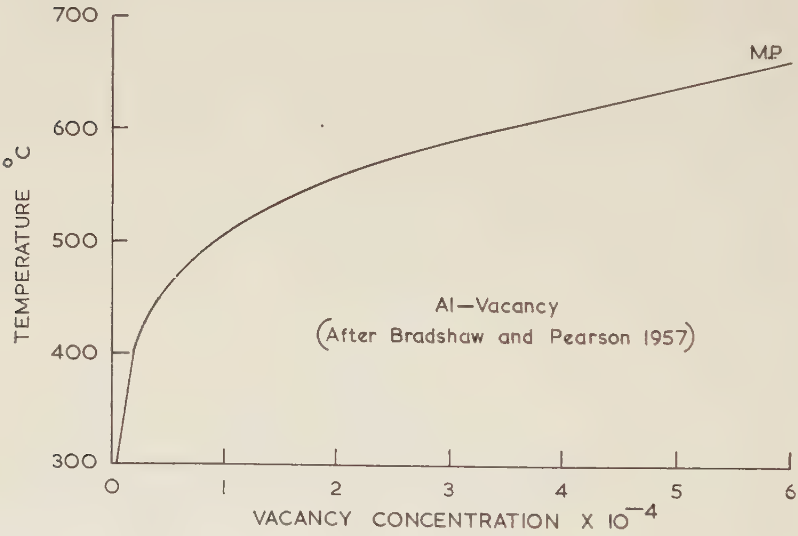

The solubility curve for vacancies in aluminium.

It is apparent from these results that (*a*) the formation of dislocation loops is favoured by high quenching temperatures and by a low solute content, and (*b*) helical dislocations are formed after quenching concentrated alloys from lower temperatures. This last point is in agreement with previous results on the aluminium 4% copper alloy (Thomas and Whelan 1959) in which many well-defined helices were observed after quenching from 500°c and 540°c.

The initial vacancy concentration required to produce the observed defects has been calculated from the densities and radii of the loops, assuming a foil thickness of $0{\cdot}1\,\mu$. The results based on calculations from many micrographs are summarized in table 1.

The vacancy concentration in the alloys quenched from high temperatures ($\sim 10^{-3}$) is much larger than in pure aluminium ($\sim 10^{-4}$, see fig. 5) and this may indicate that the presence of copper in aluminium lowers the activation energy to form a vacancy.

### 4.2. *The Al–Ag Alloys*

The results are similar to those found for the aluminium–copper alloys described in § 4.1, i.e. the density of dislocation loops decreased with decreasing quenching temperature and increasing silver content. Figure 9 (Pl. 141) shows the structure of the 1% silver alloy after quenching from 580°c and in which the loops are rectangular in shape with sides parallel to traces of [111] and [101] in the foil surface (which is $(0\bar{1}2)$). Coalescence of loops seems to have occurred at A. The density of the loops is about $10^{14}/\text{cm}^3$ and the average diameter about 300 Å. Figure 10 (Pl. 141) shows the micro-structure of the 5% silver alloy also quenched from 580°c. There are few loops and many more dislocation lines which have complicated shapes. The loops are up to 1000 Å diameter and the density is about $10^{12}/\text{cm}^3$.

Table 1

| Alloy | At % solute | Quenching temperature (°c) | Average density loops per cm³ | Loop diameter (Å) | Average vacancy concentration |
|---|---|---|---|---|---|
| Al–1% Cu | 0·45 | 540 | $10^{13}$ | 100–4000 | $3\times10^{-5}$ |
| | | 600 | $10^{16}$ | 100–300 | $5\times10^{-3}$ |
| Al–2% Cu | 0·86 | 540 | $10^{12}$ | 500 | $10^{-5}$ |
| | | 600 | $10^{15}$–$10^{16}$ | 100–500 | $10^{-3}$ |
| Al–4% Cu | 1·7 | 540 | Helical dislocations† | | $3\times10^{-5}$ |

† Taken from Thomas and Whelan (1959).

Although well-defined helical dislocations have not been observed in the 5% silver alloy the results of other workers, e.g. Smallman *et al.* (1958), Nicholson (to be published), have shown that they occur in quenched and aged aluminium 20% silver alloys. This confirms the present view that the formation of helical dislocations after quenching is favoured in alloys by increasing the solute concentration.

The initial vacancy concentrations required to produce the observed dislocation loops have been calculated and the results are summarized in table 2.

### 4.3. *The Al–Zn Alloys*

#### 4.3.1. *Al–10% Zn (5 at % Zn)*

Quenching this alloy from above 500°c produced large numbers of dislocation loops the densities of which increased from $2{\cdot}5 \times 10^{15}/\mathrm{cm}^3$ after a 540°c quench to about $10^{16}/\mathrm{cm}^3$ after a 580°c quench. The diameter of the loops varied from 100–200 Å (e.g. fig. 11, Pl. 142), so it was difficult to determine whether the loops had well-defined crystallographic shapes. In general they appear to be roughly circular. Figure 12 (Pl. 143) shows the alloy after quenching from 580°c, and it is observed that loops are not present near dislocation lines, e.g. at A. Other micrographs showed that loops were not formed near grain boundaries. The initial vacancy concentration to produce the loops was calculated to be $2 \times 10^{-4}$ for the 540°c quench and $6 \times 10^{-4}$ for the 580°c quench. The activation energy $Q$ to form a vacancy was found from resistivity measurements to be $0{\cdot}70 \pm 0{\cdot}02$ ev by Panseri and Federighi (to be published), and since $Q$ in aluminium is 0·76 ev, it appears that the binding energy between a vacancy and a zinc atom is very small. This would indicate that the effect of increasing the zinc content on the quenching characteristics would not be very marked and so an alloy of 30% zinc was examined. The results obtained with this alloy are described in the following section.

Table 2

| Alloy | At % solute | Quenching temperature (°c) | Average density loops per cm³ | Loop diam. (Å°) | Average vacancy concentration |
|---|---|---|---|---|---|
| Al–1% Ag | 0·26 | 580 | $7 \times 10^{13}$–$10^{14}$ | 300 | $1$–$4 \times 10^{-4}$ |
| Al–5% | 1·30 | 580 | $10^{12}$ | 300–1000 | $10^{-5}$ |

#### 4.3.2. *Al–30% (15 at % Zn)*

As expected from the previous considerations quenching Al–30% zinc from 510°c resulted in the formation of a high density of dislocation loops (about $10^{16}/\mathrm{cm}^3$) of diameter 100–200 Å and in which the initial vacancy concentration was estimated to be about $5 \times 10^{-4}$, i.e. very similar to the aluminium–10% zinc alloys. In a number of cases helical dislocations were also observed, e.g. at B fig. 13 (Pl. 144). Large loops can be seen at A. It is to be noted from this micrograph that there are very few loops near the helices, indicating that the vacancies in these regions have been used up by the climb of the original screw dislocations. The small loops produced by the collapse of vacancy discs can be observed at C in fig. 13

(Pl. 144). It is not certain whether the helical dislocations have been formed from residual screw dislocations or from sources operating during quenching.

Some interesting grain-boundary effects were observed in this alloy. When specimens were quenched from 540°C they disintegrated in the quenching medium and examination of the fractures showed them to be intercrystalline. After quenching from 510°C the specimens were very brittle and when examined under an optical microscope, zinc precipitates were visible at the grain boundaries. Because of this it was difficult to prepare thin foils for examination in the electron microscope, since the specimens thinned preferentially at the grain boundaries. However, an example of the structures observed is shown in fig. 14 (Pl. 144). The zinc precipitates previously at A in the grain boundary have been leached out during the preparation of the foil. Dislocation loops $\sim 100$ Å diameter are visible at B and there is a loop-free region $\sim 3\,\mu$ wide adjacent to the boundary. This indicates that the grain boundary acts as a sink for nearby vacancies. The observations showed that precipitation of zinc also occurred at the grain boundaries. This is quite surprising in view of the fact that the quenching temperature is 200°C higher than the solid solubility limit (see fig. 4). Precipitation at the boundaries must occur during the quench when large numbers of vacancies are eliminated at the grain boundaries. The result of this is the production of a loop and precipitate free region adjacent to the boundary. Vacancies away from the boundary can condense and collapse to form dislocation loops. Thus conditions are obtained for intercrystalline embrittlement, i.e. we have a matrix hardened by dislocation loops, a barrier of precipitates at the grain boundaries and a narrow, soft loop and precipitate free region between the two. The situation is analogous to the embrittlement of many precipitation-hardened alloys after ageing treatments which produce a precipitate free region between a grain boundary and the adjacent matrix (Thomas and Nutting 1959 a).

These results confirm the view that in materials where loops are visible after quenching (without artificial ageing), the aggregation of vacancies to form nuclei of collapsed discs actually occurs during quenching.

### 4.4. *The Al–Mg Alloys*

A series of alloys of increasing magnesium content from 1–7% were quenched from 550°C. It was found that the density of loops decreased as the magnesium content increased until at 7% magnesium very few loops were observed. The results of the estimated initial vacancy concentrations to produce the observed loops are summarized in table 3. Figure 15 (Pl. 145) shows the structure of the quenched aluminium 1% magnesium alloy and fig. 16 (Pl. 145) that of the same alloy after subsequent ageing for two hours at 100°C†. It is immediately apparent that after ageing the loops have grown in size, probably by absorbing quenched-in vacancies and also from the solution of the smaller loops. After ageing the loop density decreased from $2 \times 10^{15}$ to $2 \times 10^{14}$ and the vacancy concentration decreased by a factor of 2. Some of the vacancies have probably been lost during the climb of dislocations at this temperature, e.g. at B in fig. 16 (Pl. 145).

---

† The purpose of these ageing experiments was to check the work of Panseri *et al.* (1958) and is discussed in § 6.

Table 3

| Alloy | At % solute | Quenching temperature (°c) | Average density of loops per cm$^3$ | Loop diameter (Å) | Average vacancy concentration |
|---|---|---|---|---|---|
| Al–1% Mg | 1·12 | 550 | $2{\cdot}6 \times 10^{15}$ | 200 | $9 \times 10^{-4}$ |
| Al–3% Mg | 3·4 | ,, | $1{\cdot}3 \times 10^{15}$ | 200–400 | $3 \times 10^{-4}$ |
| Al–5% Mg | 5·8 | ,, | $6 \times 10^{14}$ | 400 | $2 \times 10^{-4}$ |
| Al–7% Mg | 8·2 | ,, | $10^{13}$ | 400 | $10^{-5}$ |

Figure 17 (Pl. 146) shows the structure of the 3% magnesium alloy and fig. 18 (Pl. 146) that of the 7% magnesium alloy after quenching from 550°c. From these it can be seen that the density of dislocation loops decreases considerably as the magnesium content is increased. Only a few loops are visible in fig. 18, e.g. at A, whereas a high density of dislocations in networks persists throughout the foil. These may be segments of large loops, or may be produced by plastic deformation and climb during quenching. Ageing at 100°c and 160°c† did not result in very much change of structure from that of the quenched alloy. There was no increase in the number of loops and no helical dislocations were observed at any stages of ageing even after visible precipitation had occurred. This may indicate that nearly all the vacancies are held by magnesium atoms even during ageing.

## § 5. The Dislocation Loops in Quenched Alloys

The results have shown that in all the alloys investigated precipitation of discs of vacancies and their collapse to form dislocation loops probably occurs during quenching. The density and size of the loops depend upon the quenching temperature and the solute concentration. Loops are fewer in number but have larger diameters either when the quenching temperature is lowered or when the alloy composition is increased when quenching from the same temperature. This means that the nucleation of loops becomes more difficult in these cases. Thus, increasing the solute concentration is equivalent to decreasing the quenching temperature in reducing the degree of supersaturation of vacancies. The concentration of vacancies required to produce the observed dislocation loops decreases from $10^{-3}$ to $10^{-6}$ with increasing solute concentration and decreasing quenching temperature. If we consider the same quenching temperature the effect of increasing the solute concentration is to retain more vacancies in solution provided the initial vacancy concentration does not decrease with composition. Above a certain composition limit more than 90% of the vacancies do not precipitate out on quenching. The composition limits corresponding to this situation have been estimated to be 0·9 at % Cu, 1·3 at % Ag, 8 at % Mg and > 15 at % Zn for quenching temperatures near 550°c. It follows from this that vacancies are more effectively trapped by copper atoms than by zinc atoms, so that the binding energy between a vacancy and a solute atom increases in the order zinc–magnesium silver–copper. Since the rates of movement of these solutes in aluminium decreases in this order (Clare 1958), diffusion rates in alloys must depend on the binding energy between solute atoms and vacancies. Thus precipitation in quenched alloys must be considered in terms of an equilibrium between solvent atoms, solute atoms and vacancies. If the activation energy to form a vacancy were accurately known for alloys (and this might change with composition) it should be possible to show the variation in solubility of vacancies with temperature and composition. In this way ternary phase diagrams could be constructed. This could also be done experimentally by carrying out many more quenching experiments using alloys of differing compositions. It has been possible to establish the solubility curve for vacancies in pure aluminium from the results of Bradshaw and Pearson (1957) and this is shown in fig. 5. Similar curves should be obtained for alloys.

---

† The purpose of these ageing experiments was to check the work of Panseri *et al.* (1958) and is discussed in § 6.

In all the alloy systems investigated no stacking fault contrast was observed inside the dislocation loops (figs. 6–17). This means that the loops are whole dislocations of Burgers vectors $\frac{1}{2}\langle 110 \rangle$ so that the stacking fault energy of aluminium is not appreciably altered by additions of Cu, Ag, Mg and Zn. Under a suitable stress these dislocation loops should glide by a process of prismatic slip and this can be achieved in the electron microscope simply by increasing the intensity of the electron beam. However only the loops in the aluminium–magnesium alloys have been observed to glide by this method. In these alloys the loops and the line dislocations in both quenched and aged foils glide at relatively low beam intensities. This suggests that magnesium atoms are not segregated at dislocations because if this occurred the defects should be pinned. This idea has been used by Thomas (1959) to explain the immobility of dislocations in aluminium–zinc–magnesium alloys. The dislocation lines and closed loops of dislocation have never been observed to glide in the aluminium–copper, aluminium–silver or aluminium–zinc alloys and this suggests that the solute atoms may segregate preferentially at the dislocations. The observations have shown that dislocations and grain boundaries are sinks for vacancies, so that if the binding energy between a vacancy and a solute atom is high then both vacancies and solute atoms could collect at these imperfections. However, a dislocation is a favourable site for the segregation of solute atoms only when the elastic strain energy near the dislocation lines is reduced and/or when there is a chemical or electrical attraction between the dislocation and the solute atom. If these conditions are satisfied dislocations should also be preferential sites for precipitation. In aluminium–copper alloys the segregation of copper atoms to the compression side of an edge dislocation will relieve the elastic stress around the dislocation, but in aluminium–silver alloys elastic strain effects may not be important because the atoms of silver and aluminium are nearly the same size. It is well known that dislocations are preferential sites for precipitation in aluminium–copper alloys (Castaing and Guinier 1949, Castaing 1949, Thomas and Nutting 1955, 1959 b, Wilsdorf and Kuhlmann-Wilsdorf 1955), so that segregation of copper atoms should occur at dislocation loops, as well as at other edge dislocations.

The behaviour near a screw dislocation is not as clear as in the case of an edge dislocation because in the former there is little or no dilatation. However, in quenched alloys screw dislocations can be converted into helices in which the segments of dislocation line are mainly of edge character. These can then be preferential sites for solute segregation (Thomas and Whelan 1959, Thomas and Nutting 1959 b, Nicholson (to be published).

## § 6. THE RÔLE OF VACANCIES IN SOLUTE CLUSTERING

The effects of quenching and subsequent low temperature ageing in dilute aluminium alloys containing copper, silver and zinc have been followed using electrical resistivity measurements by Rosenbaum and Turnbull (1958), De Sorbo *et al.* (1958, 1959), Turnbull *et al.* (to be published) and Panseri and Federighi (to be published). These workers assumed that the initial stages of decomposition of the supersaturated alloys were accompanied by the segregation of solute atoms into very small solute-rich clusters. They found that the rates of clustering were very much faster than would be expected from the extrapolated value of the diffusion coefficient measured at high temperatures and came to the conclusion that clustering was facilitated by excess vacancies retained during quenching. This is confirmed by the results obtained in the present investigation where it has been shown that up to $10^{-3}$ vacancies may be retained by quenching a similar series of alloys. Since an appreciable amount of diffusion takes place during the elimination of vacancies the formation and growth of clusters by the movement of solute atoms will also take place. Once there is no appreciable excess of free vacancies present the growth of clusters will practically stop. The formation of dislocation loops in dilute alloys and the condensation of vacancies at dislocations in concentrated alloys must therefore be accompanied simultaneously by solute clustering. Since the rate of elimination of vacancies is governed by the quenching temperature and alloy composition, the rate of clustering will also depend on these factors. Thus in dilute alloys quenched from high temperatures clustering can actually take place during quenching. This has been confirmed in the case of aluminium–silver alloys by the x-ray diffraction work of Walker and Guinier (1953). Because the clusters are so small they have not yet been resolved by current electron microscope techniques.

Not all of the available vacancies may be eliminated after quenching, e.g. some may still be associated with solute atoms, particularly in more concentrated alloys. On annealing the movement of any associated vacancies would be slower than that of free vacancies. This could account for the so called 'slow-reaction' which has been observed to occur after the clustering of solute atoms has ceased (Turnbull *et al.* (to be published) Panseri and Federighi (to be published)).

Panseri *et al.* (1958) found that in aluminium–magnesium alloys after quenching there was a permanent increase in resistivity of about five times the observed resistivity in quenched aluminium. Unlike aluminium and alloys containing copper, silver and zinc, recovery of resistivity in the aluminium–magnesium alloys did not occur at room temperature but was effected by ageing at 100°c. These workers explained their results by assuming that vacancies were held by magnesium atoms and were absorbed at dislocations only at 100°c in some complex way. However, it appears from the present results that many vacancies are lost during quenching or very rapidly immediately after quenching so a considerable contribution to resistivity might be expected from the magnesium atoms or from any vacancies still trapped by magnesium atoms. The fact that little or no recovery of resistivity occurs on ageing below 100°c (Panseri *et al.* 1958) suggests that no clustering of magnesium atoms takes place, but at temperatures of 100°c and above, precipitation could cause a drop in resistivity. Some recovery of resistivity due to the elimination of free vacancies would be expected on ageing at 100°c because the vacancy concentration in loops decreased by a factor of 2, i.e. vacancies are lost for example at dislocations during climb at this temperature. Since dislocations were always observed to be mobile and as no precipitation on dislocations was observed it is unlikely that magnesium atoms also collect at dislocations. Strain-ageing effects in these alloys are thus more likely to be due to vacancy dislocation interactions rather than to pinning of dislocations by magnesium atoms. At magnesium concentrations above 8 at % most of the vacancies remain in solution after quenching and are only lost during subsequent ageing by the climb of dislocations or during precipitation because loops were not observed to form. Ellwood (1951–52), from density measurements, found that the vacancy concentration in alloys of aluminium containing up to 8 at % magnesium was about $10^{-1}$. This result shows that the total vacancy concentration in these alloys is very much greater than that obtained from the density of dislocation loops ($\sim 10^{-4}$) which confirms the view that most of the vacancies are held by magnesium atoms. It is probable therefore that precipitation of the $\beta$ phase (see fig. 3) requires both vacancies and magnesium atoms.

## § 7. HELICAL DISLOCATIONS

The present work has provided more experimental results on the formation of helical dislocations. It has been shown that the formation of helices is favoured when excess vacancies have not already been lost in the formation of dislocation loops. They occur in alloys in which the solute concentration approaches the limits of solid solubility at the quenching temperatures (see figs. 1–4) so that the degree of supersaturation of vacancies is relatively low. This is precisely what would be expected because well defined helices can only form in alloys by the condensation of vacancies on screw dislocations so that a sufficient number of vacancies must be available in solution to effect the climb. Thus helices would not be expected in alloys where the dislocation loop density is high unless there are screw dislocations present which have not been annealed out at the high temperature. The possible mechanisms by which helical dislocations are formed have already been discussed in detail elsewhere (Thomas and Whelan 1959). However, it may be added here that since helices are favourable sites for precipitation, e.g. in aluminium–copper (Thomas and Nutting 1959 b) and in aluminium–silver (Nicholson, to be published) it is possible that they may only be stabilized by the segregation of solute atoms. This could occur during climb particularly if there is a strong attraction between vacancies, solute atoms and dislocations.

## § 8. CONCLUSIONS

The following conclusions have been drawn from the results discussed in the previous sections.

(1) High concentrations of vacancies in equilibrium at the high temperature can be retained in alloys by rapid quenching.

(2) In dilute alloys the aggregation of vacancies and their collapse to produce dislocation loops occurs readily during quenching. The density and size of the loops varies with the temperature of quenching as expected when the degree of supersaturation is altered. The initial vacancy concentrations to produce the defects varies from $10^{-3}$ to $10^{-6}$ as the quenching temperature is decreased and the solute concentration increased.

(3) The supersaturation of vacancies decreases with increasing solute content and decreasing quenching temperature so that in relatively concentrated solid solutions a large fraction of vacancies is retained in solution by quenching.

(4) At solute concentrations above 0·9 at % Cu, 1·3 at % Ag, 8 at % Mg and > 15 at % Zn most of the vacancies may be retained in solution after quenching from 550°C.

(5) The attraction of a vacancy for a solute atom increases in the order zinc–magnesium–silver–copper which is also the order of decreasing rates of movement of these atoms in aluminium. The rate of diffusion in alloys thus depends on the binding energy between vacancies and solute atoms.

(6) The annealing out of vacancies in aluminium–zinc, aluminium–silver and aluminium–copper alloys is probably accompanied by solute clustering. Thus the fast rates of low temperature clustering in these alloys is due to the excess vacancies retained by quenching. It is unlikely that clustering occurs in aluminium–magnesium alloys.

(7) Helical dislocations are only observed in alloys when the compositions approach the solubility limits at the quenching temperature and in which there is an attraction between solute atoms vacancies and dislocations.

(8) Grain boundaries and dislocations are sinks for vacancies. When these defects also collect solute atoms they become preferential sites for precipitation.

## ACKNOWLEDGMENTS

The author is indebted to Professor A. H. Cottrell, F.R.S., and Dr. J. Nutting for their interest and encouragement, to them and to Dr. P. B. Hirsch and Dr. M. J. Whelan for much valuable advice. Thanks are also due to Dr. D. Turnbull, Dr. T. Federighi and Mr. R. B. Nicholson for making their results available before publication.

Figures 1–4 have been taken from *Metals Handb.* (1948).

Acknowledgments for financial support are due to an I.C.I. Fellowship.

## REFERENCES

AMELINCKX, S., BONTINCK, W., DEKEYSER, W., and SEITZ, F., 1957, *Phil. Mag.*, **2,** 355.

BONTINCK, W., 1957, *Phil. Mag.*, **2,** 561.

BONTINCK, W., and AMELINCKX, S., 1957, *Phil. Mag.*, **2,** 94.

BRADSHAW, F. J., and PEARSON, S., 1957, *Phil. Mag.*, **2,** 570.

CASTAING, R., 1949, *Compt. rend.*, **228,** 1341.

CASTAING, R., and GUINIER, A., 1949, *Compt. rend.*, **228,** 2033.

CLARE, J. W. H., 1958, *Metallurgia*, **57,** 1.

COTTRELL, A. H., 1957, Inst. of Metals Monograph and Report Series No. 23, p. 1.

COULOMB, P., and FRIEDEL, J., 1957, *Report of Lake Placid Conference on Dislocations and Mechanical Properties of Crystals* (New York : Wiley), p. 555.

DASH, W. C., 1958, *Report of Cooperstown Conference on Growth and Perfection of Crystals* (New York : Wiley and Sons), p. 361.

DE SORBO, W., TREAFTIS, H. N., and TURNBULL, D., 1958, *Acta Met.*, **6,** 401.

DE SORBO, W., and TURNBULL, D., 1959, *Acta Met.*, **7,** 83.

ELLWOOD, E. C., 1951–52, *J. Inst. Met.*, **80,** 605.

FEDERIGHI, T., 1958, *Acta Met.*, **6,** 379.

FRANK, F. C., 1950, Carnegie Institute of Technology : Symposium on the Plastic Deformation of Crystalline Solids O.N.R., p. 150.

HIRSCH, P. B., SILCOX, J., SMALLMAN, R. E., and WESTMACOTT, K. H., 1958, *Phil. Mag.*, **3,** 897.

KIMURA, H. MADDIN, R., and KUHLMANN-WILSDORF, D., 1958 a, *J. Metals, N.Y.*, **10,** 93 ; 1958 b, *Bull. Amer. phys. Soc.*, **3,** 122 ; 1959, *Acta Met.*, **7,** 145.

KUHLMANN-WILSDORF, D., 1958, *Phil. Mag.*, **3,** 125.

Kuhlmann-Wilsdorf, D., Maddin, R., and Kimura, H., 1958, *Z. Mettalk.*, **49,** 584.

Maddin, R., Kimura, H., and Kuhlmann-Wilsdorf, D., 1958, *Bull. Amer. phys. Soc.*, **3,** 125.

Nicholson, R. B., Thomas, G., and Nutting, J., 1958, *Brit. J. appl. Phys.* **9,** 23.

Panseri, C., Gatto F., and Federighi, T., 1958, *Acta Met.*, **6,** 198.

Rosenbaum, H. S., and Turnbull, D., 1958, *Acta Met.*, **6,** 653.

Seitz, F., 1952, *Advanc. Phys.*, **1,** 43.

Silcox, J., and Hirsch, P. B., 1959, *Phil. Mag.*, **4,** 72.

Smallman, R. E., Coiley, J. A., Westmacott, K. H., 1958, A.E.R.E. Harwell Report M/R 2752.

Thomas, G., 1959, *Phil. Mag.*, **4,** 606.

Thomas, G., and Nutting, J., 1955, Institute of Metals Report and Monograph Series No. 18, p. 57 ; 1959 a, *J. Inst. Met.* (to be published) ; 1959 b, *Acta Met.*, **7,** 515.

Thomas, G., and Whelan, M. J., 1959, *Phil. Mag.*, **4**, 511.

Tweet, A. G., 1958, *J. appl. Phys.*, **29,** 1520.

Walker, C. B., and Guinier, A., 1953, *Acta Met.*, **1,** 568.

Wilsdorf, H., and Kuhlmann-Wilsdorf, D., 1955, *Report of Conference on Defects in Crystalline Solids* (London : The Physical Society), p. 175.

# Twinning in Cadmium Dendrites†

By P. B. Price‡
H. H. Wills Physical Laboratory, University of Bristol

[Received June 10, 1959]

## Abstract

Growth twins of cadmium with a [$1\bar{2}\bar{3}0$] twin axis and a (0001) composition plane are formed during deposition from the vapour at high supersaturation. The twin crystals grow in the form of flat 'leaf' dendrites several millimetres in length and only a few microns in thickness, while other crystals in the deposit are three-dimensional, non-dendritic, and limited in size to a few microns. The experimental conditions under which leaf dendrites appear are given, the morphology of the dendrites and the arrangement of atoms near the composition plane are described, and a connection between twinning and the dendritic growth of cadmium is proposed.

## § 1. Introduction

Although suitably oriented cadmium crystals can be twinned on the ($10\bar{1}2$) plane in the [$10\bar{1}\bar{1}$] direction by mechanical deformation, the occurrence of cadmium growth twins has not been reported. One case (Oliver 1952) has been recorded of cadmium twins with a ($10\bar{1}2$) composition plane in a melt-grown crystal, but these were, strictly speaking, mechanical twins which occurred as a result of thermal stresses set up during cooling.

Cadmium dendrites have been grown by electrodeposition (Wranglen 1955) and zinc dendrites from the melt (Weinberg and Chalmers 1952). In both cases the dendrites were single crystals whose stalks and branches grew in $\langle 10\bar{1}0 \rangle$ directions. There was no indication of twinning.

During the course of some experiments on the growth of cadmium crystals from the vapour in an inert gas (Price 1959), it was established that when the gas is very highly supersaturated with cadmium vapour ($p/p_{\mathrm{eq}} > 10^2$, where $p$ = partial pressure of cadmium vapour, $p_{\mathrm{eq}}$ = equilibrium vapour pressure) the deposit is macroscopically grainy except for occasional large dendrite growths of two main types which develop from the grainy substrate and can attain dimensions of several millimetres: (1) very thin, leaf-shaped dendrites which grow predominantly in a plane, and (2) branching, spike-shaped dendrites whose branches are not confined to a plane.

The leaf dendrites are of particular interest and importance since they invariably occur as parallel growth twins which obey a new law of twinning; these alone will be considered in this paper. We shall give the experimental conditions under which these twinned dendrites appear, describe their growth forms on the basis of x-ray diffraction, optical and electron microscopic observations, show that they have a $[12\bar{3}0]$ twin axis and a (0001) composition plane, discuss the arrangement of atoms in the composition plane, and propose a relation between twinning and the growth of dendrites to macroscopic size.

---

† Communicated by J. W. Mitchell, F.R.S.

‡ Fulbright Fellow, 1958–59. Present address: Cavendish Laboratory, University of Cambridge.

## § 2. Experimental Details

Cadmium, which crystallizes in the hexagonal close-packed structure, is the most convenient element to use in studies of the growth of metal crystals from the vapour. It has a high triple point pressure ($\sim 10^{-1}$ mm), a conveniently low melting point ($\sim 320$ °c), and it does not react with glass.

In the experiments of Price (1959), dendrites, plates, ribbons and whiskers of cadmium were grown in an inert gas on a quartz fibre which could be displaced along the line joining the centres of two plane surfaces of cadmium at different temperatures. The temperature and the cadmium vapour pressure varied linearly between the two plane surfaces. This arrangement was well suited for studying the effect of temperature and supersaturation on the growth form, but it had the disadvantage that only a few crystals at a time could be grown under the same conditions.

Fig. 1

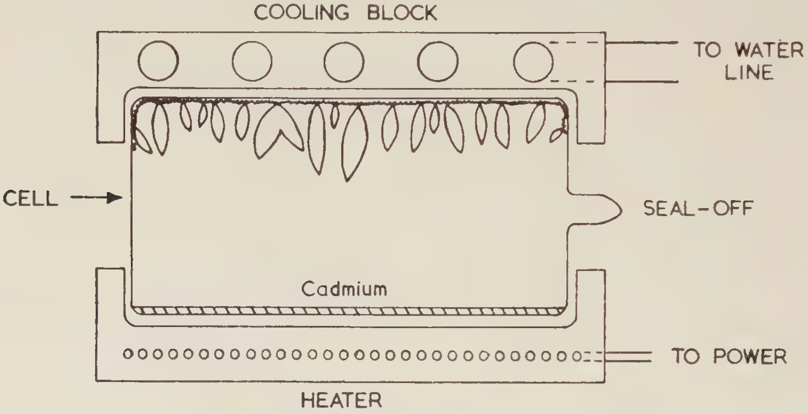

Schematic diagram of growth cell.

In the present arrangement the growth cell, shown schematically in fig. 1, was redesigned with a flat surface on which a large number of dendrites could be grown, all at the same temperature and supersaturation. The construction is extremely simple. Two Pyrex discs were sealed to the ends of a Pyrex cylinder 7 cm in diameter and 3·5 cm in length. The cylinder was joined at its side to a seal-off constriction which led to a high-vacuum system and to a three-stage distillation train containing high-purity cadmium (99·999%)†. After the cell and connecting tubing had been baked out at 500 °c for 24 hours, the cadmium was further purified by successive distillations and finally a small quantity was distilled into the cell and condensed as a layer on the bottom flat surface. Then high-purity nitrogen at a pressure of 600 mm Hg at 20°C was introduced from a Pyrex flask by means of a break-seal arrangement and the cell sealed off.

---

† Kindly supplied by the Imperial Smelting Corporation Limited.

During the growth the bottom of the cell containing the cadmium was maintained at about 320°C by a disc heater while the top surface was kept in contact with a water-cooled copper block. Soon after deposition began the cooled top surface of the cell was dotted with a very high density of nuclei which grew until the surface was completely covered with a macroscopically grainy deposit having a dull, greyish appearance. After a period of several hours leaf-shaped dendrites of visible size could be seen growing down from the grainy surface. Figure 2† shows a representative area of about 6 mm by 6 mm after about 15 hours of growth. New dendrites kept making appearances throughout the period of growth. The rate of lengthening of a given dendrite was roughly constant and of the order of a few microns per minute. Although the thickness of a 'leaf' never exceeded a few microns, its final length seemed to be limited only by the dimensions of the cell. For example, in the cell described above, where source and sink were separated by about 3·5 cm, dendrites began to develop spikes and hexagonal plates at their extremities after attaining a length of about a centimetre, probably because they were growing in a region of lower supersaturation.

## § 3. OBSERVATIONS

After the growth the cell was cut open and the crystals examined with optical and electron microscopes. Figures 3 to 7 and fig. 11 are photomicrographs at various magnifications of typical leaf dendrites which have been removed from the cell and placed flat on a microscope slide. The photographs at 1000 × were taken through a cover slip with oil between specimen and slip and between slip and a 100 × oil immersion objective.

Figures 9 and 10 are transmission electron micrographs at 4000 × and 1500 × of a carbon replica of a dendrite. After evaporation of the carbon, the film and dendrite were floated onto water and the cadmium dissolved by adding a very dilute solution of nitric acid.

### 3.1. *Classification of Dendites*

On the basis of a detailed examination of several dozen leaf crystals, it appears that there are only two types, which differ slightly in appearance. Type I (fig. 3) has a very pronounced ribbed structure, with well-developed stalk, primary and secondary branches and the beginning of tertiary branches. Often crystals of this type, in the advanced stages of growth, will develop hexagonal columns which grow perpendicularly from the main stalk. These columns provide sites from which spike dendrites, misoriented hexagonal plates, and new leaf dendrites can grow. The crystal shown in fig. 3 has developed a spike dendrite, a leaf and many hexagonal columns along its stalk, while its branches have started to develop a few hexagonal columns and a leaf. These all show up dark in the photomicrograph since the incident light is not being reflected normally from them.

---

† Figures 2 to 12 and 15 are shown as plates.

Type II, an example of which is shown in fig. 4, grows in a 'roof tile' formation consisting of layers of hexagonal plates which extend laterally. Eventually this type of dendrite may develop a branched appearance also, as illustrated in fig. 4. Figure 5 shows a portion of a 'roof tile' dendrite at 250 × . One can see that some of the 'tiles' on the same level have completely grown together, while many have almost grown together, leaving tiny spaces at the junction which eventually fill in. Figure 6 shows two such 'tiles' at 1000 × .

### 3.2. *The Direction of Growth and Branching*

For Type I dendrites the angles between stalk and primary branches and between primary and secondary branches are accurately 60°, as measured on a revolving microscope stage. Type II dendrites also branch at 60° to the dendrite axis. In none of the many dendrites examined, however, do the growth steps make a simple angle (0°, 30°. 60°, or 90°) with the stalk and the branches. In fig. 11, for example, which shows growth steps along the stalk of a Type I dendrite at 250 × , the long sides of the steps all lie along an azimuth in the basal plane about 11° clockwise from the stalk or dendrite axis. The edges of the steps on the primary and secondary branches of this crystal are also 'rotated' clock-wise by the same angle, suggesting immediately that the dendrite stalk and branches are not in low-index crystallographic directions. Close examination of the surfaces of many dendrites of both types shows that about half of them contain growth steps 'rotated' clockwise with respect to the dendrite axes and the other half contain steps 'rotated' counter-clockwise (e.g. fig. 3 is clockwise, fig. 4 is counter-clockwise). In every case the measured angle lies in the range of 10·6° to 11·1°. Since the angle between the $[12\bar{3}0]$ and $[11\bar{2}0]$ directions in the hexagonal system is 10·9°, and since the dendrite is undoubtedly made up of (0001) layers, two alternative orientations are possible:

(1) The dendrite stalk is in a $[12\bar{3}0]$ direction. The primary branches will then be in $[\bar{2}3\bar{1}0]$ and $[31\bar{2}0]$ directions and the steps will lie along the close-packed $\langle 11\bar{2}0\rangle$ directions.

(2) The dendrite stalk and branches grow in $\langle 11\bar{2}0\rangle$ directions. This requires the steps to lie along $\langle 1230\rangle$ directions, which are not close-packed.

In order to decide between these, a G.K.N. Micro Hardness Tester with a 3 g load was used to produce rosette patterns of plastic deformation on the (0001) surface of a dendrite. From observations made during previous deformation experiments with basally oriented cadmium ribbons, it was established that the patterns are traces in the basal plane of thin, lamellar deformation twins which radiate from the indented region along $\langle 11\bar{2}0\rangle$ directions. Since the directions of the deformation twin traces produced on the dendrite were parallel to its growth steps and not to its branches, it was concluded that the first alternative, that the dendrites grow and branch in $\langle 12\bar{3}0\rangle$ directions, was the correct one.

### 3.3. *Evidence for Twinning*

Near the edges of a dendrite, where the secondary and tertiary branches from two adjacent primary branches have not completely grown together, one can often see growth steps and growth layers which appear to have a different orientation from that of the main crystal. In fig. 7 can be seen several sets of 'roof tile' growth layers which would eventually meet one another and fill the gap between them if growth were allowed to continue. Under the edge of each set of 'roof tiles' another tile is protruding which appears to have a basal surface and to be rotated by about 22° with respect to the main crystal. Similar examples can be found in fig. 8 and in fig. 5. Electron microscopic observations showed that 'misoriented' layers protruded from the bottom surface of the crystal at the edges of nearly every set of 'roof tiles'. This is clearly shown in figs. 9 and 10.

In some cases (e.g. fig. 8) the 'misoriented' growth layers occupied a large enough area to deform by micro-indenting. The resulting deformation twin traces were parallel to the edges of the growth steps of these 'misoriented' areas and formed an angle of $\sim 22°$ with twin traces in the main part of the crystal caused by micro-indenting.

It was then decided to examine and photograph both of the flat sides of a dendrite. Figures 11 (*a*) and (*b*) are photomicrographs at 100× of the same regions of the 'front' and 'back' sides of a Type I dendrite. Figure 11 (*b*) has been reversed in printing so that the two surfaces appear as they would if viewed from the same side of the dendrite. The growth steps on the two faces are very clearly rotated by 10·9° in *opposite* directions about the stalk and branches, so that the angle between the two sets of steps is 21·8°. Furthermore, the details of growth on the two faces show a marked resemblance to each other.

These observations suggest that a leaf dendrite is composed of two flat crystals in contact on their basal planes but rotated by 21·8° about a common *c*-axis. Thus each crystal has a common $[12\bar{3}0]$ axis but is made up of $\langle 11\bar{2}0\rangle$ steps which are tilted in opposite directions from the axis.

This was verified by x-ray diffraction. Figure 12 is a Laue back-reflection pattern from a Type I dendrite which was mounted with its stalk vertical and its flat faces perpendicular to the beam. It is evident from the photograph that there are two sets of basal reflections of about equal intensity. When the spots are plotted on a stereographic projection, the angle between corresponding $\langle 1120\rangle$ directions turns out to be about 22°, in agreement with the optical measurements.

One set of spots may be brought into coincidence with the other by a 21·8° rotation about the common *c*-axis (or by a 38·2° rotation in the opposite direction), by a 180° rotation about the dendrite axis or any of the branch axes, or by reflection in a plane perpendicular to any of these axes. By choosing the operation of rotation through 180° about the

$[12\bar{3}0]$ axis, we are able to define the cadmium leaf dendrite as a parallel growth twin with a (0001) composition plane and a $[12\bar{3}0]$ twin axis. So far as we are aware, the cadmium dendrite grown from the vapour is the only known example of this new twinning law.

## § 4. METASTABLE INTERCRYSTALLINE BOUNDARIES

Although the two components of the $[12\bar{3}0]$ growth twin may be brought into coincidence by any one of several rotation operations, the arrangement of atoms near the composition plane can be most easily understood in terms of a rotation about the $c$-axis which is common to both components. We consider first the more general case of a rotational intercrystalline boundary, with an arbitrary angle of rotation. In § 4·2 we shall see that the angle 21·8° is a special case in which the boundary, which is the composition plane of the $[12\bar{3}0]$ twin, is metastable. Certain other angles of rotation also result in metastable boundaries. In § 4.3 it is shown that some of these boundaries can develop under certain conditions during the growth of cadmium crystals from the vapour.

### 4.1. *Coincidence Nets*

Let us start with a single crystal of the hexagonal close-packed structure with its $c$-axis vertical and divide the crystal into two halves by an imaginary horizontal plane. If we rotate the top half (component I) through an angle $\theta$ about the $c$-axis with respect to the bottom half (component II), we have two crystals whose basal planes are still parallel to the plane of the boundary. As Wilman (1951) has pointed out, a certain proportion of the atoms in the lowest basal plane of I lie in potential wells similar to those they would occupy if I and II were superposed without a rotation, but most of the atoms are raised partly out of the potential depressions.

This is illustrated in fig. 13, which shows the positions of the atoms in a basal plane of I before (filled circles) and after (open circles) a 21·8° rotation. It is seen that one out of every seven atom sites in the rotated basal plane coincides with an atom site in the unrotated plane. The positions of these coincidence atoms define a unique 'coincidence net' (indicated in fig. 13 by dotted lines) which is a multiple of the primitive net formed by the atoms in a basal plane.

It is obvious from the periodicity of the atomic arrangement that an infinite number of coincidence nets may be produced by varying the angle of rotation between two primitive nets. These coincidence nets are, in fact, rotational moiré patterns. We now investigate the relation between the angle of rotation and the size of the coincidence net.

Because of the six-fold symmetry of the primitive hexagonal net, all possible coincidence nets can be obtained by varying the angle of rotation from 0 to 30°. If the positions of atoms in the neighbouring layers are examined, however, it is seen that a rotation through $\theta$ does not produce exactly the same effect as a rotation through $60°-\theta$, so that we shall consider the range of rotations $0 \leqslant \theta \leqslant 60°$. Figure 14 is a 60° sector of a primitive net with the origin and axis of rotation at O and with the positions of atoms referred to orthohexagonal axes $\mathbf{a}$ and $\mathbf{b}$, where $|\mathbf{a}|=\sqrt{3}/2$, $|\mathbf{b}|=\frac{1}{2}$, and the interatomic distance is unity. Although $\mathbf{a}$ and $\mathbf{b}$ are not lattice vectors, the position of any atom in the net can be specified by the lattice vector $\mathbf{r}=m\mathbf{a}+n\mathbf{b}$ with the stipulation that $m$ and $n$ are both either odd or even integers. For example, a primitive lattice vector is $r=a+b$, where $m=n=1$.

Fig. 13

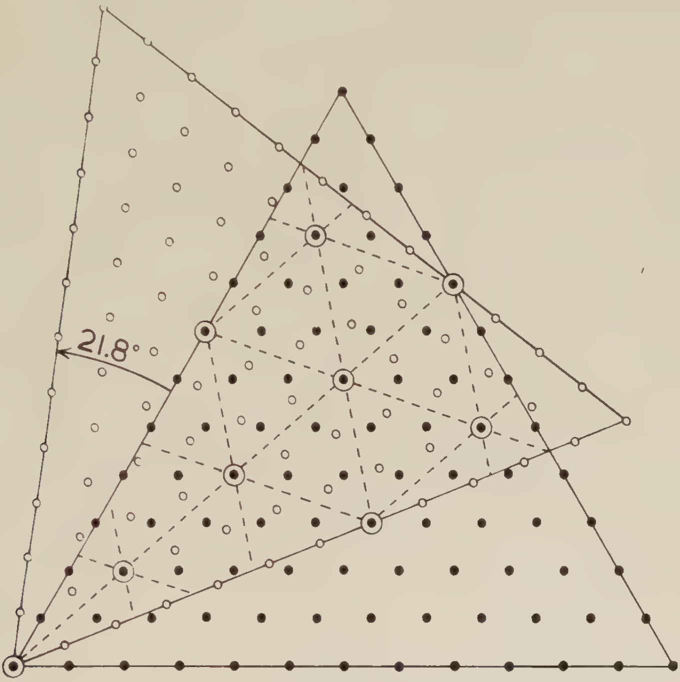

Coincidence net for a 21·8° rotation, showing the positions of atoms in a basal plane before and after rotation.

The distance from O to $[m, n]$ is given by $|\mathbf{r}|=m^2a^2+n^2b^2=\frac{1}{2}\sqrt{(3m^2+n^2)}$. From this and fig. 14 we see that for every lattice point $[m, n]$ in the upper half of the sector (defined by $0 \leqslant n \leqslant m$) there exists another lattice point $[m, -n]$ in the lower half of the sector at the same distance from O. The point $[m, -n]$ may be brought into coincidence with $[m, n]$ by rotating the primitive net through an angle $\theta$ given by

$$\tan\frac{\theta}{2}=\frac{nb}{ma}=\frac{1}{\sqrt{3}}\frac{n}{m}.$$

(For the case shown in the figure, $\theta=32{\cdot}2°$.) The same thing happens in the other five sectors of the primitive net, so that the result is a hexagonal coincidence net with a primitive lattice vector $\mathbf{r}=ma+nb$. (If $\mathbf{r}$ also happens to pass through a lattice point closer to O than $[m, n]$, then this point determines the primitive lattice vector of the coincidence net.) The ratio of the area of a unit cell in the coincidence net to the area of a unit cell in the primitive net, called the specific area, is given by $r^2 = \frac{1}{4}(3m^2 + n^2)$. The reciprocal of this, $1/r^2$, is equal to the relative density of atoms in the coincidence net.

Fig. 14

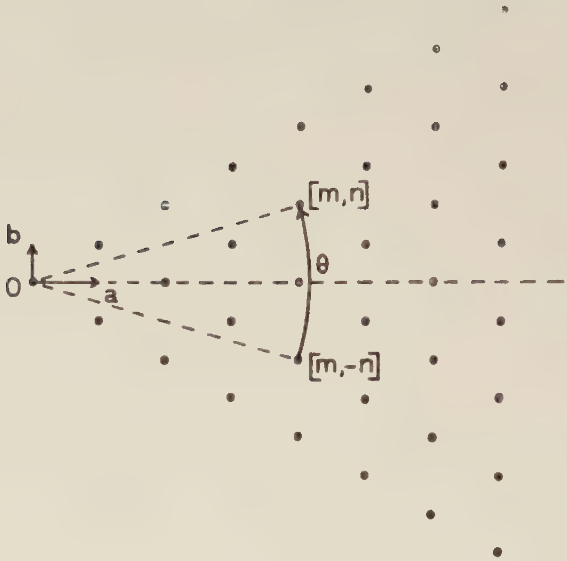

A 60° sector of a primitive net, showing a rotation which will produce a coincidence net. For the case illustrated $\theta = 32{\cdot}2°$.

Table 1. Specific Areas and Angles of Rotation for a Few Coincidence Nets

| $m$ | $n$ | $r^2$ | $\theta$ | $60° - \theta$ |
|---|---|---|---|---|
| 1 | 1 | 1 | 60° | 0 |
| 3 | 1 | 7 | 21·8° | 38·2° |
| 4 | 2 | 13 | 32·2° | 27·8° |
| 5 | 1 | 19 | 13·2° | 46·8° |
| 6 | 4 | 31 | 42·1° | 17·9° |
| 7 | 1 | 37 | 9·4° | 50·6° |
| 7 | 5 | 43 | 44·8° | 15·2° |
| 8 | 2 | 49 | 16·4° | 43·6° |
| 9 | 1 | 61 | 7·3° | 52·7° |

Values of $m$, $n$, $r^2$, $\theta$ and $60° - \theta$ for the first nine distinct coincidence nets are listed in table 1 in order of increasing $r^2$. Since the relative density of atoms in the coincidence net is a measure of the energy of the intercrystalline boundary, it may be concluded that two crystals, I and II, rotationally displaced by an angle $\theta$, can exist in metastable equilibrium only if $r^2$ is small. This may not be a sufficient condition for metastable equilibrium, however, since the energy of the boundary also depends upon the positions of atoms other than those which form the coincidence net.

### 4.2. *The Composition Plane of the* [12$\bar{3}$0] *Twin*

The first angle of rotation in table 1 simply reproduces the primitive net. If the positions of atoms in the neighbouring close-packed layers are considered, however, it is seen that the 60° rotation creates a stacking fault, which may be represented in the usual notation by the sequence . . . ABABCBCB . . . .

The next angle of rotation in the table is 21·8°, which produces the [1230] growth twin. Since these twins occur so often during growth at high supersaturation, it is reasonable to assume that the twin boundary or composition plane has a relatively low energy. This is in agreement with the fact that the coincidence net with the highest density of atoms (other than the primitive net) is the one corresponding to the 21·8° rotation.

It was pointed out in §4.1 that, when the angle of rotation is 21·8° (fig. 13), one out of seven atom sites in the bottom basal plane of I is in a coincidence position. Similarly, one-seventh of the atom sites in the top basal plane of II are unaffected by the rotation. The other atom sites in these two layers are out of their normal positions by about one-third of an interatomic distance. If the position of atoms in the neighbouring layers are also considered, it is seen that a 21·8° rotation produces a single layer stacking fault, just as in the case of a 60° rotation, so that only one out of fourteen atoms in component I occupies a coincidence position. If I is turned through $60° - \theta$ or 38·2°, however, no stacking fault is produced, and one out of seven atoms in I occupies a coincidence position. Thus for the same size coincidence net two distinct twins are obtained ($\theta = 21{\cdot}8°$, $\theta = 38{\cdot}2°$), which may differ in the energy of the twin boundary, but which are indistinguishable by goniometric measurements.

We have seen that the composition plane of the [12$\bar{3}$0] growth twin contains a larger proportion of atoms in their proper positions than any other intercrystalline boundary on the basal plane. It is concluded, therefore, that these coincidence atoms stabilize the twin orientation in spite of the fact that six out of seven atoms are displaced from their normal positions.

### 4.3. *Other Rotational Boundaries in Cadmium Crystals*

Intercrystalline boundaries corresponding to some of the other angles of rotation listed in table 1 have also been observed in cadmium crystals grown from the vapour. During an earlier investigation thin, basally oriented ribbons and platelets of cadmium were grown at low supersaturation ($p/p_{\mathrm{eq}} < 2$) on the bottom of a cylindrical cell 9 cm long and 7 cm in diameter. Several sets of ribbons were grown under different conditions, and during these experiments ribbons also grew on the sides of the cell, where the temperature and supersaturation were not known. Later, when the cell was cut open for examination of the last set of crystals which were grown on the bottom, some of the ribbons on the sides of the cell were also examined. The only observable difference between these ribbons and the ones grown on the bottom was that occasionally little 'islands' of basally oriented cadmium, up to 10 $\mu$ in height and $\sim 50\,\mu$ across and rotationally misoriented by various angles $\theta$, could be found on the former. The shapes of the 'islands' were usually parallelograms, triangles, or hexagons with angles of 60° and 120° between the edges. Values of $\theta$ for several rotational boundaries were determined by measuring the angles between the edges of those misoriented growth layers and $\langle 11\bar{2}0\rangle$ growth steps on the ribbon on which they grew. For example, fig. 15 shows a triangular island for which $\theta \simeq 7{\cdot}0°$. The results are listed in the first column of table 2 under the heading $\theta_{\text{exp}}$. The second column, $\theta_{\text{theor}}$, lists the theoretical metastable boundary from table 1 which is in closest agreement with $\theta_{\text{exp}}$. The third column gives the corresponding value of $r^2$, also taken from table 1.

Table 2. Rotationally Displaced Growth Layers on Cadmium Ribbons

| $\theta_{\text{exp}}$ | $\theta_{\text{theor}}$ | $r^2$ |
|---|---|---|
| 27·9 ± 0·3° | 27·8° | 13 |
| 13·1 ± 0·3° | 13·2° | 19 |
| 13·8 ± 0·3° | 13·2° | 19 |
| 14·0 ± 0·3° | 13·2° | 19 |
| 17·7 ± 0·3° | 17·9° | 31 |
| 18·2 ± 0·3° | 17·9° | 31 |
| 9·0 ± 0·3° | 9·4° | 37 |
| 16·5 ± 0·3° | 16·4° | 49 |
| 7·0 ± 0·3° | 7·3° | 61 |

The agreement between the measured and the calculated angles is surprisingly good. Not knowing the conditions under which these ribbons grew, it is difficult to see how the misoriented layers originated, and it is particularly surprising that some of the boundaries corresponding to large values of $r^2$ occurred, since a very low density of atoms on the rotational boundary would be in their proper positions. These are the only intercrystalline boundaries which have been observed and measured in cadmium crystals grown from the vapour. Attempts to produce boundaries under known conditions have, except in the case of leaf dendrites, been unsuccessful.

### 4.4. *Related Observations on Copper*

A few years ago Kronberg and Wilson (1949) studied the orientations of the large grains that are produced during the secondary recrystallization of twin-bearing cubically aligned copper. Their observations indicated that the large grains were formed by a process of nucleation and development of new orientations, with nucleation apparently occurring at twin boundaries. Two types of orientation were found, which were related to the ideal cubic orientation by rotations of 21·8° about [111] poles and of ~19° about [100] poles. It is interesting that the coincidence net in the (111) plane formed by a 21·8° rotation about a [111] axis is identical to the net in fig. 13. This is a result of the fact that the face-centred cubic (111) plane has the same structure as the hexagonal close-packed (0001) plane.

## § 5. Relation between Twinning and Dendritic Growth

A detailed examination at high magnification of the sandlike layer of tiny cadmium crystals on the top surface of the cell showed no evidence of growth layers rotated by 21·8° on basal surfaces. On the other hand, there were many examples of crystals which had grown into each other and formed twisted boundaries. Because of the high density of growing crystals with random orientations, it seems likely that some adjacent crystals will have nearly the proper orientations to form 21·8° rotational boundaries when they grow together. With some amount of distortion they could then continue to grow as $[12\bar{3}0]$ twins.

Fig. 16

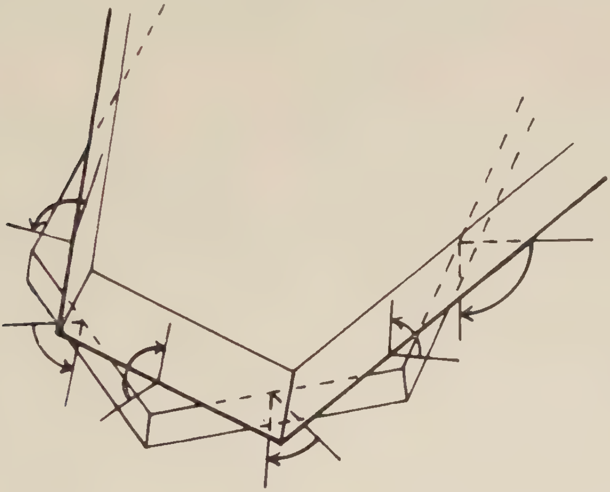

Re-entrant angles at a $[12\bar{3}0]$ twin boundary.

Regardless of how the twin originates, once it is formed there will be a re-entrant angle at the boundary between the two components. This is shown schematically in fig. 16. Nucleation will be easier and growth will occur more rapidly at the twin boundary than at the edges of other crystals.

This gives the twin a chance to extend itself rapidly in lateral directions, and unless the common *c*-axis is nearly normal to the surface of the cell it can grow down and out of the region of tiny, randomly oriented crystals, where growth is occurring only slowly.

This gives a qualitative picture of why only twinned crystals can reach macroscopic size. If the supersaturation were low, the rapid lateral growth would probably result in a thin, tabular twin with rather flat basal surfaces. The 'roof tile' appearance of the leaf dendrite is probably due to the high supersaturation, which favours nucleation of new layers on both sets of basal surfaces. These layers then spread toward the edges of the dendrite as growth proceeds.

Because of the rotational nature of the [1230] twin, the side faces of the two components are not parallel to each other, so that the re-entrant angle persists throughout the growth of the dendrite. A consequence of this is that the stalk and branches grow in [1230] compromise directions, halfway between the $\langle 10\bar{1}0\rangle$ directions which the two components would take if they were single crystal dendrites.

Since growth has to occur predominantly in a downward direction if the dendrite is to reach a macroscopic size, usually only one, two or at most three main dendrite arms at 60° to one another develop. If the substrate were a point or line source then the dendrite might be able to extend six arms symmetrically into a cadmium 'snowflake'. In fact, several dendrites which were grown on a quartz fibre have developed stalks in all six directions, although not symmetrically because of the presence of the fibre.

## § 6. SUMMARY

Cadmium which is deposited from the vapour at high supersaturation ($p/p_{\mathrm{eq}} \gtrsim 10^2$) in an atmosphere of an inert gas usually takes the form of microscopic crystals with random orientations. Occasionally an unusual parallel growth twin is formed, which rapidly grows into a leaf dendrite several mm in lateral dimensions and only a few microns in thickness. The plane of the dendrite is the (0001) composition plane of the twin, and the dendrite stalk is the $[12\bar{3}0]$ twin axis. The primary and secondary branches also grow along $\langle 12\bar{3}0\rangle$ directions making 60° angles with the stalk.

The arrangement of atoms in the composition plane of the twin may be visualized by rotating one two-dimensional net through an angle of 21·8° with respect to another. This produces a rotational moiré pattern with hexagonal symmetry and with the smallest mesh size which is possible other than the identity pattern. One out of every seven atom sites on either side of the composition plane is unchanged by the rotation. Although there is evidence of rotational boundaries in cadmium crystals corresponding to other moiré patterns with larger mesh sizes, only the twinned dendrites can be grown under reproducible conditions.

One component of the $[12\bar{3}0]$ twin may be brought into coincidence with the other by a 180° rotation about the twin axis or by a 21·8° rotation about the common *c* axis. Growth steps on opposite sides of the dendrite are rotated by 21·8° angles to each other, and the branches and stalk grow in compromise directions, halfway between the $\langle 10\bar{1}0 \rangle$ directions which the two components would take if they were separate single crystal dendrites.

The re-entrant angles at the edges of a dendrite provide a site for easy nucleation and thus increase the rates of growth in lateral directions, allowing the twinned crystal to reach macroscopic size.

## ACKNOWLEDGMENTS

It is a pleasure to acknowledge the valuable discussions which were held with Dr. J. W. Mitchell and Professor F. C. Frank during the course of the work. The growth cells were constructed by J. H. Burrow, whose help is gratefully acknowledged. The photomicrographs were taken with equipment purchased with the assistance of a grant from the Department of Scientific and Industrial Research. This work was carried out during the tenure of a Fulbright grant by the U.S. Government and is a continuation of research begun at the University of Virginia with Professor N. Cabrera.

## REFERENCES

KRONBERG, M. L., and WILSON, F. H., 1949, *J. Metals, N.Y.*, **1,** 501.
OLIVER, D. S., 1952, *Research, Lond.*, **5,** 45.
PRICE, P. B., 1959 (to be published).
WEINBERG, F., and CHALMERS, B., 1952, *Canad. J. Phys.*, **30,** 488.
WILMAN, H., 1951, *Proc. phys. Soc. Lond.* A., **64,** 329.
WRANGLEN, G., 1955, *Trans. roy. Inst. Tech.* (Stockholm), No. 94.

# Accurate Determination of the Lattice Parameters of Beryllium†

By D. R. SCHWARZENBERGER
Tube Investments Research Laboratories, Hinxton Hall, Cambridge

[Received July 10, 1959]

## ABSTRACT

The lattice parameters of a single crystal of beryllium have been determined from observations on a divergent-beam transmission x-ray photograph of the crystal. Diffraction in the crystal leads to a pattern of deficiency lines on a photographic plate, the geometry of which is determined by the lattice parameters of the crystal, and the wavelength of the radiation, but is independent of the exact experimental arrangement. The values obtained are

$$a=2\cdot2866\pm0\cdot0006\ \text{Å},\quad c=3\cdot5833\pm0\cdot0009\ \text{Å},\quad c/a=1\cdot5671.$$

## § 1. INTRODUCTION

THE lattice parameters of a single crystal with simple symmetry may in suitable cases be determined accurately from observations on divergent x-ray beam photographs of the crystal. If a highly divergent x-ray beam is transmitted through a crystal, diffraction leads to a characteristic pattern of deficiency lines on a photographic plate placed in the path of the beam. The lattice parameters are then determined from observations on accidental coincidences in the intersections of these lines, particular to the wavelength of the characteristic radiation used or, in favourable circumstances, from measurements on inexact but near coincidences. This method was first considered by Kossell (1936), and is discussed by James (1954). A full account of the application of the method to the determination of the C–C distance in diamond has been given by Lonsdale (1947) and to Cunico alloy phases by Geisler *et al.* (1948). In the present investigation the method has been used to determine $a$ and $c$ in a single crystal of the metal beryllium.

It is an advantage, particularly with beryllium, to be able to determine the lattice parameters accurately for a single crystal so that deformation of the lattice and introduction of impurity are completely avoided in the specimen preparation.

## § 2. FORMATION OF THE DIVERGENT-BEAM PATTERN

### 2.1. *Experimental Procedure*

The specimen was a single crystal of beryllium, about 99·6% Be, approximately $1\times0\cdot5\times0\cdot5\ \text{cm}^3$, the residue from a distillation experiment, supplied by A.W.R.E., Aldermaston. The x-ray source, about 1 $\mu$ in diameter, was provided by an x-ray projection microscope of the Cosslett–Nixon design (1952), using a copper target with an accelerating voltage of 25 kv. The specimen was placed as near to the target as possible, about 0·1 cm for the near face, and the plate was placed 4 cm from the target. The exposure time was 15 sec with an Ilford Special Lantern Contrasty emulsion.

---

† Communicated by Dr. J. W. Menter.

Photographs of good contrast of the deficiency lines were obtained with this specimen, and no attempt was made to improve the contrast by variation of the specimen thickness.

### 2.2. *Beryllium Pattern*

In the typical photograph shown in fig. 1 (Pl. 151) $(10\bar{1}0)$ was normal to the photographic plate, and a range of just over 60° of the [001] zone was recorded approximately along the length of the plate. Two types of contrast are seen. The dark conics are the deficiency lines, with fine structure due to the CuK$\alpha_1$ and $\alpha_2$ characteristic lines, about 0·02 cm apart on the print. The strongest lines also have associated faint K$\beta$ lines about 0·5 cm away. Some lines are also split further, or become wavy from substructure in the crystal. All observations were made in regions of the photograph free from such sub-structure. Superimposed is a shadow micro-radiograph of the crystal, showing impurity particles and absorption contrast from the shape of the specimen.

From the known approximate values of the lattice parameters, $a$ and $c$, a stereographic projection of the expected pattern of conics for CuK$\alpha$ radiation was drawn. Comparison of the photograph with the expected pattern gave the orientation of the crystal, and allowed the deficiency lines to be indexed.

## § 3. INTERSECTIONS OF DEFICIENCY LINES

On such a photograph, intersections of three or more curves at a single point may occur. These may be independent of the wavelength, $\lambda$, and depend only on the geometry of the lattice, e.g. $20\bar{2}0$, $1\bar{1}02$ and $2\bar{1}\bar{1}2$ for beryllium. (An $hkl$ conic is formed by reflection at $(hkl)$ planes.) Some such coincidences, however, depend on the ratio of $\lambda$ to the lattice parameters. The radius of a deficiency circle is $\cos^{-1}(\lambda/2d)$, so that as $\lambda$ decreases, the circles expand, and the positions of the intersections vary. If at a particular wavelength, two or more intersections happen to coincide, then geometrical requirements give a relation between $\lambda$ and the lattice parameters. For a cubic crystal, one such relation is sufficient to determine $a$ in terms of the known wavelength. For a hexagonal crystal, both $a$ and $c$ are required, so two multiple intersections which are exact for the same wavelength must be considered. The powers of $a$ and $c$ involved must also be such that either parameter may be eliminated, to obtain an expression for the other in terms of $\lambda$.

For beryllium, two such multiple intersections accidental to the wavelength, which appear to be exact, are:

A. $01\bar{1}2$, $01\bar{1}\bar{2}$, $10\bar{1}2$, $10\bar{1}\bar{2}$ circles for CuK$\alpha_2$;

B. $20\bar{2}0$, $20\bar{2}\bar{1}$, $02\bar{2}1$, $02\bar{2}\bar{2}$ circles for CuK$\alpha_2$.

Figure 2 shows indexed tracings of an enlarged print of these intersections.

Calculations on these coincidences gave the value of $a/\lambda = 1{\cdot}480625$.

Then taking the wavelength of CuK$\alpha_2$ radiation to be 1·54433 Å,

$$a = 2{\cdot}2866\ \text{Å}, \quad c = 3{\cdot}5833\ \text{Å}, \quad c/a = 1{\cdot}5671.$$

Fig. 2

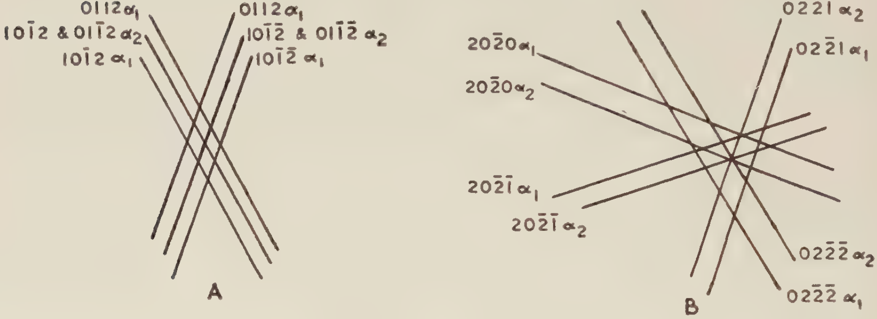
$01\bar{1}2\alpha_1$
$10\bar{1}2$ & $01\bar{1}2\alpha_2$
$10\bar{1}2\ \alpha_1$
$01\bar{1}\bar{2}\alpha_1$
$10\bar{1}\bar{2}$ & $01\bar{1}\bar{2}\ \alpha_2$
$10\bar{1}\bar{2}\ \alpha_1$
A
$20\bar{2}0\alpha_1$
$20\bar{2}0\alpha_2$
$20\bar{2}\bar{1}\ \alpha_1$
$20\bar{2}\bar{1}\ \alpha_2$
$02\bar{2}1\ \alpha_2$
$02\bar{2}1\ \alpha_1$
$02\bar{2}\bar{2}\ \alpha_2$
$02\bar{2}\bar{2}\ \alpha_1$
B

Indexed tracings of an enlarged print of intersections A and B.

## § 4. SOURCES OF ERROR

(i) The wavelength of CuK$\alpha$ is known accurately to 0·001% in kX units. The conversion factor to Å units is correct to 0·003% (1 Å = 1·00202 kX) so the wavelength in Å units is accurate to 0·004% or 1 unit in the 4th decimal place in $a$ or $c$.

(ii) The temperature was not recorded, but can be taken to be within a few degrees of room temperature (22°C). From the results of Gordon (1949) or of Owen and Richards (1936) on the variation of lattice parameter with temperature, a change of about 10°C near room temperature gives a change of about 0·01% in $a$ or $c$. Thus if the temperature was in fact out by as much as 5°C either way, the value of $a$ or $c$ would not change by more than 0·005%.

(iii) No correction was made for the refractive index of X-rays in beryllium, as this only affects the 5th decimal place in $a$ or $c$, introducing an error of about 0·001%.

(iv) The impurity content of the beryllium was about 0·4%.

(v) The main source of error is introduced in the width of the lines, in measuring the distance between lines, or, as here, deciding whether the intersections are exactly coincident.

The possible error at the A intersection was estimated from cathetometer measurements, on the enlarged print, of the width and separation of the CuK$\alpha_1$ and $\alpha_2$ lines. This showed that the separation of the two $\alpha_2$ circles which appeared just to touch, $10\bar{1}2$ and $01\bar{1}2$, or $01\bar{1}2$ and $10\bar{1}2$, could not be greater than $0{\cdot}1\,\delta$, where $\delta$ is the $\alpha_1$–$\alpha_2$ separation, without being detected. Thus the possible error in the radius of one of these circles is $0{\cdot}05\,\delta$. The radius of one of these circles equals

$$\cos^{-1}\frac{\lambda}{2d}=\cos^{-1}\lambda\left(\frac{1}{c^2}+\frac{1}{a^2}\right)^{1/2}.$$

The percentage change in $\lambda/2d$ as $\lambda$ changes from CuK$\alpha_1$ to $\alpha_2=\pm 0{\cdot}25\%$. This gives the possible error in $\lambda/2d$ from misjudging the coincidence of the $\alpha_2$ lines as $\pm 0{\cdot}013\%$.

Similar measurements and calculations for the B intersection also give an error in $\lambda/2d$ of $\pm 0{\cdot}013\%$.

Thus the error in a single determination of the lattice parameters is less than $\pm 0{\cdot}03\%$.

This gives, for the present result on a single crystal of beryllium,

$$a=2{\cdot}2866\pm 0{\cdot}0006\,\text{Å}.$$

## § 5. DISCUSSION

The present determination gave

$$a=2{\cdot}2866\pm 0{\cdot}0006\,\text{Å},\quad c=3{\cdot}5833\pm 0{\cdot}0009\,\text{Å},\quad c/a=1{\cdot}5671.$$

Previous determinations, summarized by Owen (1952) appear to have all been made on powder or fine-grained specimens. Among these, the back reflection focusing method used by Gordon (1949) appears to have the highest potential accuracy (0·005%). The present entirely different method gives a result agreeing with this to better than 0·04%, i.e. effectively within the limits of the experimental error of the present determination. The present method of determining lattice parameters depends on the existence of accidental relationships between deficiency lines. If a more perfect single crystal of beryllium was used, a photograph with sharper lines and no splitting due to substructure would be obtained. Then more useful accidental relationships, exact or near, between deficiency lines might be found, giving further estimates of $a$ and $c$ values, enabling the error to be reduced. In addition, other wavelengths might be used to photograph the specimen. In these circumstances it might then be possible to approach the accuracy of ±0·002% obtained by Lonsdale (1947) for the lattice constant of diamond.

It is clear however that even with a reasonably good single crystal of beryllium, the divergent x-ray beam technique provides a simple method of determining the lattice parameters, and yields a result of considerable accuracy without the necessity for refined experimental conditions.

## ACKNOWLEDGMENTS

I wish to thank Dr. J. W. Menter and Dr. J. Sawkill for helpful discussions. This work is published by permission of the Chairman of Tube Investments Ltd.

## REFERENCES

COSSLETT, V. E., and NIXON, W. C., 1952, *Proc. roy. Soc.* B, **140,** 422.
GEISLER, A. H., HILL, J. K., and NEWKIRK, J. B., 1948, *J. appl. Phys.*, **19,** 1041.
GORDON, P., 1949, *J. appl. Phys.*, **20,** 908.
JAMES, R. W., 1954, *The Optical Principles of the Diffraction of X-rays* (G. Bell & Sons).
KOSSEL, W., 1936, *Ann. Phys., Lpz.*, **26,** 533.
LONSDALE, K., 1947, *Phil. Trans. roy. Soc.*, **240,** 219.
OWEN, E. A., 1952, *Proc. phys. Soc. Lond.* A, **65,** 294.
OWEN, E. A., and RICHARDS, T. I., 1936, *Phil. Mag.*, **22,** 304.

# The Solar Diurnal Variation of the Intensity of the Nucleonic Component of the Cosmic Radiation†

By P. L. Marsden and Qamrun Nessa Begum
Physics Department, University of Leeds

[Received August 11, 1959]

## Abstract

The diurnal variation of the intensity of the nucleonic component of the cosmic radiation detected at this laboratory through the period 1954–58 has been analysed. The results, together with previously reported neutron data, show that the direction of the anisotropy causing the diurnal variation has remained substantially constant at 60–70° east of the line joining the earth to the sun except during 1954 when the direction changed abruptly to become west of the earth–sun line. The amplitude of the diurnal wave shows considerable variation, closer in correlation with the planetary amplitude of magnetic activity $A_p$, than with relative sunspot numbers.

## § 1. Introduction

A neutron monitor has been in continuous operation in these laboratories from September 1954 to the present time; from the data so recorded we have determined the solar diurnal variation of the intensity of the nucleonic component at monthly and yearly intervals from September 1954 to December 1958. During this period the solar activity has changed appreciably, varying from minimum in 1954 to the very active maximum in late 1957. In view of this and because the diurnal maximum of the intensity of the hard component probably follows a 22-year cycle related to solar activity (Thambyahpillae and Elliot 1953), it is of particular interest to study the change of phase of the diurnal maximum of the intensity of the nucleonic component. In addition we have made use of earlier data, for 1951–52 given by Firor *et al.* (1954), for 1953–55 given by Conforto and Simpson (1957) to extend the period through which we can follow the phase of the maximum. Current theories of the diurnal variation are based on models in which corpuscular streams issuing from the sun carry ordered magnetic fields. Cosmic ray particles passing through the streams are accelerated or decelerated, causing a small increase or decrease in the intensity of the radiation in a given direction in space, which as the earth rotates is recorded as a daily variation (Alfvén 1949, Dorman 1957). The results presented here are discussed in terms of these ideas.

---

† Communicated by Professor J. G. Wilson.

## § 2. APPARATUS

From January 1955 to April–June 1957 the results reported here were obtained using two cubical neutron monitors (Marsden and Doran 1956), with separate electronic circuits for each monitor. For the International Geophysical Year the arrangement was changed to conform to the internationally accepted type of monitor (Simpson 1957). The change was made in two stages so that the counting rate of the earlier monitors could be normalized to the increased counting rate of the IGY type monitor. During the change over period (~three months) the variations of response of the two types of monitor were compared and found to be indistinguishable. Throughout the whole time covered in this paper a daily comparison of the counting rates from each half of the monitor was made and also at frequent intervals standardizing checks were made with a neutron source.

## § 3. RESULTS

The bi-hourly counting rates from each part of the monitor have been combined and corrected for barometric pressure variations using an exponential correction. Days on which there were Forbush decreases have been rejected from the diurnal analysis but days following the decreases have been included after making an allowance for the recovery of the intensity. The data have been grouped together to give average monthly and yearly bi-hourly counting rates and curves of period one day which give the best fit with the experimental observations have been calculated. The method of computation and calculation of the uncertainty is that given by Whitaker and Robinson (1946). In some trial periods attempts to fit the data more closely by including higher harmonics have been made but in general the second harmonic is not significant and only results for the first harmonic are reported here.

The data are conveniently summarized by means of a summation dial, shown in fig. 1, in which the monthly vectors representing the amplitude and phase of the diurnal variation are joined successively. Certain features of the changes in the diurnal variation which we discuss in more detail below are immediately obvious from this figure; thus it is clear that there have been considerable changes in the amplitude and that apart from the early section of the record, i.e. from the end of 1955, the time of the maximum has remained fairly constant. This latter fact is more striking when it is recalled that from January 1955 to the end of 1958 the intensity of the nucleonic component, as recorded for example at Leeds, has decreased some 20% and from late 1956 onwards has been extremely disturbed.

## § 4. DISCUSSION

In fig. 2 the variation of the amplitude of the first harmonic through the period under consideration is shown. The solid curve corresponds to the individual monthly mean amplitudes, the dashed curve is for the data grouped into three monthly running means. The same grouping of data is followed in the second set of curves of fig. 2 showing the equivalent planetary amplitude of the intensity of geomagnetic activity, $A_p$. Also shown are the relative sunspot numbers.

Fig. 1

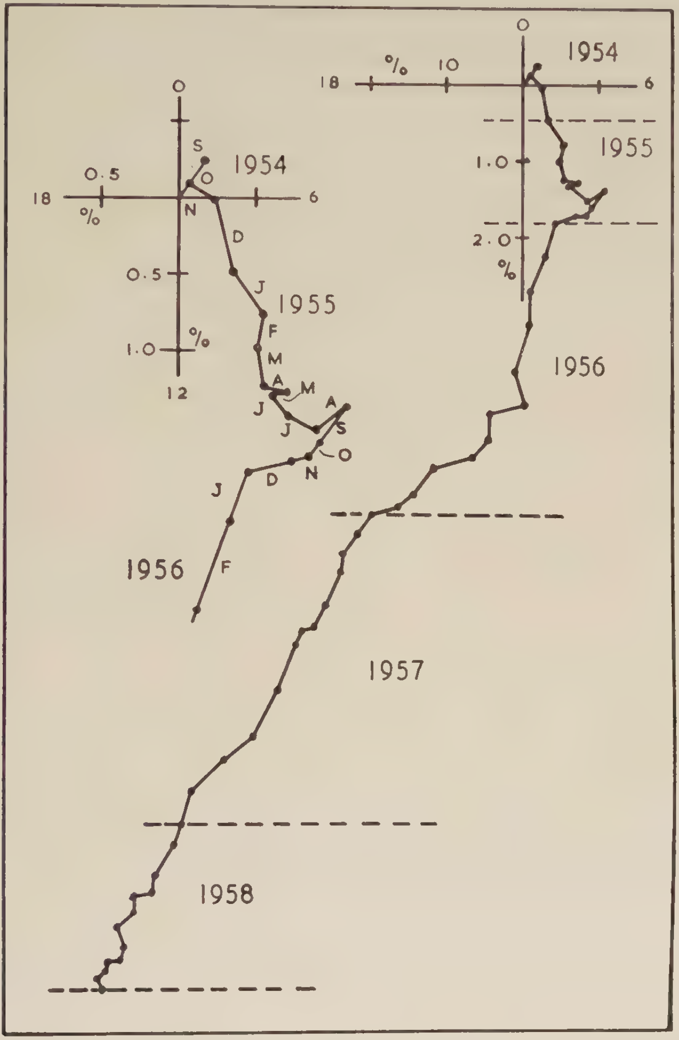

Mean monthly diurnal vectors for successive months during the period September 1954–December 1958 recorded at Leeds. The period September 1954–February 1956 has been replotted on twice the scale of the main graph.

The correlation between the sunspot numbers and the cosmic ray diurnal amplitude is not close and a considerably closer correlation is apparent with the magnetic amplitude; this is in agreement with recent observations on the hard component reported by Venkatesan and Dattner (1959). Comparison of the record reported here with other neutron monitor data confirms the general variation, in that the amplitude was large in October 1956, decreased until mid 1957 and was then followed by very large amplitudes in August–September 1957, although detailed comparison reveals significant differences. The amplitude decreased very markedly from September 1957 to December 1958. This is in contrast to the change in the total nucleon intensity, the mean level of which has remained depressed but fairly constant throughout 1958 and indicates a distinction between the mechanism responsible for the depression of the cosmic ray intensity associated with solar activity and that producing the diurnal variation.

Fig. 2

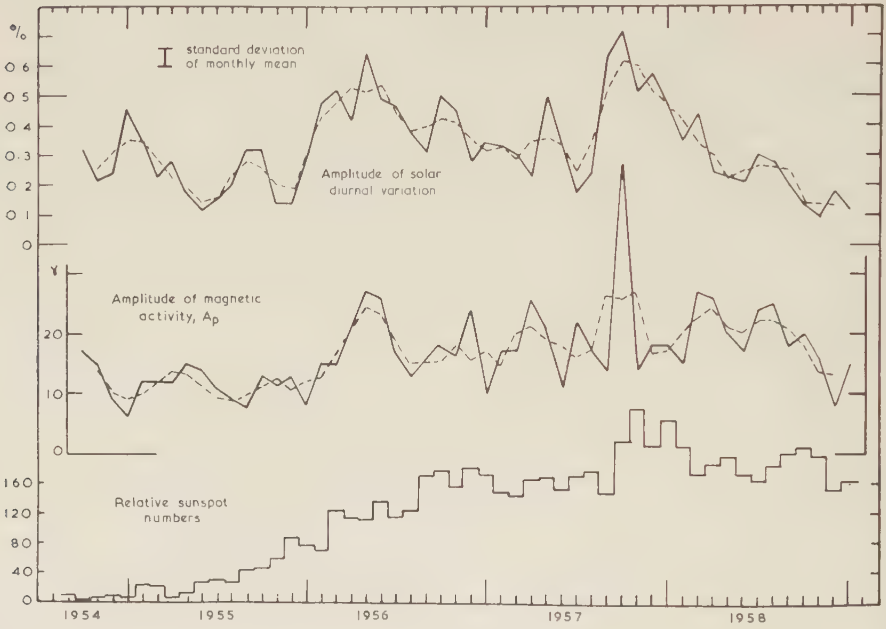

Amplitude of the diurnal variation of the nucleonic component recorded at Leeds, equivalent planetary amplitude of magnetic activity and relative sunspot numbers during the period September 1954–December 1958.

The close correlation of the amplitude of the diurnal intensity with the amplitude of magnetic activity, which is a measure of the magnetic disturbance due to corpuscular emission from the sun, suggests that the same streams which are thought to be responsible for the magnetic phenomena are also connected with diurnal variation. Dorman (1957) has suggested that the streams giving rise to the magnetic disturbances are streams originating in the vicinity of sunspots (streams of the second kind) which carry away 'frozen in' magnetic fields from the sunspot areas. The direction of the magnetic field in the beam might be expected to have considerable effect upon the phase of the maximum of the diurnal wave.

We draw attention to two aspects concerning the time of the maximum: first that from 1956 onwards the time of maximum has remained almost constant, thus the times of maximum for the years 1956, 1957 and 1958 are 1340, 1350 and 1300 h local solar time respectively. Secondly that in 1955 the phase changed abruptly between August and September; the resultant time of maximum through the period November 1954 to July 1955 is 1050 h and from September 1955 to February 1956 it is 1430 h.

Fig. 3

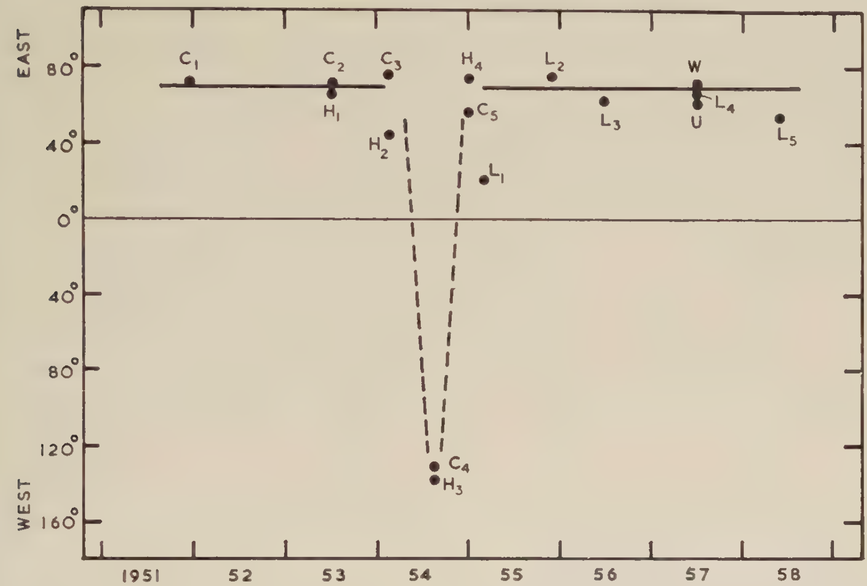

Direction of the anisotropy causing the diurnal variation in the nucleonic component during the period 1951–58. Key: $C_1$, Climax, Nov. (1951)–Jan. (1952); $C_2$, Climax, 1953; $C_3$, Climax, Jan. (1954)–March (1954); $C_4$, Climax, July (1954)–Sept. (1954); $C_5$, Climax, Nov. (1954)–Feb. (1955); $H_1$, Huancayo, 1953; $H_2$, Huancayo, Jan. (1954)–March (1954); $H_3$, Huancayo, July (1954)–Sept. (1954); $H_4$, Huancayo, Nov. (1954)–Feb. (1955); $L_1$, Leeds, Nov. (1954)–July (1955); $L_2$, Leeds, Sept. (1955)–Feb. (1956); $L_3$, $L_4$, $L_5$, Leeds, 1956, 1957, and 1958; W, Weissenau, 1957; U, Uppsala, 1957.

When allowance is made for the deflection of the trajectories of particles in the earth's magnetic field the direction of anisotropy causing the diurnal maximum may be calculated from the time of maximum. Following the method given by Dorman (1957) we have calculated this direction; it is found to be 64°, 67° and 55° east of the line joining the sun and earth for the years 1956, 1957 and 1958 respectively. We consider the uncertainty in these values to be ~15°, chiefly on account of the uncertainty in the effective geomagnetic latitude of the station. The directions are plotted in fig. 3 together with other neutron data from Climax for a short period, 1951–52, from Climax and Huancayo for the years 1953 and 1955, together with data for 1957 from Weissenau and Uppsala. For all stations the method of computation has been that given by Dorman.

Fig. 4

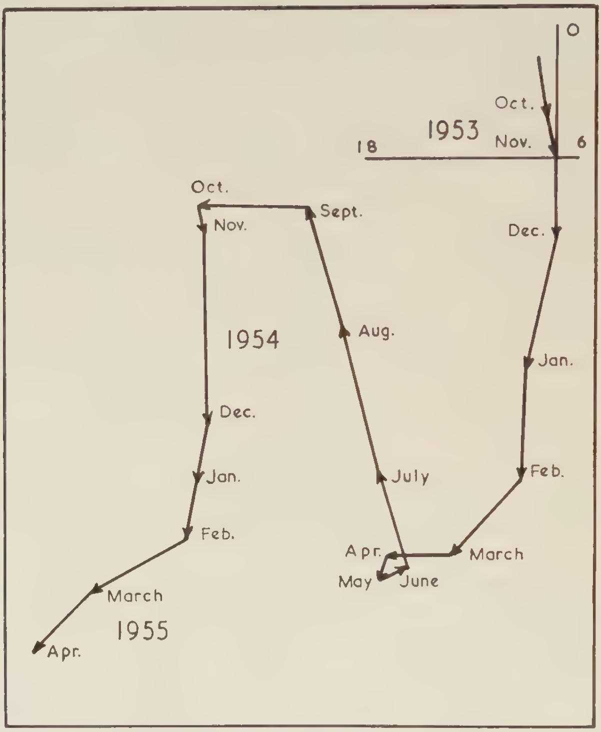

Monthly average vectors for successive months during period October 1953–April 1955 for Climax (Conforto and Simpson 1957).

It appears that the direction of the anisotropy responsible for diurnal variation detected by neutron monitors was substantially the same for the years preceding and following the sunspot minimum year 1954. The record for 1954 has been discussed by Conforto and Simpson (1957) and explained tentatively in terms of a sidereal variation. However another interpretation of the data given by these authors appears possible, suggested particularly by the data from Climax reproduced here in fig. 4. There are three distinct periods of a few months duration, viz. January–March (1954), July–September (1954) and November (1954)–February (1955), during which the time of maximum appears to be roughly constant but different in each of the three groups of months. Thus for January–March the resultant time of maximum is 1315 h, July–September 2300 h and for November–February 1200 h (local solar time). The months not included in these groups and separating them could be regarded as the months covering the transition periods between the times of maximum given above. The neutron data from Huancayo are much more complicated than those for Climax but even here grouping according to the same months the time of maximum shows large changes between the groups. In addition Venkatesan and Dattner (1959) have noted that there are sudden changes in the times of maximum occurring in the ion chamber data from several stations for the period June–November 1954; for all the stations considered the phase becomes much earlier than usual during these few months. The Climax and Huancayo data grouped in the manner given above for 1954 have been plotted in fig. 3 and show an extremely sharp minimum; the direction of the anisotropy appears to have swung to the west of the earth–sun line. Also plotted are the results from Leeds for November 1954–July 1955 and September 1955–February 1956 which are in general agreement with the discontinuity in the Climax and Huancayo records.

A large change in the direction of the anisotropy at the time of sunspot minimum, as the sunspot field changes polarity, might reasonably be expected but it is difficult to see why the direction should return to the same value as before the solar minimum: the sunspot field previous to 1954 was in such direction that if it were 'frozen in' the beams it would have given an early morning maximum and after 1954 a maximum shortly after noon.

If the poloidal field of the sun were the field which became frozen in the beams emitted by the sun then the direction of field for much of the time covered here would be such as to give rise to an early morning maximum. In addition, if the general field of the sun was important in this context, large changes in phase would have been expected in the cosmic ray record about June 1957 when the 'south pole' reversed its polarity (Babcock and Livingston 1958) and again in late 1958 when the field at the 'north pole' also reversed (Babcock 1959, private communication). No such changes in the time of maximum are evident and indeed it does not seem probable that the much weaker poloidal fields could influence the direction of the anisotropy at this stage of the solar cycle when there was considerable sunspot activity.

It is possible that the sharp change in the direction of the anisotropy at the time of sunspot minimum is connected with the general field of the sun. The direction of the poloidal field at this time would be in such a direction as to make the direction of the anisotropy giving rise to the maximum west of the earth–sun line. At this stage of the solar cycle the general field may well become dominant, because in addition to the small number of spots, the resultant effect of the beams on cosmic ray particles may be further reduced on account of sunspot groups of opposite polarities appearing simultaneously on the sun.

In conclusion we emphasize the essential feature of the results reported here; that, apart from the discontinuity at sunspot minimum, the direction in space of the source of particles giving the diurnal maximum has remained constant.

## ACKNOWLEDGMENTS

We are pleased to acknowledge the help and advice of Professor J. G. Wilson in the preparation of this paper. We are also indebted to Professor Emhert and Dr. Sandström who kindly made their data available to us. The help of the Royal Society in providing financial assistance is gratefully acknowledged.

## REFERENCES

ALFVÉN, H., 1949, *Phys. Rev.*, **75,** 11.
BABCOCK, H. D., and LIVINGSTON, W. C., 1958, *Science*, **127,** 1058.
CONFORTO, M., and SIMPSON, J. A., 1957, *Nuovo Cim.*, **5,** 1052.
DORMAN, L. I., 1957, *Cosmic Ray Variations* (Moscow: State Publishing House for Technical and Theoretical Literature).
FIROR, J. W., FONGER, W. H., and SIMPSON, J. A., 1954, *Phys. Rev.*, **94,** 1031.
MARSDEN, P. L., and DORAN, G. A., 1956, *Proc. phys. Soc. Lond.* A, **69,** 894.
SIMPSON, J. A., 1957, *Annals of the International Geophysical Year, IV*, part VII (London: Pergamon Press).
SIMPSON, J. A., FONGER, W. H., and TREIMAN, S. B., 1953, *Phys. Rev.*, **90,** 934.
THAMBYAHPILLAE, T., and ELLIOT, H., 1953, *Nature, Lond.*, **171,** 918.
VENKATESAN, D., and DATTNER, A., 1959, *Tellus*, **11,** 116.
WHITAKER, E., and ROBINSON, G., 1946, *The Calculus of Observations* (London: Blackie & Son).

# A Non-mesonic Decay of a ${}^{11}_{\Lambda}$B Hyperfragment[†]

By D. EVANS, B. D. JONES and J. ZAKRZEWSKI[‡]
H. H. Wills Physics Laboratory, Bristol

[Received August 8, 1959]

## ABSTRACT

An event is described which is interpreted as the non-mesonic decay of ${}^{11}_{\Lambda}$B into ${}^{8}$Li, a deuteron and a proton. Any other interpretation is seen to have a negligible probability of being correct. The binding energy of the $\Lambda^0$-hyperon in the ${}^{11}_{\Lambda}$B hypernucleus is found to be $11 \cdot 3 \pm 0 \cdot 8$ MeV.

## § 1. INTRODUCTION

IT has been observed that the decay of a hyperfragment of $Z > 3$ does not often involve the emission of a $\pi$-meson. When a $\pi$-meson is not emitted the energy release of the $\Lambda^0$-hyperon decay is 177 MeV, and many channels are available for the decay process, most of which involve the emission of neutrons. The observed features of most decays of such hypernuclei are therefore not capable of unique interpretation. Even if a $\pi$-meson is emitted, there is little chance of the residual nucleus being affected by the low-energy proton from the bound $\Lambda^0$-decay, and the resulting events in emulsion are usually associated with very short tracks due to the recoiling nuclear core of the hyperfragment. The identity of the recoil is then impossible to ascertain; even if the charge is determined from other considerations, it is unlikely that the mass number would be uniquely defined.

The decays of ${}^{8,9}$Li and ${}^{8}$B give a characteristic T-shaped track in emulsion (a 'hammer' track) and a hypernucleus decaying in such a way that these nuclear fragments are produced has a chance of being uniquely identified. The present communication describes an event observed in a K5 emulsion stack exposed to 80 MeV $K^-$-mesons from the Bevatron at Berkeley. A $K^-$-meson is captured at rest, and produces an event which is interpreted as being due to the creation of a ${}^{11}_{\Lambda}$B hypernucleus which subsequently decays into ${}^{8}$Li, a deuteron and a proton. Any other interpretation is seen to have a negligible probability of being correct. To our knowledge, this is the first example of a uniquely defined non-mesonic decay of a ${}^{11}_{\Lambda}$B hyperfragment, although a number of events have been observed which, among other possibilities, could be due to boron hypernuclei (Levi-Setti *et al.* 1958)[§].

---

[†] Communicated by the Authors.

[‡] On leave from the University of Warsaw.

[§] See note added in proof.

## § 2. EXPERIMENTAL DETAILS AND RESULTS

The photograph (Pl. 152) shows the K$^-$-meson absorption star, consisting of a very steep $10\,\mu$ track, which could be due to a nucleus of charge one or two, one of low grain density which is due to a $\pi$-meson, and a $1{\cdot}8\,\mu$ interconnecting track to a second star, S. The latter consists of three tracks: (*a*) which is 17·2 mm long and, from the variation of ionization with range, must be due to a proton; (*b*) which has a length of 5·5 mm; and (*c*) which ends after $64\,\mu$ in the characteristic hammer shape described in §1.

The value of the exponent of the gap length distribution, $g$, (Fowler and Perkins 1955) was measured on track (*b*) near its origin. The values of $g$ expected if (*b*) were due to a proton, deuteron and triton respectively were found from measurements on ten ending K$^-$-mesons of small dip and four ending protons having a dip angle similar to that of (*b*). Blob counts on four light tracks due to the background beam, in each of the plates where the above measurements of $g$ were done, showed that any variation in the sensitivity to ionization of the emulsions was less than 5%, and this effect was therefore neglected. Table 1 displays the results.

Table 1

| Expected for track (*b*) at emission if due to: | $g/100\,\mu$ from measurements on : | |
|---|---|---|
| | Flat $K^-$-mesons | Protons ~ 30° dip |
| Proton | $210 \pm 10$ | $233 \pm 13$ |
| Deuteron | $287 \pm 13$ | $300 \pm 15$ |
| Triton | $348 \pm 20$ | $372 \pm 31$ |
| $g/100\,\mu$ on track (*b*) (32° dip) $= 304 \pm 27$ | | |

Although there appears to be a systematic increase in $g$ of about 7% for measurements on the steeper tracks, it seems almost certain from table 1 that track (*b*) must have been due to a deuteron. Interpretation as a proton is very unlikely and the expected $g$ for a triton is $1\frac{1}{2}$ standard deviations from the measured value.

The angular directions of the projections in the plane of the emulsion of the three tracks from S, and their angles of dip with respect to that plane, were measured a number of times by three observers and the standard deviations of the sets of results were used in the estimation of errors.

The ranges were measured of protons from 17 decays at rest of $\Sigma^+$-hyperons. Three of the protons had a dip angle $> 60°$ in processed emulsion. The emulsions in which these measurements were made, and the one containing the event being reported, were kept under the same humidity conditions. Using the procedure described by Fry and White (1953), the shrinkage factor under our standard conditions was found to be

2·36 ± 0·04. The mean range of the protons from the $\Sigma^+$-hyperon decays was found to be $1663 \pm 10\,\mu$, giving a stopping power of 1·009 ± 0·006 times that of the emulsion used by Barkas (1958) in his range–energy determination. This range–energy relation, adjusted by the measured stopping power, is used in the discussion.

Table 2 summarizes the range and angle measurements on the tracks from S.

Table 2

| Track from S | Range in $\mu$m | Plane angle | Dip angle (unprocessed emulsion) |
|---|---|---|---|
| (*a*) Proton | 17 173 ± 215 | 138·4 ± 0·5° | 22 ± 1° |
| (*b*) Deuteron | 5 538 ± 38 | 215·9 ± 0·5° | 32 ± 1° |
| (*c*) 'Hammer' | 64 ± 1 | 0 ± 1·5° | 11·5 ± 2° |

The errors on range are the expected straggling, and those on the angle measurements include observational uncertainty, as deduced from the spread found in repeated measurements, combined with the uncertainty in direction due to multiple Coulomb scattering over the length of track used for measurement.

## § 3. DISCUSSION

The track connecting S to the $K^-$-meson star is too short to offer any assistance in the interpretation. The observed energy release in star S is at least 145 MeV, assuming the 'hammer' track to be due to ${}^8$Li. Taking into account the energy required to remove the observed fragments from any nucleus, star S could clearly not have been the result of a $\pi$-meson absorption.

The three tracks from S are coplanar to within the errors of measurement (± 2°), suggesting an interpretation in terms of a hyperfragment decay at rest. The resultant momentum, $R$, of the proton and deuteron has a magnitude of 580 ± 5 MeV/c. A ${}^8$Li of this momentum has a range of $64 \pm 2\,\mu$m, which can be compared with the observed range of 64 $\mu$m for the 'hammer' track. A ${}^9$Li fragment would have had a range of $50 \pm 2\,\mu$m. However, the direction of the vector $\mathbf{R}$ makes an angle of 2·4 ± 2·1° to the measured direction of the 'hammer' track. The total measured resultant momentum of the three particles is 25 ± 22 MeV/c if track (*c*) is taken to be due to ${}^8$Li. Table 3 displays the above discussion and deduces the binding energy of the $\Lambda^0$ ($B_\Lambda$), if S is taken to be the decay of ${}^{11}_{\Lambda}$B. The errors include those shown in table 2, combined with those due to uncertainties in shrinkage factor, stopping power and range–energy relation.

The value of the binding energy assumes the nuclear fragment to be produced in the ground state. If a neutron is introduced to take the measured resultant momentum, there is insufficient energy available and $B_\Lambda$ becomes $-1 \pm 1$ Mev. It is seen, therefore, that star S can be uniquely defined as the decay of ${}^{11}_{\Lambda}\mathrm{B}$, if it is caused by a hyperfragment.

It is instructive to discuss the position if the inter-connecting track from the $\mathrm{K}^-$-star were taken to be due to a $\Sigma^-$-hyperon. Since the energy release is 145 Mev, clearly the $\Lambda^0$ produced was trapped and decayed, the whole process releasing 257 Mev.

Table 3

| Track | Energy in Mev | Momentum in Mev/c | Range of (*c*) for momentum balance ($\mu$m) | Measured resultant momentum | $B_\Lambda$ for ${}^{11}_{\Lambda}\mathrm{B}$ Mev |
|---|---|---|---|---|---|
| (*a*) Proton | $71{\cdot}3 \pm 0{\cdot}6$ | $372{\cdot}7 \pm 1{\cdot}6$ | $64 \pm 2$ | $25 \pm 22$ Mev/c | $11{\cdot}3 \pm 0{\cdot}8$ |
| (*b*) Deuteron | $50{\cdot}5 \pm 0{\cdot}4$ | $438{\cdot}3 \pm 1{\cdot}8$ | | | |
| (*c*) ${}^{8}\mathrm{Li}$ | $22{\cdot}5 \pm 0{\cdot}2$ | $580{\cdot}0 \pm 2{\cdot}8$ | | | |

A capture in a heavy nucleus would have to lead to 122 Mev being taken by the deuteron and proton, with the subsequent evaporation at a nuclear excitation of at most 135 Mev giving a Li or B fragment (track (*c*)) of $\sim 20$ or $\sim 40$ Mev respectively. Further, by chance, for a Li fragment, the evaporation momentum must balance that of the proton and deuteron from the initial knock-on process, and for a B fragment, the products must be coplanar. The probability of any process involving the capture of a $\Sigma^-$-hyperon in a heavy nucleus leading to the observed features of star S is estimated to be $< 10^{-6}$. Even taking into account the number of $\Sigma^-$-stars which have been observed, the probability that S is due to a $\Sigma^-$-hyperon capture in a heavy nucleus remains very small.

The capture of a $\Sigma^-$-hyperon in a light nucleus must again lead to an intermediate stage in which a hyperfragment is produced. The only reactions which can conserve charge, energy and momentum in both the initial absorption and final hyperfragment are:

$$\Sigma^- + {}^{12}\mathrm{C} \rightarrow n + n + {}^{11}_{\Lambda}\mathrm{B} \quad \text{or} \quad n + {}^{12}_{\Lambda}\mathrm{B}.$$

(For example, there is insufficient energy to produce ${}^{11}_{\Lambda}\mathrm{Be}$ and a $\Lambda^0$-particle could not be bound in a lighter fragment.) If ${}^{12}_{\Lambda}\mathrm{B}$ is produced, its range should be $\sim 5\,\mu$m, whereas star S is centred on the end of the interconnector to the $\mathrm{K}^-$-star. Further, as is shown above, S cannot be interpreted as the decay of ${}^{12}_{\Lambda}\mathrm{B}$. It seems therefore, for any reasonable probability, that star S must be due to the decay of ${}^{11}_{\Lambda}\mathrm{B}$ even if the track connecting it to the $\mathrm{K}^-$-star is produced by a $\Sigma^-$-hyperon.

## § 4. CONCLUSION

The only interpretation that can adequately describe the event shown in the photograph is one in terms of a ${}^{11}_{\Lambda}\mathrm{B}$ decaying according to the scheme:

$${}^{11}_{\Lambda}\mathrm{B} \rightarrow {}^{8}\mathrm{Li} + d + p.$$

The binding energy of the $\Lambda^0$ in ${}^{11}_{\Lambda}\mathrm{B}$ is then $B_{\Lambda} = 11{\cdot}3 \pm 0{\cdot}8$ MeV, the error including measurement and calibration uncertainties. The value taken for the $Q$ of the $\Lambda^0$ decay was 37·2 MeV (Levi-Setti 1958).

This binding energy value assumes ${}^8\mathrm{Li}$ to be formed in the ground state. There are three low lying levels of ${}^8\mathrm{Li}$ at about 1 MeV, 2 MeV and 3 MeV respectively, and no bound states of higher excitation are reported (Lauritsen and Ajzenberg-Selove 1957). The 2 MeV and 3 MeV levels decay by neutron emission and are therefore excluded in the present case, since the distinctive $\beta$ and $\alpha$-particle decay chain is observed. There is no reason to exclude the 1 MeV level; for example, in low energy neutron reactions the 1 MeV level and ground states are often produced with comparable frequency.

There remains the possibility that the ${}^{11}_{\Lambda}\mathrm{B}$ is in an excited state when it decays. It may be noted here that ${}^{10}\mathrm{B}$ has an excited level at 0·7 MeV with a lifetime of $\sim 10^{-9}$ sec. The presence of an analogous excited level in ${}^{11}_{\Lambda}\mathrm{B}$ may perhaps be detected when further determinations of binding energy have been made.

## ACKNOWLEDGMENTS

We should like to thank Professor C. F. Powell, F.R.S., for his hospitality and encouragement. We are very grateful to Dr. P. H. Fowler, who pointed out a number of important features of the analysis, to Dr. E. J. Lofgren, Dr. Levi-Setti and the Bevatron team for handling the exposure and to Professor G. Occhialini and his colleagues at the University of Brussels for processing the stack.

We acknowledge the help given by the scanning team at this laboratory. B. D. Jones thanks the Department of Scientific and Industrial Research, and J. Zakrzewski the Institute for Nuclear Research, Warsaw, for maintenance awards.

*Note added in proof.*—An event has been reported to us (private communication R. Levi-Setti, University of Chicago) the most probable interpretation of which is as the mesonic decay of ${}^{11}_{\Lambda}\mathrm{B}$. The value of $B_{\Lambda}$ is found to be $9{\cdot}9 \pm 0{\cdot}6$ MeV when the $Q$ value for the free $\Lambda^0$-hyperon decay is taken as 37·6 MeV.

## REFERENCES

BARKAS, W. H., BARRETT, P. H., CÜER, P., HECKMAN, H. H., SMITH, F. M., and TICHO, H. K., 1958, *Nuovo Cim.*, **8**, 185.

FOWLER, P. H., and PERKINS, D. H., 1955, *Phil. Mag.*, **46**, 587.

FRY, W. F., and WHITE, G. R., 1953, *Phys. Rev.*, **90**, 207.

LAURITSEN, T., and AJZENBERG-SELOVE, F., 1957, *American Institute of Physics Handbook.*

LEVI-SETTI, R., SLATER, W. E., and TELEGDI, V. L., 1958, *Nuovo Cim.*, Suppl., **10**, 68.

# The Plastic Deformation of Single Crystals of an Aluminium–Silver Alloy†

By A. Kelly‡, A. Lassila and S. Sato§
Department of Metallurgy, Northwestern University, Evanston, Illinois

[Received June 29, 1959]

## Abstract

Tensile tests have been carried out at a variety of temperatures between 77°K and 373°K on single crystals of an aluminium—20 wt % silver alloy. The crystals were aged either at room temperature, or at 160°C, within the cold-hardening range. Single crystals of this material are very ductile. Stress–strain curves have been obtained and the change of flow stress with temperature, during deformation, has been measured and compared with the change of elastic modulus over the same temperature range. Observations have been made with the optical microscope of the appearance of slip lines on polished surfaces of the specimens.

The stress–strain curves are approximately linear showing a rate of work hardening about the same as that of pure aluminium in stage II of the stress–strain curve. The temperature dependence of the flow stress is small, varying less than does the elastic modulus over the temperature range investigated. The temperature dependence of the flow stress is compared with new measurements of the same quantity in pure aluminium single crystals. The crystals deform by a ⟨110⟩ {111} slip mechanism but cross slip is profuse at all stages of the deformation and at all temperatures. This is attributed to the very high flow stress of these single crystals which is two orders of magnitude greater than that shown by pure aluminium.

## § 1. Introduction

Despite much recent work on the plastic properties of single crystals of pure metals few experiments have been reported on the deformation of crystals containing coherent precipitates of known structure. In this investigation the deformation of single crystals of an aluminium–silver alloy has been studied in an attempt to understand the nature of the interaction between dislocations and the precipitates which leads to the great strength of the alloy crystals compared to crystals of aluminium.

The aluminium rich end of the Al–Ag phase diagram shows that alloys of less than 50 wt % Ag should be age-hardenable. Many publications (see for example Köster and Braumann 1952) have shown that age hardening does occur and in two stages—a cold and a warm hardening stage. The crystals used here were all aged within the cold-hardening range. X-ray investigations (Walker and Guinier 1953) have shown that in the cold-hardening stage there are present in the alloy approximately spherical clusters of atoms very rich in silver, each surrounded by a spherical shell rich in aluminium. The marked cold hardening observed is attributed to the presence of these spherical Guinier–Preston zones. Studies of the plastic properties of this alloy are of particular interest because aluminium and silver possess closely the same Goldschmidt radius and hence lattice strains around the zones are expected to be unimportant as the cause of hardening.

---

† Communicated by the Authors.

‡ Now at Department of Metallurgy, University of Cambridge.

§ Now at Institute of Scientific and Industrial Research, Osaka University, Japan.

In an investigation of this nature it is imperative to use single crystals because polycrystalline specimens are quite brittle at room temperature showing elongations to fracture of only a few per cent whilst single crystals are very ductile, often showing glide strains of greater than 80%. This difference in behaviour is attributed to the markedly different ageing behaviour of material close to grain boundaries.

Stress–strain curves have been obtained, and the change of flow stress with temperature has been measured during deformation. Observations have been made of the slip lines on the surface of the crystals. In connection with the study of the change in flow stress with temperature measurements have been made of the change in Young's modulus over the same temperature range and also of the change in flow stress with temperature of pure aluminium single crystals.

## § 2. EXPERIMENTAL DETAILS

Rods of aluminium–20 wt % silver were made by vacuum melting in a graphite crucible. The aluminium used was of 99·99% purity supplied by Alcoa and the silver of 99·996% purity from the Belmont Smelting and Refining Co. After melting the rods were cleaned in sodium hydroxide and swaged and rolled with intermediate annealing treatments to a thickness of 0·06 in.

No success was obtained in growing single crystals from the strip by a strain–anneal method, which is very easy in the aluminium–copper system (Kelly and Chiou 1958). This is attributed to recrystallization which occurs on over-ageing of Al–Ag alloys of this composition (Geisler *et al.* 1943). Such does not occur in the Al–Cu system, and it is impossible to avoid over-ageing when attempting to grow single crystals by the strain–anneal method. Single crystals were obtained from the melt by a modified Bridgman technique. Specimens were cut to shape from the rolled strip, packed in alumina and passed through a horizontal furnace with a steep temperature gradient at a speed of about 1 in. per hour. Single crystals of rectangular cross section of dimensions about 0·06 in. × 0·25 in. × 1·5 in. were obtained. After etching in warm NaOH solution to check that specimens were single crystals they were lightly ground to ensure uniformity of cross section and then heavily etched. They were then homogenized for 5–7 days at 560°C and quenched into water at room temperature. The orientation of the crystals was determined by a Laue back-reflection method and then specimens were either held at room temperature until tested or were rehomogenized at 560°C for twelve hours, quenched into water and immediately placed in an oven at 160°C and aged for eight hours, after which they were quenched to room temperature and held at this temperature until tested. The specimens aged eight hours at 160°C show maximum cold hardness (Köster and Braumann, 1952) and were produced specifically for this investigation of the tensile properties of these alloys. Those aged at room temperature were produced for an x-ray examination of the change of shape of the Guinier–Preston zones produced by deformation of single crystals which will be described elsewhere. Their tensile properties will be described here. They were aged at room temperature because this produces zones of smaller size than does ageing at 160°C and the smaller zone size is more convenient for the x-ray investigation.

Reversion of one specimen after ageing for eight hours at 160°C was accomplished by placing the specimen in an oven for 15 min at 220°C. In these alloys complete reversion, i.e. a return to the zone free condition, is not obtained (Belbeoch and Guinier 1955) as it is in the Al–Cu system.

Single crystal specimens were polished for the examination of slip lines in a bath of orthophosphoric acid, ethyl alcohol and water using a voltage of 30.

Table 1. Temperatures of Deformation

| Bath | Measured temperature (°K) |
|---|---|
| Liquid nitrogen | 77 |
| Solid and liquid ‘ Freon 12 ’ | 119 |
| *n*-propyl alcohol | 155 |
| Acetone and solid $CO_2$ | 196 |
| Solid and liquid $CaCl_2$ solution | 233 |
| Ice and brine | 258 |
| Ice and water | 273 |
| Room temperature | 295–301 |
| Boiling water | 373 |

Specimens were deformed in an Instron tensile testing machine at a strain rate of $10^{-4}\,\mathrm{sec}^{-1}$. Temperature was controlled by immersion of the specimen in one of the baths detailed in table 1. Crystals aged at room temperature were tested at this temperature or at 77°K. Those aged at 160°C were tested at temperatures up to 373°K. When changing the temperature of a specimen during a tensile test the specimen was brought to the desired temperature determined on a thermocouple placed close to it and held at this temperature for 5–10 min before continuing the test. The time between tests at two different temperatures was between 15 and 30 min.

## § 3. Results

### 3.1. *Critical Resolved Shear Stress*

The orientations of the tensile axes of the crystals examined are shown in fig. 1. The values of the critical resolved shear stress (CRSS) of a number

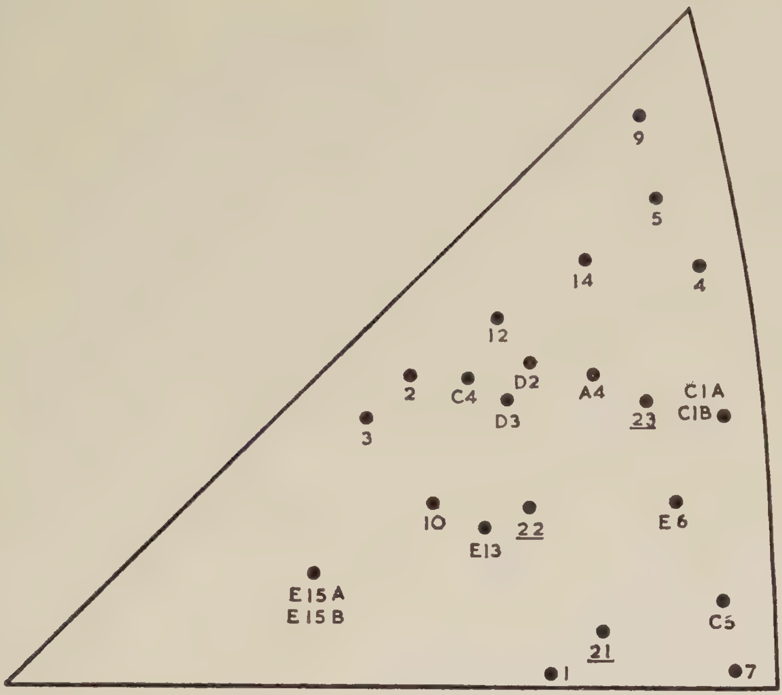

Fig. 1. Orientation of tensile axes of specimens used. Specimens of which the number is underlined were of pure aluminium.

Table 2. Values of Critical Resolved Shear Stress

| Crystal | Ageing treatment | Temperature of test | CRSS (kg/mm$^1$) |
|---|---|---|---|
| 1 | 8 hrs at 160°c | 273°K | 8·5 |
| 2 | " | " | 8·5 |
| 3 | " | " | 7·6 |
| 4 | " | " | 9·0 |
| 9 | " | " | 9·1 |
| 5 | " | 77°K | 9·6 |
| 14 | Aged at 160°c and reverted | 273°K | 6·5 |
| A4 | Aged at room temperature | 300°K | 6·2 |
| D2 | " " " | " | 7·5 |
| D3 | " " " | " | 6 8 |
| E6 | " " " | " | 7·2 |
| E13 | " " " | " | 6·6 |
| C1A | " " " | " | 7·5 |
| C1B | " " " | " | 6·6 |
| E15A | " " " | " | 6·4 |
| C4 | " " " | 77°K | 6·2 |
| C5 | " " " | " | 7·1 |
| E15B | " " " | " | 7·4 |

of the alloy crystals are listed in table 2, assuming ⟨110⟩{111} slip—see § 3.3. The values of CRSS of crystals aged at room temperature are less than those of crystals aged at 160°C. The reverted crystal shows a CRSS, the same as that of those aged at room temperature. The values of CRSS thus follow exactly the change of hardness with ageing temperature determined on polycrystalline specimens of these alloys (Köster and Braumann 1952). For any one condition of ageing and temperature of testing, the values of CRSS show a spread of values amounting to at most 20% of the lowest value. No systematic variation of CRSS with orientation is apparent. This range of values of CRSS is about the same as that found in pure metal single crystals. The values of CRSS obtained in crystals tested at 77°K are not very different from those found at room temperature. This result is strikingly different from that found with pure metals and other age-hardened single crystals (Kelly and Chiou 1958) and indicates a very small temperature dependence of CRSS.

### 3.2. *Stress–Strain Curves*

Load-extension curves were obtained for a number of crystals at 77°K, 273°K and 300°K. In single crystal work, provided one is dealing with a specimen of uniform cross section, the load-extension curve is usually plotted as resolved shear stress against glide strain, derived from the measured load and elongation and the known initial orientation of the crystal. This procedure assumes homogeneous slip throughout the gauge length and is often a poor approximation as single crystals usually exhibit marked deformation bands and other inhomogeneities during extension and slip on secondary systems is often observed. Diehl (1956) followed these inhomogeneities of extension in detail in copper single crystals. A similar procedure was followed here. Measurements were made of the elongation in adjacent regions along the gauge length of a crystal by measuring the change in the separation of light scratches on the surface of the crystal. Table 3 shows the measured elongation in nine adjacent regions of single crystal D3 deformed to an average elongation of 9·7%. This is a typical result and quite large variations in the elongation in adjacent regions of the crystal are found. Crystal D2 showed the smallest variations of any examined and the results for this crystal at an average elongation of 12·5% are also shown in table 3. The inhomogeneities in the case of crystal D2 are much the same as those found by Diehl in pure copper. In the case of crystal D3 they are larger if the regions near the grips are included. The occurrence of quite marked deviations from the average elongation appears then to be of general occurrence in crystals of alloys and of pure metals and should be borne in mind when stress–strain curves are plotted.

Assuming homogeneous ⟨100⟩{111} glide and using the equations given by Schmid and Boas 1950, the shear stress–glide strain curves of a number of crystals are shown in figs. 2 and 3. The crystals aged and deformed at room temperature were not extended to fracture but unloaded and used in the X-ray examination. The crystals shown in fig. 3 were extended to

Table 3

| Crystal D3 | Crystal D2 |
|---|---|
| Elongation in adjacent regions each *c.* 3 mm in length | Elongation in adjacent regions each *c.* 3 mm in length |
| 7·8% | 10·8% |
| 9·7 | 13·2 |
| 11·5 | 13·1 |
| 13·6 | 12·9 |
| 13·0 | 12·7 |
| 11·4 | 12·1 |
| 8·7 | 12·7 |
| 7·0 | |
| 4·7 | |
| Average elongation 9·7% | Average elongation 12·5% |

Fig. 2

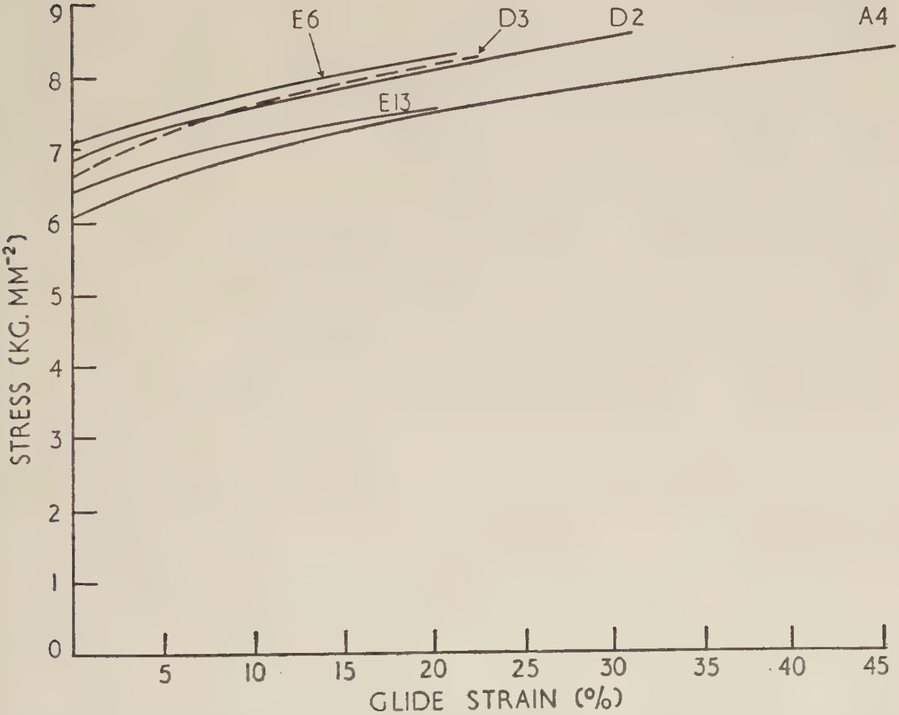

Stress–strain curves of five crystals, aged at room temperature and tested at room temperature.

Fig. 3

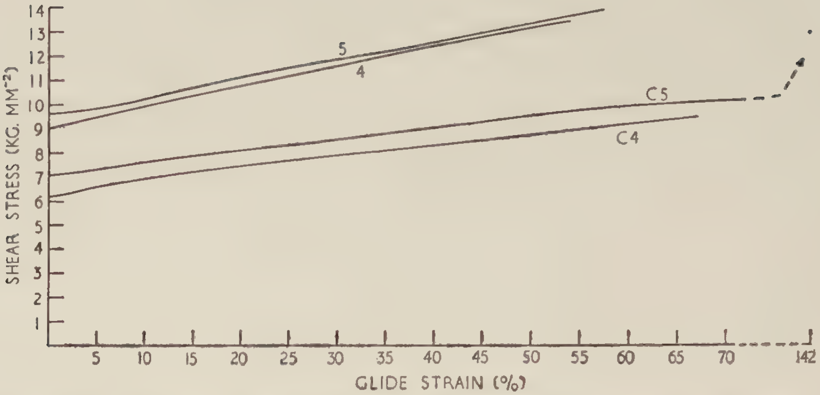

Stress–strain curves of two crystals aged at 160°c and deformed at 77°k (5), and at 273°k(4). Crystals C4 and C5 were aged at room temperature and deformed at 77°k.

fracture. Crystal C5 broke at a resolved shear stress of 12·43 kg mm$^{-2}$ at a glide strain of 142%. All the curves are quite similar in shape. A little easy glide is sometimes seen at 77°k. The curves are almost linear but show a slight concavity to the strain axis over most of their length. Average values of the rate of work hardening were found from the curves excluding any portion of easy glide. Crystals aged at room temperature showed rates of work hardening of about 6·0 kg mm$^{-2}$ and those aged at 160°c a slightly higher rate, about 7·5 kg mm$^{-2}$. Within both of these groups the rate of work hardening was lower at lower temperatures of testing. The rates of work hardening quoted correspond to $2{\cdot}4\times10^{-3}G$ and $3\times10^{-3}G$ where $G$ is the rigidity modulus. These values are much the same as those found in stage II of the stress strain curve of pure aluminium using the figures of Staubwasser (1959) and Sato and Kelly (1959).

### 3.3. *Examination of Slip Lines*

During deformation of these single crystals the change of orientation of the crystal lattice with respect to the direction of tension was observed by x-ray back-reflection photographs during the course of the deformation. The change of orientation observed was always consistent with slip on a $\langle 110\rangle\{111\}$ system. The change of orientation of the tensile axis was followed for a number of crystals to large deformations. Usually slip was observed on secondary systems before the boundary of the unit triangle was reached, but even so overshoot of the tensile axis amounting to some 3°–4° was usually observed.

In examining slip lines on polished surfaces of metal crystals attention must be paid to the orientation of the surface of examination with respect to the slip direction. During the course of deformation the slip pattern was observed on two surfaces of the crystals, viz. a face containing the tensile direction and the direction of glide (side surface) and a face normal to the first and containing the direction of tension (top surface). The appearance of slip lines on these two surfaces are quite dissimilar. On the side surface the slip lines are straight and follow accurately the trace of a {111} plane (fig. 4 (*a*), Pl. 153). On the top surface the slip lines observed at low magnification also follow on the average the trace of the same {111} plane but at higher magnification are seen to be extraordinarily wavy and to branch and follow no single crystallographic plane (fig. 4 (*b*), Pl. 153). This behaviour is found in all conditions of ageing and at all temperatures of deformation, though crystals deformed at 77°K show slip lines on the top surface which are rather less wavy. The marked waviness is found at the smallest deformation at which crystals were examined —1% glide strain— and continues up to fracture. At large deformations when other glide systems become active the secondary glide systems also show wavy slip lines. This gives rise to an extremely complicated array of branched, and wavy intersecting slip lines (fig. 5, Pl. 154)†.

This appearance of the slip lines is quite different from that normally observed in pure aluminium crystals and is similar to that found in body-centred cubic metals—see for example Maddin and Chen (1954) and Low and Guard (1959). There is a difference, however, in that in the Al–Ag alloy the slip lines observed on a top surface run much more nearly parallel to the trace of a single plane, the (111) plane, than do those in body-centred cubic metals when each is examined at high magnification. In view of this the plotting of the load elongation curves in terms of resolved shear stress versus glide strain on a $\langle 110\rangle\{111\}$ system is considered reasonable.

The type of fracture observed in these crystals is illustrated in fig. 6 (Pl. 154). Fracture occurs by extensive glide on a plane approximately parallel to the main slip plane. Large amounts of deformation occurred in a narrow region and no neck was observed to form. It appears that after extensive deformation the resistance to shear of the slide planes in a particular region of the crystal is much reduced with respect to the rest of the crystal leading to extensive shear on one plane, or on a set of closely spaced parallel planes, leading to parting of the crystal. A very similar type of fracture has been observed previously in aluminium zinc single crystals (Elam 1927).

### 3.4. *Temperature Dependence of the Flow Stress*

#### 3.4.1. *Alloy crystals*

The results reported in §§ 3.1 and 3.2 on the critical resolved shear stress and stress–strain curves show that the variation with temperature of these parameters is small. A more accurate assessment of the temperature dependence of the plastic properties, which is not complicated by changes due to difference in orientation and possible differences in the state of ageing of the crystals, can be obtained by measuring the change in flow stress when the temperature is changed during the deformation of one crystal. This method was originally developed by Cottrell and Stokes (1955) and the procedure is as follows. A crystal is strained a few per cent at a certain temperature and then unloaded so that a small stress of about 0·5 kg mm$^{-2}$ is maintained to hold the alignment. The temperature is changed and again the crystal strained plastically a few per cent. The crystal is unloaded, the temperature altered to the original temperature and the procedure repeated. The ratio of the flow stresses at the two temperatures for a crystal in the cold-worked state at which the transition is made is then found directly from the load values of the Instron chart.

---

† A very slight waviness of the slip lines is sometimes observed on the side surface of the crystals. This is attributed to the departure of the orientation of the side surface from the ideal orientation since the side surface is never quite parallel to the slip vector, and to a surface effect connected with the formation of a thick oxide film produced during the polishing of the alloys.

Table 4. Values of the Ratio $\sigma_{77}/\sigma_{273}$ for Crystals 2 and 14

| Crystal 2 (fully cold hardened) | | Crystal 14 (reverted) | |
|---|---|---|---|
| Elongation (%) | $\sigma_{77}/\sigma_{273}$ | Elongation (%) | $\sigma_{77}/\sigma_{273}$ |
| 1·5 | 1·111 | 2·8 | 1·150 |
| 2·6 | 1·110 | 5·4 | 1·165 |
| 3·6 | 1·110 | 7·4 | 1·181 |
| 4·8 | 1·105 | 9·3 | 1·169 |
| : | : | 13·6 | 1·184 |
| : | : | 17·6 | 1·169 |
| 17·6 | 1·106 | 22·6 | 1·187 |
| 18·7 | 1·110 | 27·9 | 1·172 |

The values found for crystal 2 for transitions between 77 °K and 273 °K are shown in table 4. The ratio is seen to be independent of the elongation, i.e. independent of the cold worked state. By using a number of temperatures the ratio of the flow stress at temperature $T$ ($\sigma_T$) to that at 273 °K ($\sigma_{273}$), i.e. values of the quantity $\sigma_T/\sigma_{273}$, can be found.

Figure 7 shows a typical series of transitions between 77 °K and 273 °K for each of the crystals numbers 1, 2, 3 and 9. The nature of the yield point and the shape of the stress–strain curve varies from crystal to crystal. Jerky flow was found only in crystal 1 during deformation at 273 °K. Yield drops were most pronounced in crystal 1 at 77 °K, they were less obvious in crystals 2, 3 and 14 and were absent in crystal 9. In all crystals showing them they were progressively less marked as the temperature of testing was raised above 77 °K. The occurrence of the yield drop seems to depend on the orientation of the crystal, but the necessary condition for its appearance is that the crystal be prestrained at a higher temperature if the effect is to be found at a certain temperature. In some cases, however, the yield drop did not occur at a low temperature after prestrain at 373 °K. This yield drop is not a work-softening effect, observed in pure aluminium, since the necessary condition for work softening at a given temperature is prestrain at a lower temperature. This yield point effect bears some similarities to that observed in pure metal single crystals of face-centred cubic structure (Haasen and Kelly 1957, Makin 1958 a).

Consistent values of the ratio $\sigma_T/\sigma_{273}$ could be obtained from all crystals if the upper yield point was taken as representing the flow stress, when a yield drop occurred. The ratio $\sigma_T/\sigma_{273}$ was independent of the total strain to which a crystal was subjected to better than 2% in all crystals. As the ratio of the flow stress determined in this way was independent of elongation, transitions between a variety of temperatures and 273°K were often made on the same crystal, thus eliminating any effects due to different ageing behaviour and to differences in orientation between crystals. There was no significant difference between the ratio $\sigma_T/\sigma_{273}$ found when the temperature was raised and when it was lowered, thus no irreversible annealing or work softening occurred in these crystals. As crystal 1 showed such a marked yield drop at 77°K the ratio $\sigma_{77}/\sigma_{273}$ was also measured for the lower yield point. In this case the change of flow stress is only one-half that for the upper yield point. The values of the ratio $\sigma_T/\sigma_{273}$ for all the crystals tested are tabulated in table 5. Each value listed is the mean of at least four determinations.

Fig. 7

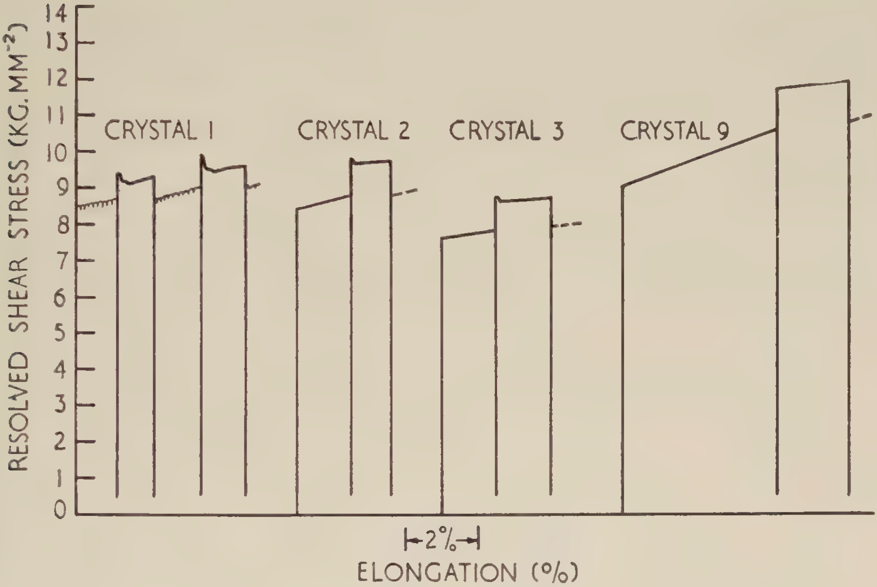

Portions of stress–elongation curves of crystals, 1, 2, 3 and 9, deformed alternately at 273°K and at 77°K.

The values are carried to four figures. The only error in the measurement of the ratio $\sigma_T/\sigma_{273}$ is due to measurement of the load and of the temperature.

Table 5. Flow Stress at Temperature $T$ Relative to that at 273°K

| Temperature | 77°K | 155°K | 196°K | 373°K |
|---|---|---|---|---|
| Crystal | | | | |
| 1 | 1·107<br>(1·054)† | — | — | 0·975 |
| 2 | 1·109 | — | 1·045 | 0·986 |
| 3 | 1·111 | 1·069 | 1·046 | 0·952 |
| 9 | 1·110 | — | — | — |

† Values for lower yield point.

The temperature was well controlled and the flow stress varies very slowly with temperature. Load values can be easily read to four significant figures in terms of the full-scale deflection on the Instron chart as unity.

Figure 8 shows a plot of the quantity $\sigma_T/\sigma_{273}$ against temperature. The average value for all crystals has been taken for each temperature. The ratio $\sigma_{77}/\sigma_{273}$ for the lower yield point of crystal 1 is also plotted. The change of flow stress with temperature is seen to be very small.

Fig. 8

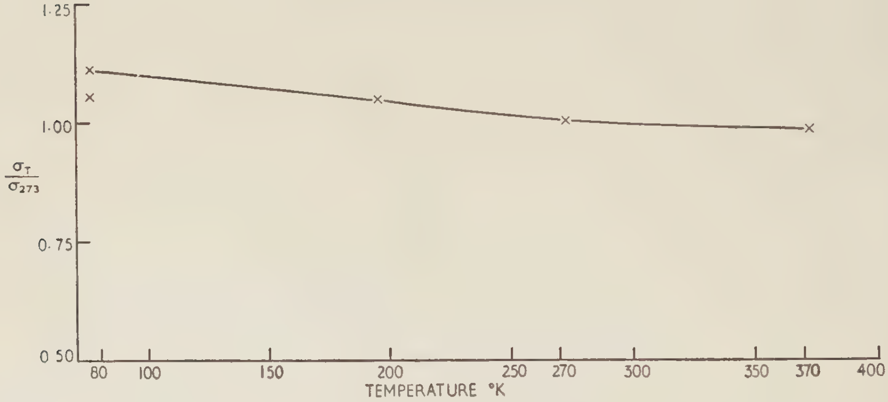

Plot of the quantity $\sigma_T\ \sigma_{273}$ against temperature for the fully cold-hardened alloy crystals. The two points at 77°K represent the values of the upper and lower yield points.

It is of interest to know how the temperature dependence of the flow stress compares with that of the elastic moduli for these crystals. Values of Young's modulus for a polycrystalline specimen of the same composition as the single crystals and quenched and aged in an identical manner were found at four temperatures from resonant frequency measurements using a dynamic method described by Fine (1957). The values obtained are shown in table 6. A plot was made of these and a smooth curve drawn through the points. By extrapolation and interpolation values of Young's modulus

Table 6. Values of Young's Modulus of an Alloy Polycrystal Aged 8 hours at 160°C

| Temperature (°K) | Young's Modulus ($10^3$ kg mm$^{-2}$) |
|---|---|
| 101 | 7·710 |
| 201·5 | 7·368 |
| 274·6 | 7·082 |
| 325·0 | 6·880 |

($E_T$) were found at the temperatures at which the tensile tests were made. Most dislocation theories of plastic flow relate the flow stress to the rigidity modulus rather than to Young's modulus. The variation of Young's modulus with temperature for these alloy crystals is identical with that of Young's modulus and of the rigidity modulus for pure aluminium, derived from the results of Sutton (1953) and of the same two quantities for Al–4% Cu alloys aged to contain Guinier–Preston zones (Byrne, private communication). Thus it can be assumed that the rigidity modulus and Young's modulus show the same variation with temperature in these alloys.

Table 7 compares the temperature variation of the quantity $\sigma_T/\sigma_{273}$ with $E_T/E_{273}$. The flow-stress ratio represents the maximum change with temperature, since values of the upper yield point were always taken when a yield drop was observed. It is seen that over the temperature range 77°K to 373°K the elastic modulus varies more with temperature than does the flow stress. From 77°K to 273°K the variation of the two quantities is about the same.

Table 7. Comparison of Values of $\sigma_T/\sigma_{273}$ and $E_T/E_{273}$

| Temperature | 77°K | 155°K | 196°K | 273°K | 373°K |
|---|---|---|---|---|---|
| Flow stress | 1·109<br>(1·054)† | 1·069 | 1·045 | 1·000 | 0·975 |
| Elastic modulus | 1·100 | 1·063 | 1·044 | 1·000 | 0·943 |

† Lower yield point.

By changing the temperature during deformation values of the quantity $\sigma_{77}/\sigma_{273}$ were found for crystal 14, which was reverted after ageing. The values are shown in table 4. It is seen that the ratio $\sigma_{77}/\sigma_{273}$ increases with elongation for small elongations but reaches a constant value at elongations greater than about 5%. This value is different from that of the fully cold-hardened crystals. Assuming the same variation of elastic moduli with temperature as that found in the crystals aged at 160°C, the flow stress varies between 77°K and 273°K about 8% more than do the elastic moduli.

### 3.4.2. *Pure aluminium crystals*

It is of interest to compare the temperature dependence of the flow stress in these alloy crystals containing Guinier–Preston zones with that of the pure matrix metal, aluminium. The temperature dependence of the flow stress of pure aluminium has been measured by Cottrell and Stokes (1955). However, the temperature dependence of the flow stress of pure copper single crystals has been measured in three investigations, Adams and Cottrell (1955), Makin (1958 b) Basinski (1959). The agreement is not very good. With th isin mind similar measurements to those carried out on the alloy crystals were made on three single crystals of pure aluminium. One of these (23) was slowly cooled and the other two, 21 and 22, were quenched from a temperature corresponding to about the same fraction of the melting point as the alloy crystals had been, to see if any effect due to the quenching is apparent. The CRSS of the slowly cooled crystal was 120 g/mm$^2$ and of crystals 21 and 22, 260 and 450 g/mm$^2$ respectively. No other difference was found between the behaviour of the three crystals. The ratio of the flow stress obtained at any two temperatures became constant after an elongation of a few per cent. Work softening was observed after 10% elongation and values of the ratio $\sigma_T/\sigma_{273}$ were then taken only for temperature transitions when the temperature was lowered. Figure 9

Fig. 9

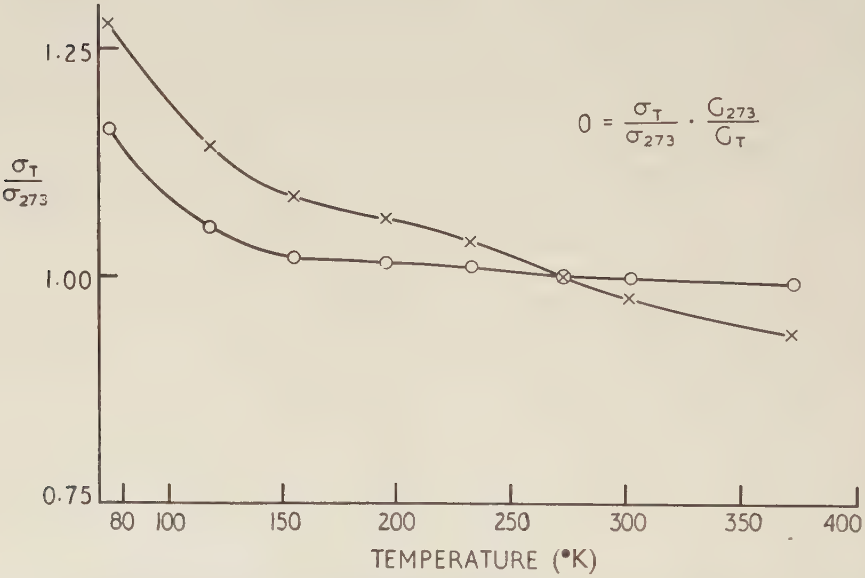

Plot of the quantity $\sigma_T/\sigma_{273}$ against temperature for pure aluminium single crystals, points X. Points O represent the quantity $\frac{\sigma_T}{\sigma_{273}} \cdot \frac{G_{273}}{G_T}$.

shows a plot of the quantity $\sigma_T/\sigma_{273}$ against temperature and of the quantity $\sigma_T/\sigma_{273} \cdot G_{273}/G_T$ where $G_T$ is the rigidity modulus at temperature $T$ calculated from Sutton's (1953) extensive data on aluminium crystals of similar purity to these used here. The results are very similar to those obtained by Cottrell and Stokes (1955) and by Basinski (1959). There is a sharp drop in the flow stress as the temperature increases from 77°K to 150°K and another slight fall between 240°K and 270°K; outside these temperature ranges the flow stress falls uniformly with rise in temperature at a rate a little faster than the decrease in the elastic moduli.

### 3.5. *Quenching Experiments*

The CRSS of these alloy crystals is about two orders of magnitude greater than that of pure aluminium crystals. This large increase in strength can be attributed to the presence within the alloy of the GP zones if other strengthening effects can be shown to be small. Two possible effects which come to mind are the strengthening of aluminium due to the presence of silver in solid solution and also the effect of quenching from the $\delta$-phase field. Quenching is always necessary in age-hardening alloys when it is desired to produce precipitate structures stable only at around room temperature or slightly above. In the case of the Al–Cu system the effect of copper in solid solution on the CRSS can be found by testing a reverted crystal (Kelly and Chiou 1958), i.e. one which has been aged at a low temperature and heated for a few minutes at about 200°C, when GP zones dissolve to give a supersaturated solid solution. Using this procedure the effects of quenching can be assumed to be eliminated. This procedure is not possible in these Al–Ag alloys because no heat treatment leading to complete reversion is known.

The effect of silver in solid solution on the CRSS of aluminium crystals is not detectable (Haessner and Schreiber 1957), but aluminium only dissolves silver to the extent of 0·16 at % at room temperature and the crystals used here contain 6 at %. In an attempt to evaluate the effects of the quench and of silver in solid solution the following experiments were performed.

Pure aluminium polycrystals quenched from 560°C to 0°C in a manner identical to that used with the alloys show no increase in initial flow stress, with respect to slowly cooled specimens. Polycrystals of the alloy were quenched from 560°C into iced brine and tested within 10 min of quenching at 258°K. They showed an initial flow stress of 4 kg mm$^{-2}$ and exhibited extremely rapid work hardening to a nominal tensile stress of *c.* 15 kg mm$^{-2}$, which is the value of the initial nominal tensile stress of polycrystals quenched and aged at room temperature. The same type of experiment was repeated on single crystals. The crystals had to be solution treated with the grips in place. The results were erratic, two crystals (10 and 12) showed a CRSS of *c.* 4 kg mm$^{-2}$ and one (number 7) a value of 0·6 kg mm$^{-2}$ at 258°K. All three showed extremely rapid work hardening at 258°K to a resolved shear stress of between 6 and 7 kg mm$^{-2}$, which is the same as the CRSS of crystals quenched and aged at room temperature. Quenching the specimens in this manner with the grips in place may lead to some deformation and hence to accelerated zone formation. The one crystal showing a CRSS of $0{\cdot}5\,\mathrm{kg\,mm^{-2}}$ is considered significant and indicates that the effect of 6 at % silver in solid solution is small. This conclusion is justifiable because all disturbing effects, such as quench hardening and plastic flow, during the quench will raise the CRSS rather than lower it.

## § 4. DISCUSSION

The values of the CRSS of the alloy crystals show the same relative change for different ageing conditions as are shown by the hardness values of other workers. The CRSS values of the fully cold hardened crystals are two orders of magnitude greater than those of pure aluminium crystals. From the results of Haessner and Schreiber and the quenching experiments reported here this increase in the flow stress must be attributed to the presence of GP zones in the alloy.

The temperature dependence of the strength is very small. In aluminium crystals a large temperature dependence of the flow stress is found, particularly below *c.* 150°K. This large temperature dependence is usually attributed to the thermally activated glide of dislocations through a forest of other dislocations threading the glide plane. This in general requires the formation of jogs in dislocation lines. Curves such as those in fig. 9 are interpreted (Seeger 1954) by writing the flow stress

$$\sigma = \sigma_G + \sigma_S$$

where $\sigma_G$ is supposed to depend on temperature as do the elastic moduli and $\sigma_S$ is due to the cutting process. Above a certain temperature the process of jog formation becomes so easy that $\sigma_S$ may be set equal to zero. We may take this temperature as about 155°K in the case of aluminium. We shall now show that the values of $\sigma_S$ are such that its contribution to the flow stress in these alloys will be inappreciable and we conclude from this that the density of the forest in these alloys, which is directly related to $\sigma_S$, is no greater than that in pure aluminium.

We have from the results for the pure aluminium crystals

$$\sigma_{77} = \sigma_{G(77)} + \sigma_{S(77)}$$

and

$$\sigma_{273} = \sigma_{G(273)}.$$

Whence

$$\frac{\sigma_{77}}{\sigma_{273}} = \frac{\sigma_{G(77)}}{\sigma_{G(273)}} + \frac{\sigma_{S(77)}}{\sigma_{G(273)}}$$

$$= 1{\cdot}10 + \frac{\sigma_{S(77)}}{\sigma_{G(273)}}.$$

The value of $\sigma_{77}/\sigma_{273} = 1{\cdot}28$ and the maximum value of the flow stress in aluminium crystals deformed at 273°K is *c.* $1{\cdot}5\,\mathrm{kg\,mm^{-2}}$ whence $\sigma_{S(77)}$ is at most equal to $0{\cdot}27\,\mathrm{kg\,mm^{-2}}$. This value is about 3% of the flow stress of the alloy crystals and hence is not observed in our experiments.

This conclusion is supported by the results on the reverted crystal shown in table 4 where, when the flow stress of the alloy is lower, a larger relative change of flow stress with temperature is detected.

In the case of pure aluminium the values of $\sigma_G$ and $\sigma_S$ increase together so that the ratio $\sigma_S/\sigma_G$ remains constant during deformation. In the alloy crystals the maximum increase in flow stress during deformation is *c.* 4·5 kg mm$^{-2}$ yet there is no evidence of the appearance of a component of the flow stress which depends more rapidly on temperature than do the elastic moduli. We conclude that the nature of the work-hardening processes is different in the alloy from that found in pure aluminium.

There is also a striking difference in the slip lines observed in these alloys compared to those seen in pure aluminium. The slip lines seen on a top surface are always very wavy and do not follow a single crystallographic plane. The explanation of this behaviour would seem to be that the screw components of dislocations are behaving approximately as if they are undissociated and hence not confined to motion on a single plane. This could arise from the very high stresses to which the crystals must be subjected before slip occurs. It is not known whether the screw dislocations move solely on close packed planes. If they do, the calculation of Schoeck and Seeger (1954) of the stress dependence of the activation energy for cross slip of a single screw dislocation should apply. These authors find that under a stress of 7·0 kg mm$^{-2}$ the activation energy for this process is 0·5 ev. This corresponds to an energy of 20 $kT$ at room temperature and 80 $kT$ at 77°K. The calculation is complicated; no account is taken of the decrease in separation of the partial dislocations under an applied stress and the model assumed may not correspond to the lowest activation energy (Friedel 1957), particularly because cross slip may occur easily at a jog and screw dislocations in quenched and aged Al–Ag alloys contain many jogs (Thomas, private communication). Thus, these figures for the activation energy correspond to an upper limit and the cross slip of single screws may well be occurring in this alloy.

We may now consider the mechanism of hardening. The material contains silver-rich clusters of atoms which are spherical in shape and a large fraction of the silver atoms are present in these clusters. Mott and Nabarro (1940) identify the flow stress of age-hardened alloys with the average internal shear stress due to the difference in size of atoms in the matrix and in the cluster. They evaluated the average for the case of spherical clusters which leads to

$$\sigma = 2G\epsilon f \quad . \quad . \quad . \quad . \quad . \quad . \quad . \quad . \quad . \quad . \quad . \quad (1)$$

where $\epsilon$ is a misfit parameter and $f$ is the volume fraction of clusters. If we evaluate this relation in the present case, assuming all the silver atoms are in the clusters, we find $\sigma = 2{\cdot}0$ kg mm$^{-2}$. This value is rather low compared to the observed CRSS of *c.* 9·0 kg mm$^{-2}$ in the fully cold-hardened state. According to eqn. (1) the flow stress should depend on temperature, as does the elastic modulus. The experiments show that the strength depends on temperature rather less than does the elastic modulus.

It has been proposed (Kelly and Fine 1957) that the strength of this alloy is due to a change in the number of like and unlike near neighbours, which tends to reverse the process of clustering, when a dislocation cuts through a cluster. The evidence that large numbers of dislocations cut through the clusters during deformation is very good (Jan 1955), and has been confirmed by experiments on single crystals in this laboratory. An estimate of the stress necessary to force a dislocation through the clusters (Kelly 1958) gives a stress of *c.* 7 kg mm$^{-2}$, which is close to that observed. This estimate uses the measured heat of reversion to calculate the change in energy on changing the number of Al–Ag near neighbours in the alloy. Apart from a small variation of flow stress with temperature equal to that of the lattice parameter no variation of flow stress with temperature is predicted. However, the free energy change on altering the number of like and unlike bonds across the slip plane would be expected to show a decrease with increasing temperature due to the existence of an entropy term (Fine, private communication).

The small temperature dependence of the flow stress in these Al–Ag alloys is in very marked contrast to that shown by Al–Cu alloys containing GP I zones (Kelly and Chiou 1958), which shows a large temperature dependence of the flow stress below about 160°K. This difference can be readily understood because of the difference in shape of the zones. In Al–Cu the zones have the shape of a plate and in one dimension are only one atom thick. In the Al–Ag case the zones are spherical and about fourteen atoms in diameter. A calculation due to Liebfried (1956) convinces one that thermal fluctuations are quite unable to provide the necessary activation energy to appreciably reduce the stress necessary to force a dislocation through the zones in Al–Ag, but could do so in Al–Cu.

## ACKNOWLEDGMENTS

The authors are very grateful to Professor M. E. Fine for constant encouragement and helpful discussion. This work was supported by the U.S. Air Force under Contract No. AF 18(600)1468.

## REFERENCES

ADAMS, M. A., and COTTRELL, A. H., 1955, *Phil. Mag.*, **46,** 1187.
BASINSKI, Z. S., 1959, *Phil. Mag.*, **44,** 393.
BELBEOCH, B., and GUINIER, A., 1955, *Acta Met.*, **3,** 370.
COTTRELL, A. H., and STOKES, R. J., 1955, *Proc. roy. Soc.* A, **243,** 17.
DIEHL, J., 1956, *Z. Metallk.*, **47,** 411.
ELAM, C. F., 1927, *Proc. roy. Soc.* A, **115,** 133.
FINE, M. E., 1957, *Rev. Sci. Instrum.*, **28,** 643.
FRIEDEL, J., 1957, *Dislocations and Mechanical Properties of Crystals* (New York: Wiley), p. 555.
GEISLER, A. H., BARRETT, C. S., and MEHL, R. F., 1943, *Trans. Amer. Inst. min. (metall.) Engrs*, **152,** 182.
HAASEN, P., and KELLY, A., 1957, *Acta. Met.*, **5,** 192.
HAESSNER, F., and SCHREIBER, D., 1957, *Z. Metallk.*, **48,** 263.
JAN, J-P., 1955, *J. appl. Phys.*, **26,** 1291.

Kelly, A., 1958, *Phil. Mag.*, **3,** 1472.
Kelly, A., and Chiou, C., 1958, *Acta. Met.*, **6,** 565.
Kelly, A., and Fine, M. E., 1957, *Acta Met.*, **5,** 365.
Köster, W., and Braumann, F., 1952, *Z. Metallk.*, **43,** 193.
Leibfried, G., 1956, *Dislocations and Mechanical Properties of Crystals* (New York : Wiley), p. 495.
Low, J. R., and Guard, R. W., 1959, *Acta Met.*, **7,** 171.
Makin, M. J., 1958 a, *Phil. Mag.*, **3,** 309; 1958 b, *Ibid.*, **3,** 287.
Maddin, N., and Chen, N. K., 1954, *Progr. Met. Phys.*, **5,** 53.
Mott, N. F., and Nabarro, F. R. N., 1940, *Proc. phys. Soc. Lond.*, **52,** 86.
Sato, S., and Kelly, A., 1959, *Trans. Amer. Inst. min.* (*metall.*) *Engrs*, **215,** 413.
Schmid, E., and Boas, W., 1950, *Plasticity of Crystals* (London : Hughes).
Schoeck, G., and Seeger, A., 1954, *Rep. Conf. Defects in Crystalline Solids* (London : The Physical Society), p. 340.
Seeger, A., 1954, *Phil. Mag.*, **45,** 771.
Staubwasser, W., 1959, *Acta Met.*, **7,** 43.
Sutton, P. M., 1953, *Phys. Rev.*, **91,** 816.
Walker, C. B., and Guinier, A., 1953, *Acta Met.*, **1,** 568.

# CORRESPONDENCE

## Lattice Vibrational Spectrum of Sodium Chloride†

By J. R. Hardy‡
H. H. Wills Physics Laboratory, University of Bristol

[Received November 10, 1959]

The advent of diffuse x-ray and inelastic neutron scattering as means of studying the lattice vibrations of crystals has given a new impetus to theoretical work in this field. The normal modes are plane waves whose angular frequencies $\omega_i$, for a wave vector $\mathbf{q}$, are given by the roots of the equation, first deduced by Born and von Kármán (1912):

$$\left| \begin{Bmatrix} K & K' \\ \alpha & \beta \end{Bmatrix}_{\mathbf{q}} - \omega^2 \delta_{\alpha\beta} \delta_{KK'} \right| = 0 \qquad . \quad . \quad . \quad . \quad . \quad \text{(i)}$$

$\alpha$ (or $\beta$) = 1, 2, 3 denotes a set of orthogonal Cartesian axes, and $K$ (or $K'$) = 1, . . . . , $n$, denotes the $n$ constituent Bravais lattices. The matrices

$$\begin{Bmatrix} K & K' \\ \alpha & \beta \end{Bmatrix}_{\mathbf{q}}$$

depend on the interatomic force constants, and recent theoretical work has been concerned with the determination of these constants from the experimental $\omega$ v. $\mathbf{q}$ dispersion curves for waves travelling along directions of high crystal symmetry. Examples of such work are provided by that of Foreman and Lomer (1957) on aluminium and Cole and Kineke (1958) on germanium and silicon.

Once the force constants are known the distribution function $N(\omega)$, or number of normal modes per unit frequency at $\omega$, can be found by solving eqn. (i) for a representative sample of points in $\mathbf{q}$ space. However, the foregoing results are not consistent with any very simple models of the crystals in question.

The aim of this communication is to present $N(\omega)$ v. $\omega$ distribution curves for sodium chloride based on two fairly simple models of the crystal, which are, however, more realistic than that used earlier by Kellermann (1940). He assumed the crystal to be composed of rigid point charges, held apart by nearest neighbour repulsion. The second assumption is supported by Löwdin's (1948) theoretical work and is retained. The modification introduced here is the inclusion of the effect of the dipole moment which each ion acquires when displaced from its equilibrium position. This may be split into two parts, the first of which arises because the displaced ion is in an electric field. The second part arises from the redistribution of charge about an ion when it is displaced relative to its nearest neighbours. To the first order this can be described by a point dipole associated with each sodium–chlorine bond situated at the centre of the chlorine ion and the size of which is proportional to the repulsive potential. This is the 'deformation' dipole first introduced by Szigeti (1950). Two frequency spectra have been calculated from these assumptions. That in fig. 1 results when the 'deformation' dipoles are neglected and each ion is assumed to acquire a dipole moment given by the product of its polarizability in the crystal (as given by Shockley 1946) and the field. The spectrum in fig. 2 is calculated including both effects, the magnitude of the 'deformation' dipoles being chosen, following Szigeti, to fit the observed

---

† Communicated by Professor M. H. L. Pryce, F.R.S.

‡ Now A.E.I. Research Fellow, Physics Research Laboratory, University of Reading.

Fig. 1

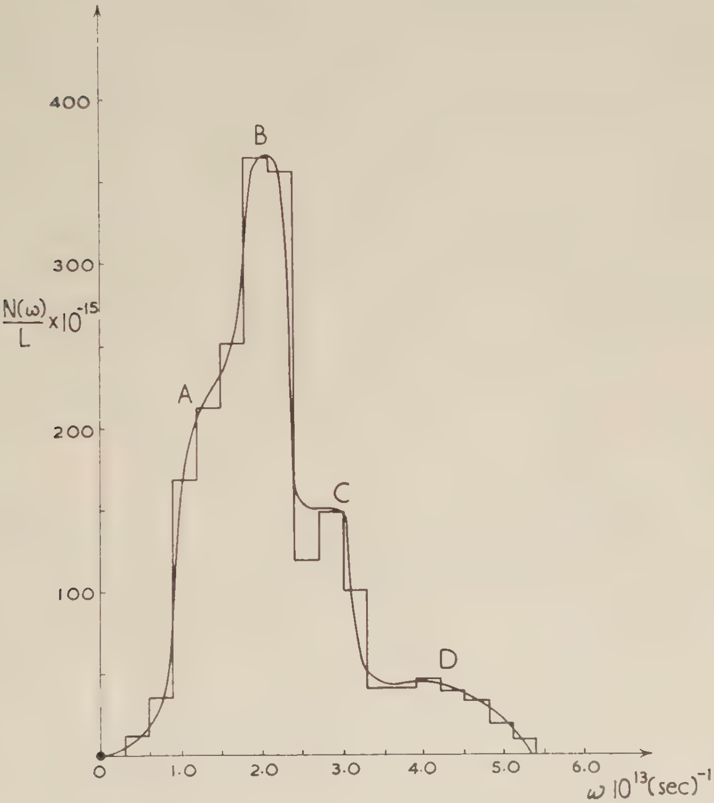

The frequency spectrum of the lattice vibrations of sodium chloride calculated omitting 'deformation' dipole effects.

ratio of the static and optical frequency dielectric constants and the value of the infra-red dispersion frequency.

All the data used are room temperature data and the sample of points in **q** space is the same as that used by Kellermann. It is thus possible to use his values for the Coulomb parts of

$$\begin{Bmatrix} K & K' \\ \alpha & \beta \end{Bmatrix}_{\mathbf{q}}$$

but the repulsive parts are taken from Karo's (1957) data which embody an improved value of the compressibility ($4{\cdot}26 \times 10^{-12}$ cm$^2$/dyne). The smooth curves are inferred from the histograms obtained by counting the number of modes in each interval of $0{\cdot}3 \times 10^{13}$ sec$^{-1}$ (the curves refer to one mole containing $L$ ion pairs). The van Hove (1953) singularities are not apparent with this small sample of points. One can, however, distinguish

Fig. 2

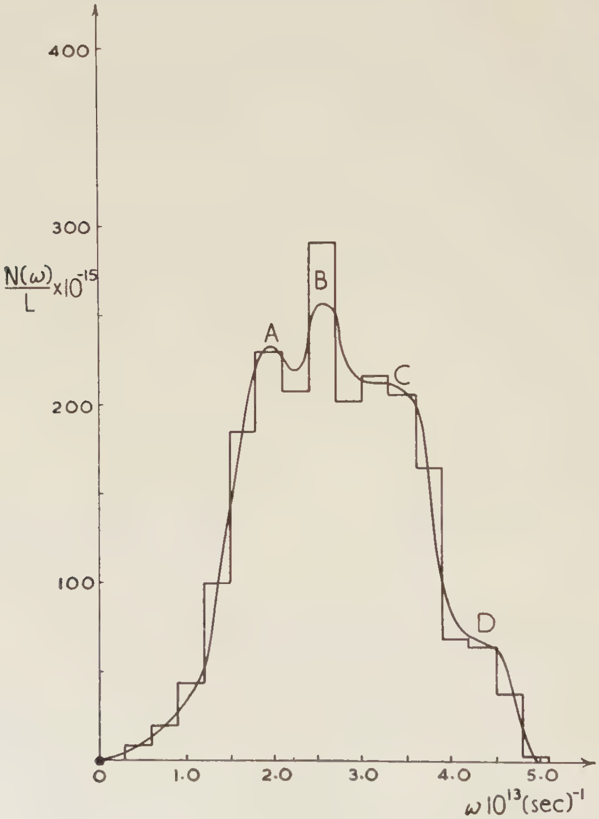

The frequency spectrum of the lattice vibrations of sodium chloride when 'deformation' dipole effects are included in the calculation.

in fig. 1 the shoulders A and C caused respectively by transverse and longitudinal acoustic modes, and the maxima B and D due to the corresponding optical modes. Figure 2 is less clear, although A and D definitely arise from transverse optical and longitudinal acoustic modes respectively, but B and C are due to a superposition of transverse optical and longitudinal acoustic modes, C probably being associated with the former. The importance of the 'deformation' dipole effect is most clearly shown by the displacement of this peak (corresponding to B in fig. 1). This suppresses the sharp rise in $N(\omega)$ for small $\omega$ and produces a close similarity to Kellermann's curve in this region. This supports the second model, as Kellermann's spectrum reproduces the observed low temperature effective Debye temperatures very well, which indicates that the low frequency part is correct. However, Lundqvist *et al.* (1959) have shown that if absolute zero data are used, this agreement is no longer present. They introduce an 'effective' charge independent of $\mathbf{q}$ and thus obtain better agreement. The resulting spectrum is very different from fig. 2 as the 'deformation' mechanism is equivalent to introducing an 'effective' charge which depends on $\mathbf{q}$. This seems more consistent, but to test this model in the same way one must use absolute zero data throughout. A more direct test would be an experimental determination of $\omega$ v. $\mathbf{q}$ curves for specific directions similar to the work on germanium, etc. If this could be done at room temperature, the results could be related directly to the theoretical work described here.

## ACKNOWLEDGMENTS

I should like to thank Professor M. H. L. Pryce, F.R.S., Dr. A. M. Karo, and the Bristol Aircraft Company's Computer Division for their help during this work, and to express my gratitude to the Department of Scientific and Industrial Research for the Research Studentship which made this work possible.

## REFERENCES

BORN, M., and VON KÁRMÁN, TH., 1912, *Phys. Z.*, **13,** 297.
COLE, H., and KINEKE, E., 1958, *Phys. Rev. Letters*, **1,** 360.
FOREMAN, A. J. E., and LOMER, W. M., 1957, *Proc. phys. Soc., Lond.* B, **70,** 1143.
KARO, A. M., 1957, *Quart. Rep., M.I.T. Solid State Group*, **24,** 20 (and private communication).
KELLERMAN, E. W., 1940, *Phil. Trans. roy. Soc.* A, **238,** 513 (see also BORN, M., and HUANG, K., 1954, *Dynamical Theory of Crystal Lattices* (Oxford).
LÖWDIN, P. O., 1948, *A theoretical Investigation into Some Properties of Ionic Crystals* (Uppsala: Almqvist and Wiksells).
LUNDQVIST, S. O., LUNDSTRÖM, V., TENERZ, E., and WALLER, I., 1959, *Ark. Fys.*, **15,** 193.
SZIGETI, B., 1950, *Proc. roy. Soc.* A, **204,** 51.
SHOCKLEY, W., 1946, *Phys. Rev.*, **70,** 105 A.
VAN HOVE, L., 1953, *Phys. Rev.*, **89,** 1189.

## An Extension of Boltzmann's *H*-Theorem

By S. Simons and P. J. Higgins
Queen Mary College, University of London

[Received July 16, 1959]

We proceed to extend Boltzmann's $H$-Theorem, showing that the entropy of an assembly of gas molecules can never decrease, to the case when the gas is enclosed in a finite vessel, whose walls act as rigid boundaries scattering the incident molecules in any prescribed manner. To deal with the boundary scatter at a general point $\mathbf{R}$ of the surface, we shall call the velocity $\mathbf{v}$ of a molecule positive if it approaches the surface, and negative if it leaves it. Then for positive values of $\mathbf{v}$ and $\mathbf{w}$, there is a probability $P(\mathbf{w},\mathbf{v},\mathbf{R})\,d\mathbf{v}$ of a molecule incident at $\mathbf{R}$ with velocity $\mathbf{w}$ being scattered into a state with velocity lying in the range $d\mathbf{v}$ about $-\mathbf{v}$. It follows that since energy is conserved in boundary collisions, $P(\mathbf{w},\mathbf{v},\mathbf{R})$ will be non-zero only if $v=w$, and from the definition of probability

$$\int' P(\mathbf{w},\ \mathbf{v},\ \mathbf{R})\,d\mathbf{v}=1 \quad . \quad . \quad . \quad . \quad . \quad . \quad . \quad . \quad (1)$$

for all $\mathbf{w}$ and $\mathbf{R}$, where $\int' d\mathbf{v}$ implies that the integral is taken over all positive values of $\mathbf{v}$. The function $P(\mathbf{w},\mathbf{v},\mathbf{R})$ must satisfy the analogue of the general principle of microscopic reversibility (Garcia-Moliner and Simons 1957) which states that if the molecules are equally distributed in position-velocity phase space, then the rate of transitions from $\mathbf{w}$ to $-\mathbf{v}$ equals that from $\mathbf{v}$ to $-\mathbf{w}$; that is

$$w'(\mathbf{R})\,P(\mathbf{w},\mathbf{v},\mathbf{R})=v'(\mathbf{R})\,P(\mathbf{v},\mathbf{w},\mathbf{R}), \quad . \quad . \quad . \quad . \quad . \quad (2)$$

where $v'(\mathbf{R})$, $w'(\mathbf{R})$ are respectively the magnitudes of the components of $\mathbf{v}$ and $\mathbf{w}$ normal to the surface at $\mathbf{R}$.

If $f(\mathbf{v},\mathbf{r},t)\,d\mathbf{v}\,d\mathbf{r}$ is the number of gas molecules which at time $t$ are situated in the volume element $d\mathbf{r}$ about $\mathbf{r}$ and have velocities lying in the range $d\mathbf{v}$ about $\mathbf{v}$, then we readily see from the definition of $P(\mathbf{w},\mathbf{v},\mathbf{R})$ and from eqn. (2), that at the boundary point $\mathbf{R}$, $f(\mathbf{v},\mathbf{r},t)$ will satisfy

$$f(-\mathbf{v},\mathbf{R},t)=\int' P(\mathbf{v},\mathbf{w},\mathbf{R})f(\mathbf{w},\mathbf{R},t)\,d\mathbf{w}. \quad . \quad . \quad . \quad . \quad (3)$$

The general principles of statistical mechanics give the entropy $S$ for our system in the form $S=-kH$ where $k$ is Boltzmann's constant and

$$H=\iint f(\mathbf{v},\ \mathbf{r},\ t)\ln f(\mathbf{v},\ \mathbf{r},\ t)\,d\mathbf{v}\,d\mathbf{r}, \quad . \quad . \quad . \quad . \quad . \quad (4)$$

the integral being taken over *all* velocities and throughout the volume of the enclosed gas. We now proceed to prove Boltzmann's $H$-Theorem, which states that $(\partial H/\partial t)\leqslant 0$, equality being attained only when the gas possesses the Maxwell distribution. From eqn. (4) we have

$$\partial H/\partial t=\iint(\ln f+1)(\partial f/\partial t)_c\,d\mathbf{v}\,d\mathbf{r}-\iint \mathbf{v}\,.\,\mathrm{grad}\,(f\ln f)\,d\mathbf{v}\,d\mathbf{r}, \quad . \quad (5)$$

making use of the Boltzmann transport equation, which in the absence of external forces takes the form $(\partial f/\partial t) = (\partial f/\partial t)_c - \mathbf{v} \, . \, \mathrm{grad} \, f$, where $(\partial f/\partial t)_c$ is the rate of change of $f$ due to intermolecular collisions. Now it is shown in the usual proof of the $H$-Theorem (Chapman and Cowling 1952), that owing to the explicit form taken by $(\partial f/\partial t)_c$, the first term on the right-hand side of eqn. (5) is always less than or equal to zero. It therefore remains for us to show that

$$\int\int \mathbf{v} \, . \, \mathrm{grad} \, (f \ln f) \, \mathbf{dv} \, \mathbf{dr} \geqslant 0. \qquad . \quad . \quad . \quad . \quad . \quad . \quad . \quad (6)$$

To prove this, we employ the inequality that for all $x \geqslant 0$, $x \ln x - x + 1 \geqslant 0$. We then let $x = f(\mathbf{w}, \mathbf{R}, t)/f(-\mathbf{v}, \mathbf{R}, t)$, when multiplying the resultant inequality by $v'(\mathbf{R}) \, P(\mathbf{v}, \mathbf{w}, \mathbf{R}) \; f(-\mathbf{v}, \mathbf{R}, t)$, and integrating over all positive $\mathbf{v}$ and $\mathbf{w}$ with fixed moduli $v = w = k$, we obtain

$$\int v' f(\mathbf{v}, \mathbf{R}, t) \ln f(\mathbf{v}, \mathbf{R}, t) \, \mathbf{dv} \geqslant 0, \qquad . \quad . \quad . \quad . \quad . \quad . \quad . \quad (7)$$

making use of eqns. (1), (2) and (3), where the integration is now taken over both positive and negative values of $\mathbf{v}$ with $v = k$. It follows from the inequality (7) that $\int_S \int v' f \ln f \, \mathbf{dv} \, dS \geqslant 0$, where $dS$ is an element of the surface $S$ enclosing the gas, and where the $\mathbf{v}$ integration is now over *all* values of $\mathbf{v}$. Hence, by Green's theorem, the inequality (6) holds and from eqn. (5), $\partial H/\partial t \leqslant 0$. It readily follows that if any other distribution is imposed on the gas molecules, this distribution will alter with continual production of entropy until a Maxwell distribution with zero mean gas velocity is attained.

### REFERENCES

CHAPMAN, S., and COWLING, T. G., 1952, *The Mathematical Theory of Non-Uniform Gases*, chapter 4 (Cambridge : University Press).
GARCIA-MOLINER, F., and SIMONS, S., 1957, *Proc. Camb. phil. Soc.*, **53,** 848.

---

## Electrical Resistance in Liquid Metals and the Change on Melting

By D. K. C. MACDONALD
Division of Pure Physics, National Research Council, Ottawa

[Received August 10, 1959]

THE interpretation of the resistance increase which, apart from one or two 'pathological' cases, is normally observed when a metal melts, has been discussed in the past by Simon (1924) and Mott (1934) in particular. Essentially it would appear that Mott ignored any direct influence of spatial disordering at the melting point on the resistance, and assumed rather that the increase could be accounted for by the reduction in the characteristic temperature, $\theta$, in the liquid state. That is, ignoring any anharmonic effects, if we write for the resistance $R = CT/M\theta^2$ where $C$ is an electron-lattice coupling constant and $M$ is the atomic mass, then, assuming that $C$ remains more or less unchanged, an increase of resistance by typically a factor of 1·5 to 2 on melting could be accounted for by a drop in $\theta$ of about 20% to 40%. At the Ottawa Conference (Ottawa 1956) there was some discussion of this topic and at that time MacDonald suggested that perhaps one could equally well account for the increase in resistance in terms of the generation of something rather less than 5% of lattice 'vacancies' on melting. This interpretation would rest essentially on the assumption that the increased resistance was due primarily to spatial disorder occurring at the melting point, rather than to change of $\theta$.

It would appear of some interest to be able to assess more definitely what role each of these mechanisms plays in the resistance of the liquid state and particularly so also because recently Bernal has suggested that essentially the liquid state may be regarded as an entirely random assembly of atoms, the only correlation or 'order' occurring because of the necessity to fit atoms into the available space. An attempt was made here some years ago to measure the variation with temperature of resistance at *constant volume* in the liquid state, since this should then enable one to distinguish with some certainty between the component of resistance on the one hand due to thermal lattice vibrations (and hence dependent directly on an effective $\theta$) and on the other hand any additional 'residual' resistance introduced at the melting point (and hence presumably to be assigned to a specific increase in spatial atomic disorder). Some attempts were made to measure the electrical resistivity of some of the alkali metals by using a sealed capillary method as suggested by Gubar and Kikoin (1945) who suggested this method for experiments on the resistance of liquid mercury†. The results we obtained were by no means entirely satisfactory in all cases, but a fairly typical set of data are shown in fig. 1 and from this, as indicated

---

† Gubar and Kikoin in fact also mention that "experiments carried out by us with alkali metals in liquid state have shown that for them also the temperature coefficient of resistance at constant volume is lower than that commonly determined at constant pressure, but this decrease is not so great as for mercury". This accords qualitatively with our findings but we have not yet come across the detailed publication of their work on the liquid alkali metals.

Gubar and Kikoin's results on mercury seem interesting in themselves. The resistance of mercury is rather anomalous (cf. Mott and Jones, 1936, p. 278) in that the liquid resistance is around four times greater than that of the solid while in other metals the resistance increase on melting is a factor of about 1·5 to 2; this contributes to a considerably smaller electron mean free path in liquid mercury than one might expect in other liquid metals. Now the temperature coefficient of resistance at constant volume in liquid mercury is found by Gubar and Kikoin to be very small and, it appears, even negative. Ignoring here any particular significance of a negative resistance coefficient in the liquid, the *small* temperature coefficient of resistance would suggest, in terms of our discussion, that the component of resistance due to spatial disorder is dominant in liquid mercury. This conclusion therefore appears concordant with the very fact of a short electron mean free path in liquid mercury.

Fig. 1

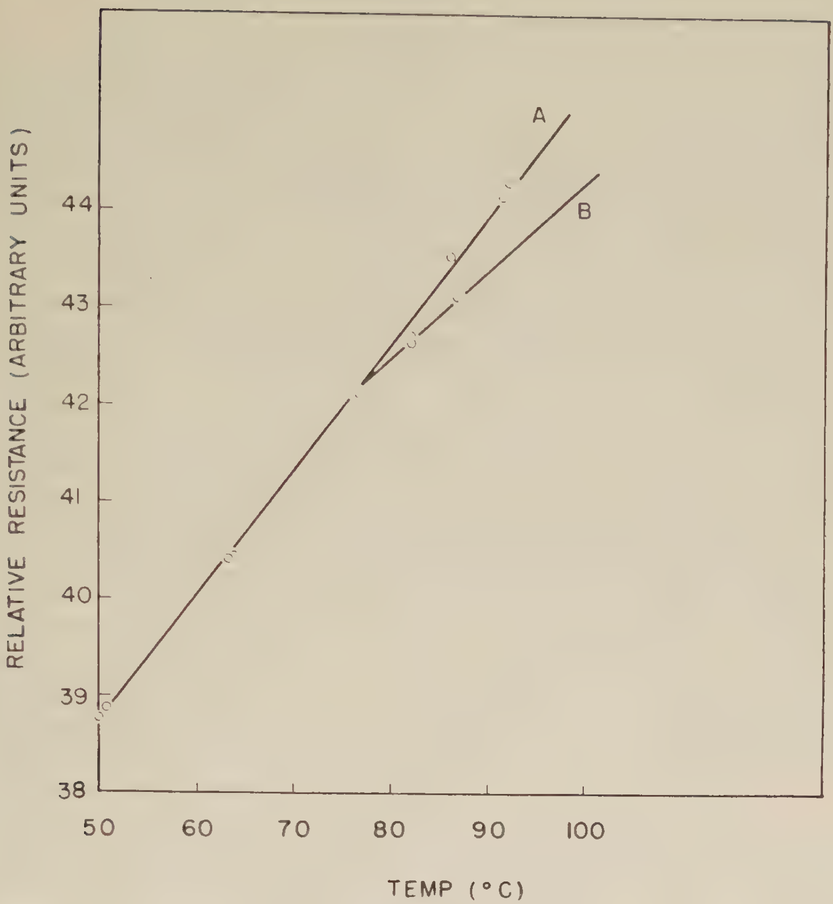

Resistance as measured of rubidium sample (experiment : April 19, 1954) in liquid state. A, resistance at constant pressure ($p \sim 0$) ; B, resistance at constant volume.

Fig. 2

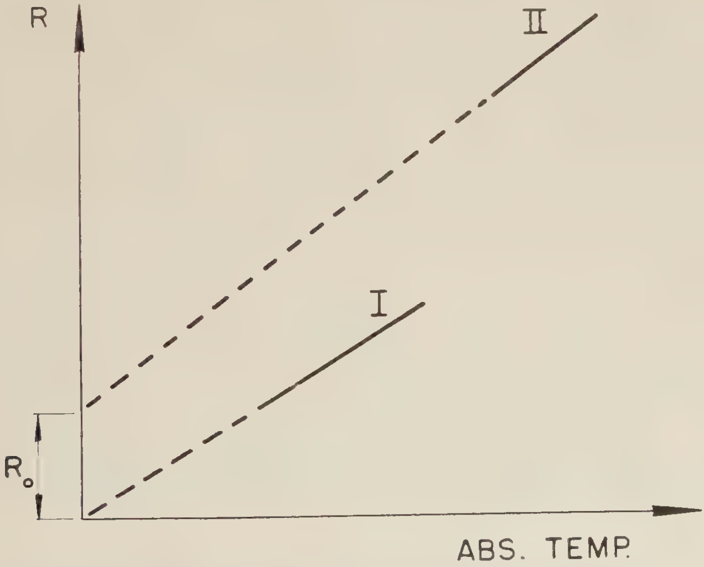

Rough sketch of resistance of pure metal in solid and liquid states. I, resistance in solid state ; extrapolates approximately to zero at absolute zero for pure metal. II, resistance at constant volume in liquid state ; extrapolation to absolute zero indicates 'residual' resistance, $R_o$.

in fig. 2, we can estimate that an apparent additional residual resistance amounting to around one-quarter of the total change of resistance on melting is introduced there. Such results as we obtained on the other alkali metals appeared not inconsistent with this estimate.

It is suggested therefore that in considering the electrical resistance of the liquid state both spatial disorder *and* the change of $\theta$ must be taken into account, and that the influence of the former is by no means negligible. All this of course assumes that a quasi band model of the electrical resistance is justified in some sense for discussing the resistance in the liquid state.

### References

Gubar. S., and Kikoin, I., 1945, *J. Phys., Moscow*, **9**, 52.
Mott, N. F., 1934, *Proc. roy. Soc.* A, **146**, 465.
Mott, N. F., and Jones, H., 1936, *Theory of Properties of Metals and Alloys*, (Oxford: University Press).
Ottawa, 1956, *Canad. J. Phys.*, **34**, 1341 (Proc. Int. Conf. on Electron Transport . . . special issue No. 12A, 1956).
Simon, F. E., 1924, *Z. Phys.*, **27**, 157.

---

## Facets and Anomalous Solute Distributions in Indium–Antimonide Crystals

By K. F. Hulme and J. B. Mullin
Ministry of Supply, Royal Radar Establishment,
Great Malvern, Worcestershire

[Received September 28, 1959]

We have found that, during the growth of InSb crystals from the melt, the presence of a planar crystallographic {111} facet at the solid liquid interface can profoundly affect the solute distribution in the growing solid. The effect is not due to a solute-enriched boundary layer existing because of inadequate stirring, but to a genuine difference in $k^*$, the distribution coefficient on and off a {111} facet ($k^*$ = ratio of solute concentrations in solid and liquid *at the interface*, under the given growth conditions; see eqn. 13, Burton *et al.* 1953). The difference can be large for Te, and for a residual donor impurity (which might also be Te).

Our evidence was obtained from crystals pulled from the melt by the Czochralski technique using rotation rates of $\sim 100$ r.p.m., pull rates of $\sim 2$ cm/hr and seed crystals oriented close to a $\langle 111 \rangle$ direction.

The ends of these crystals when parted from the residual melt by a sharp increase in pull rate often showed a planar facet on an otherwise curved surface. X-ray orientation determinations have shown that, with one exception so far, the facets are {111} planes; we have observed a {100} facet on a heavily twinned crystal, but have not attempted to determine the effect of {100} facets on solute distributions. The facet sizes ranged from ~2 mm to ~3 cm diameter, depending on the general interface curvature (the solid interface is convex in our case, at least in the final stages of crystal growth). If the seed is slightly off the ⟨111⟩ orientation the facet is off-axis (see fig. 1, Pl. 155); the rings on the end are thought to be associated with the way in which the rotating crystal parted from the melt rather than a true growth feature.

The autoradiograph shown in fig. 2 (Pl. 155) is a section parallel to the growth axis of a single crystal doped with radio-Te. The Te is concentrated on one side of the crystal: the straight lines present in the area of enhanced concentration were found to be parallel to a {111} plane, and are attributed to fluctuations in the growth conditions; they indicate that a {111} facet was present during growth at one side of the interface. The end of this crystal showed a facet at the appropriate side. The donor concentrations obtained by Hall constant measurements were $1{\cdot}5 \times 10^{19}$ and $2{\cdot}4 \times 10^{18}$ per $\mathrm{cm}^3$ respectively in and out of the Te-enhanced region—thus Te is in true atomic solution in both regions. On the basis of previous measurements of distribution coefficients (Mullin 1958, Strauss 1959) and the concentration ratio of ~6 quoted above, we conclude that, for growth rates of ~2 cm hr $k^* \sim 3$ on a {111} facet and $k^* \sim 0{\cdot}5$ off a facet—a striking difference, the values being on opposite sides of unity; the value of ~0·9 obtained with polycrystalline material (Harman 1956, Hulme and Mullin 1957, Mullin and Hulme 1958) represents a weighted mean.

For a series of undoped crystals, regions were often found, in slices taken perpendicular to the growth direction, in which the donor concentrations were 6–15 times greater than the donor concentrations in adjacent regions of the slice. In two crystals where slices were taken close to the ends which showed {111} facets the area of high donor concentration corresponded in size and position to the facet. In these two cases the melt was vigorously swirled in the opposite direction to the crystal rotation, by means of a 400 cycle rotating magnetic field; the effect cannot, therefore, reasonably be ascribed to inadequate stirring. In two other crystals, a single twin grew, in which the growth direction was now almost ⟨511⟩; in slices showing both orientations the {111} area showed the usual high donor density region surrounded by a low donor density region whereas the twinned area, on which a {111} facet would not be expected to appear, was uniform and had low donor concentration. These observations indicate that $k^*$ for the residual donor impurity is also markedly different on and off a {111} facet.

InSb belongs to the point group $\bar{4}3m$ and faces of the form $\{\bar{1}\bar{1}\bar{1}\}$ show etch pits in CP4, whereas faces of the form {111} do not (Allen 1957, Dewald 1957). All the observations quoted apply to crystals in which the face exposed to the melt did not show etch pits and was therefore {111}; reliable information on $\{\bar{1}\bar{1}\bar{1}\}$ facets is at present lacking.

As far as the authors are aware the possible importance of facets on segregation in melt-grown crystals has not been previously demonstrated

—although for Ge there have been indications (Burton, Kolb, Slichter and Struthers 1953, Burton, Prim and Slichter 1953, Hall 1953) of ~10% variations in $k$ with growth direction. In crystal growth from aqueous solution the effect is well known (i.e. 'hour-glass' crystals, Buckley 1951). It must be attributed to differential adsorption on the interface and the values of $k^*$ on $\{111\}$ facets will be expected to depend markedly on growth rate, and perhaps on concentration. The values of $k^*$ off a $\{111\}$ facet might be expected to depend to a lesser extent on interface orientation, growth rate, and concentration. It would be interesting to know whether there are other examples of the effect in melt-grown crystals as clearly manifested as that involving Te in InSb, and whether $\{100\}$ and other facets are important. This work will be published in greater detail together with further observations in due course.

## ACKNOWLEDGMENTS

It is a pleasure to acknowledge the experimental contributions of O. Jones and W. H. E. Wilgoss and the assistance of J. Wright, J. Elcox, M. Crofts and M. Stevens, and also valuable discussions with Dr. W. Bardsley.

This letter is published by permission of the Controller, H.B.M. Stationery Office.

## REFERENCES

ALLEN, J. W., 1957, *Phil. Mag.*, **2,** 1475.

BUCKLEY, J. E., 1951, *Crystal Growth* (London : Chapman & Hall), p. 416.

BURTON, J. A., PRIM, R. C., and SLICHTER, W. P., 1953, *J. chem., Phys.*, **21,** 1987.

BURTON, J. A., KOLB, E. D., SLICHTER, W. P., and STRUTHERS, J. D., 1953, *J. chem. Phys.*, **21,** 1991.

DEWALD, J. F., 1957, *J. electrochem. Soc.*, **104,** 244.

HARMAN, T. C., 1956, *J. electrochem. Soc.*, **103,** 128.

HALL, R. N., 1953, *J. phys. Chem.*, **57,** 86.

HULME, K. F., and MULLIN, J. B., 1957, *J. Electron. Contr.*, **3,** 160.

MULLIN, J. B., and HULME, K. F., 1958, *J. Electron. Contr.*, **4,** 170.

MULLIN, J. B., 1958, *J. Electron. Contr.*, **4,** 358.

STRAUSS, A. J., 1959, *J. appl. Phys.*, **30,** 559.

# REVIEWS OF BOOKS

*Ferrites.* By J. Smit and H. P. J. Wijn. (Philips Technical Library, 1959.) [Pp. 369.] 72*s*.

This is a most welcome book, filling an important gap in the technological literature. It presents a simply written account of the properties of the large class of magnetic oxides known as ferrites, starting from the basic concepts in magnetism and ending with a wide selection of experimental results on actual materials which are of interest for practical applications. As such it is a book which will be of greater interest to engineers than to theoretical physicists, but everyone concerned with ferromagnetism will find it a useful, and so far unique, summary of the experimental results and theoretical ideas. In some parts the choice of material is rather biased towards the work done in the authors' own laboratories, the Philips Research Laboratories at Eindhoven, where ferrites were first developed under Snoek over twenty years ago, and where much has been done since. This bias is freely admitted in the preface and it is largely offset by an authoritative handling of the facts which are presented, but the uninitiated reader may gather a somewhat distorted picture of present day trends in this field. For example garnets are discussed in four pages and there is no discussion of the important recent advances in the methods of growing single crystals, which have made possible such devices as parametric microwave amplifiers. In any book dealing with a field expanding as rapidly as ferromagnetism it is necessarily very difficult to cover all the latest advances and it would be useful to have an explicit statement giving the last date covered, together with a list of omitted topics and further references. This book is profusely illustrated with both diagrams and experimental results and it is well produced. W. P. W.

*Vector Space.* By M. J. Buerger. (New York: John Wiley & Sons, Inc., 1959.) [Pp. 347.] 96*s*.

The experimental data obtained from a crystal by x-ray diffraction depend on the crystal structure, but cannot immediately be transformed to give this structure, since only the intensities and not the phases of the diffracted x-ray beams can be measured. It was, however, shown by A. L. Patterson some twenty-five years ago that a Fourier transformation of the intensities (corrected for certain geometrical factors) in principle gives the interatomic vectors in the crystal. This book deals with methods by which the positions of the atoms can in turn be deduced from the Patterson function. It is definitely a book for the specialist in crystal structure analysis; for example, it contains only one reference to another text book (by the same author). Within these limits, it is a clear and comprehensive account which should be read by every crystallographer. It is to be hoped that the book may sometime also fall into the hands of a topologist, who might thereby be stimulated to study the problem of when a point set (the crystal structure) is uniquely determined by its vector set (the Patterson function).

Professor Buerger's account of the historical development of the subject is not entirely chronological; the work of Wrinch, which really founded this subject, preceded that of the author, which is not the impression that would be given to the casual reader of page 326. W. C.

*The Many Body Problem.* Cours donnés a l'École d'Éte de physique Théorique. (Paris: Dunod; London: Methuen; New York: Wiley, 1959.) [Pp. 675.] £5.

THE pleasant and valuable custom of holding summer schools, where experts contribute courses of lectures on a single general theme, seems to have been started at Les Houches, and is now well established. An important corollary is the publication of the lectures, as in this volume. This is particularly useful where the subject is new, fashionable, and developing rapidly. Until one or other of the leading authorities can be persuaded to withold for a year or two from research and write a proper treatise, this volume may be the only complete account of this new branch of quantum theory, outside of the original papers which are difficult and confusing. The actual contributions are of varying style and substance. There is not room here to mention them all, but the reader is advised to start with the two admirable chapters by Brueckner, which give a clear general guide to the theory and its results, then to study the chapters by Hugenholtz, Beliaev, Bohm, and Huang, where the various formal techniques are set out, and finally to read the other sections were the special properties of nuclear matter, of electrons in metals (including superconductivity) and of liquid Helium, are discussed separately in detail. A collection of lectures has one great advantage over the usual compilations of review articles: instead of trying to fit in every paper, however bad, that has been written on his subject, each author makes a real effort to be intelligible. In this work they have almost all succeeded. J. M. Z.

*Absorption and Dispersion of Ultrasonic Waves.* By KARL F. HERZFELD and THEODORE A. LITOVITZ. (New York and London: Academic Press, 1959.) [Pp. xviii+535.] Price $14.50.

MEASUREMENTS of velocity and absorption of ultrasonic waves in gases and liquids have provided valuable information on the kinetics of molecular processes during the past 30 years. The literature associated with the subject has grown apace and there have been a number of good review articles. Now we have a book. Herzfeld and Litovitz have produced a volume which will become, at once, the accepted work in this field.

The book is written by two experts and the text reflects their individual interests. Since his classical paper with F. O. Rice, in 1928, Professor Herzfeld has been interested in the rate of exchange of energy between molecules. 90 pages (chapter VII) of this 550 page book are devoted to the detailed theory of vibrational and rotational energy exchange. The section on liquids is woven around the research of Professor Litovitz and carries his own emphasis on the importance of bulk and shear viscosity. The methods available for measuring ultrasonic absorption and velocity are dismissed briefly in chapters V and IX, 20 pages in all. The book is concerned chiefly with relating the measured ultrasonic quantities to thermodynamic and kinetic parameters characteristic of relaxing processes, and with the interpretation of these parameters in terms of theories of the gaseous and liquid states.

After an Introduction which warns the reader of things to come, the book opens with a careful discussion of the classical absorption formulae, the chapter ending with a formal introduction of bulk viscosity. Relaxation is introduced in chapter II with a useful description of the mechanisms of relaxation in a compressed gas and crystal: this leads naturally to the concept of effective specific heat. The assumed additivity of classical and relaxational absorption is mentioned, but it is not assessed. Developing the connection between the dispersion of sound and the effective specific heat, the authors emphasize the limitations of approximate formulae. Examples of the basic reaction equation are sought in the two-state and simple harmonic cases, and then more complicated matters are encountered with series and parallel reactions. It is shown that quantum mechanical calculations yield a different behaviour from classical theory, although not in as remarkable a way as Figure 24–2 would have us believe. The second bump in curve D does not survive recalculation. Chapter II ends with the full thermodynamic treatment of a general chemical reaction.

After a brief digression in chapter III into the effects of scattering and large amplitude, the aspects of relaxation theory peculiar to gases are considered in chapter IV, together with a summary of the experimental results in chapter VI. Problems relevant to the liquid state are dealt with in chapters VIII to XIII. In particular, ' Kneser liquids ' are shown to behave like condensed gases, while associated liquids are linked with the glassy state.

The most serious omission in this excellent book is a chapter on aqueous solutions. I look forward to reading, in a second edition, a new section on aqueous solutions written with the same authority and inspiration as the present text. J. H. A.

*Plasma Physics and the Problem of Controlled Thermonuclear Reactions.* Vol. III. Editor M. A. Leontovich. Translator J. B. Sykes. (Pergamon Press, 1959.) [Pp. 422.] £8.

Russian work on controlled thermonuclear reactions started in 1951. This is the third of four volumes describing progress up to the time of the 1958 Geneva Conference and it consists mainly of work done in the three years 1955 to 1957. Many of the papers have not appeared in English before and Pergamon Press and the translator, J. B. Sykes, are to be congratulated on presenting them to a wider public.

Most of the papers in this volume are theoretical but they cover a wide range of subjects. Basic physics is represented by the calculation of rates of radiation from a plasma and by several papers describing the behaviour of a rarified plasma in a strong magnetic field. One paper which is of special interest is that by Trubnikov on the rate of magnetic bremsstrahlung from a plasma layer as he shows that this may determine the minimum size of a self-sustaining fusion reactor. The critical size is shown to be rather large, even for a D-T reactor.

Other papers discuss special techniques for confining high temperature plasmas. Osovets describes a ring discharge produced in a cylinder instead of a torus. Such a discharge can contract towards the centre of the cylinder and he shows how it can be used to produce a plasma ball. Budker discusses the basic principles of a magnetic mirror machine and also the problem of direct conversion of thermonuclear energy into electrical energy. Kadomtsev proposes a device which, although basically a mirror machine, has some similarity to the Princeton stellarator. Two mirror machines are connected by two semicircular end sections and in addition the mirror fields are corrugated to help compensate for the toroidal drift of particles. As yet this complicated device has not been built.

A useful plasma must be confined in a stable manner. Braginsky shows that some of these instabilities are geometrical in the sense that they do not occur if the plasma surface has the correct shape. Required shapes of plasma surface can be obtained by surrounding it with suitably placed metallic conductors. In another paper Sagdeev shows that, if particle distribution functions are anisotropic, there may exist instabilities which have not been predicted by earlier hydromagnetic treatments. R. J. T.

## BOOK NOTICES

*Fonctions Sphériques de Legendre et Fonctions Sphéroïdales*, Tome III. Par L. Robin. (Paris : Gauthier-Villars, 1959.) [Pp. 289, bound.] 6000 f.

*Photopiles au Sélénium.* By G. Blet. (Paris : Gauthier-Villars, 1959.) [Pp. 150.] 1100 f.

*Advances in Chemical Physics*, Vol. II. Edited by I. Prigogine. (New York : Interscience Publishers, 1959.) [Pp. 412.] 87*s*.

*Contributions to the Theory of Games*, Vol. IV. Edited by A. W. Tucker and R. D. Luce. Annals of Mathematics Studies, Number 40. (Princeton : University Press ; London : Oxford University Press, 1959.) [Pp. 453.] 48*s*.

*Quantum Particle Dynamics.* By J. McConnell. (Amsterdam : North-Holland Publishing Company, 1958.) [Pp. 252.]

*Applications of the Theory of Matrices.* By F. R. Gantmacher. Translated by J. L. Brenner. (New York : Interscience Publishers, 1959.) [Pp. 317.] 63*s*.

*Reports on Progress in Physics*, Vol. XXII. Executive Editor, A. C. Stickland. (London : The Physical Society, 1959.) [Pp. 634.]

This volume is a thick one and contains the following review articles :

Applications of Quantum Mechanics in Theoretical Chemistry. By G. G. Hall.
Progress in Vacuum Technology. By J. Pollard.
The Propagation of Elastic Waves in Crystals and other Anisotropic Media. By M. J. P. Musgrave.
Relativity. By H. Bondi.
Double Beta Decay. By H. Primakoff and S. P. Rosen.
Physical Problems of Thermoelectricity. By A. F. Joffe and L. S. Stil'bans.
Paramagnetic Resonance Data. By J. W. Orton.
Experimental Investigations of the Ionospheric E-Layer. By B. J. Robinson.
Radio-frequency Spectroscopy of Excited Atoms. By G. W. Series.
The Theory of a Fermi Liquid. By A. A. Abrikosov and I. M. Khalatnikov.
Invariance in Elementary Particle Physics. By N. Kemmer, J. C. Polkinghorne and D. L. Pursey.
Nuclear Magnetism in Pure Liquids. By J. G. Powles.
Experimental Work with $^3$He. By V. P. Peshkov and K. N. Zinov'eva.
The Two-Nucleon Interaction. By R. J. N. Phillips.

---

[*The Editors do not hold themselves responsible for the views expressed by their correspondents.*]

Fig. 6

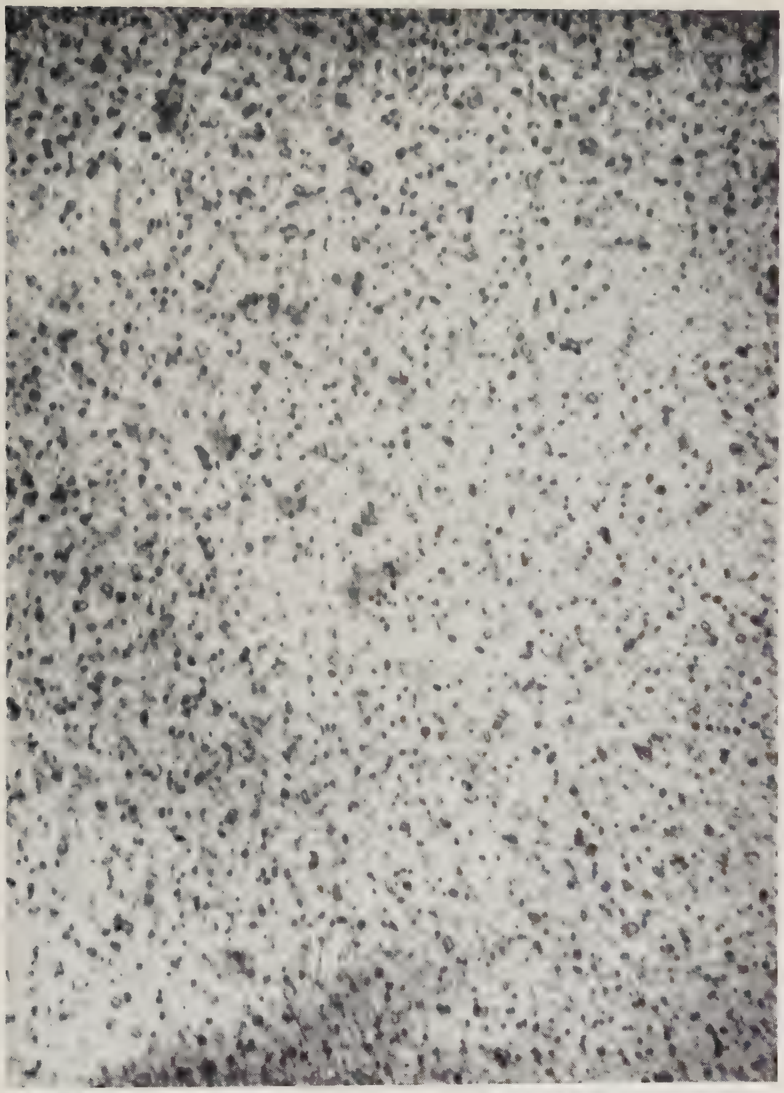

Al–1% Cu. Quenched from 600°c. Foil orientation [001] showing dislocation loops 100–300 Å diameter. ×64 000.

Fig. 7

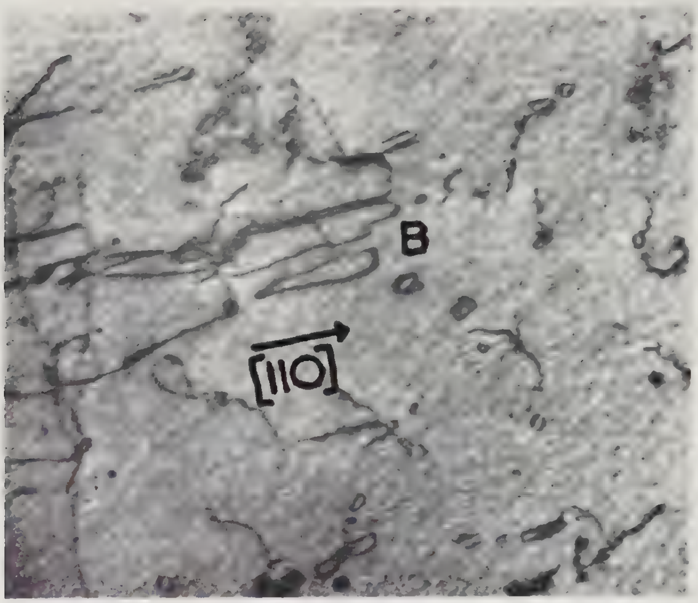

Al–1% Cu. Quenched from 540°c. Foil orientation [001]. Note elongation of loops B in [110]. ×36 000.

Fig. 8

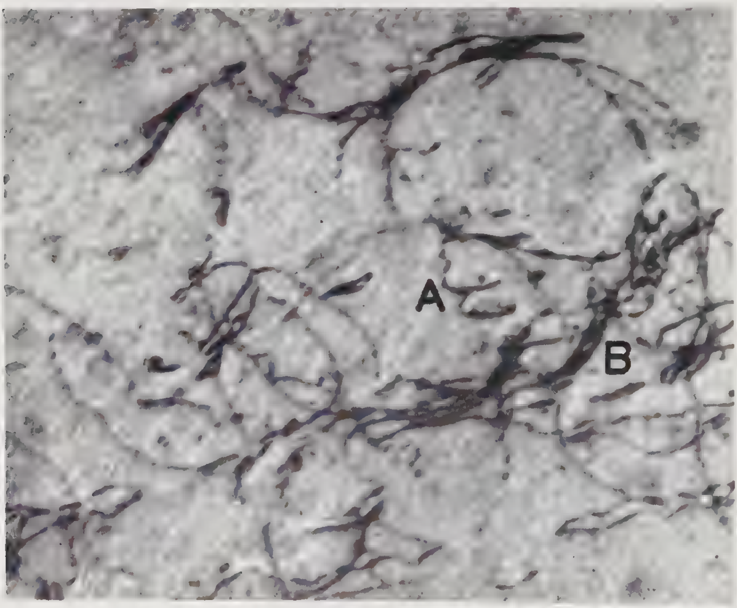

Al–2% Cu. Quenched from 540°c. Foil orientation [0$\bar{1}$1]. Helical dislocation at A. There are very few loops in this specimen but complex dislocation networks at B. ×36 000.

Fig. 9

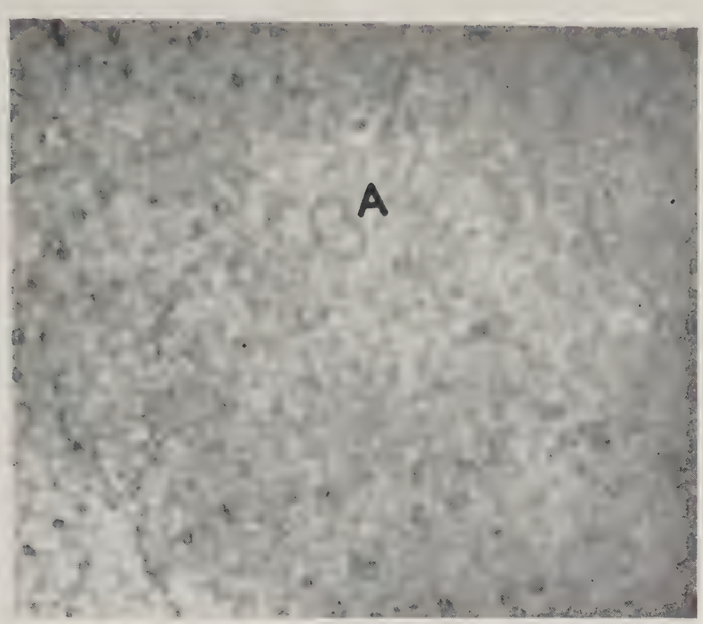

Al–1% Ag. Quenched from 580°c. Foil orientation $[0\bar{1}2]$. Loops have parallelogram, shapes. Coalescence may have occurred at A. ×36 000.

Fig. 10

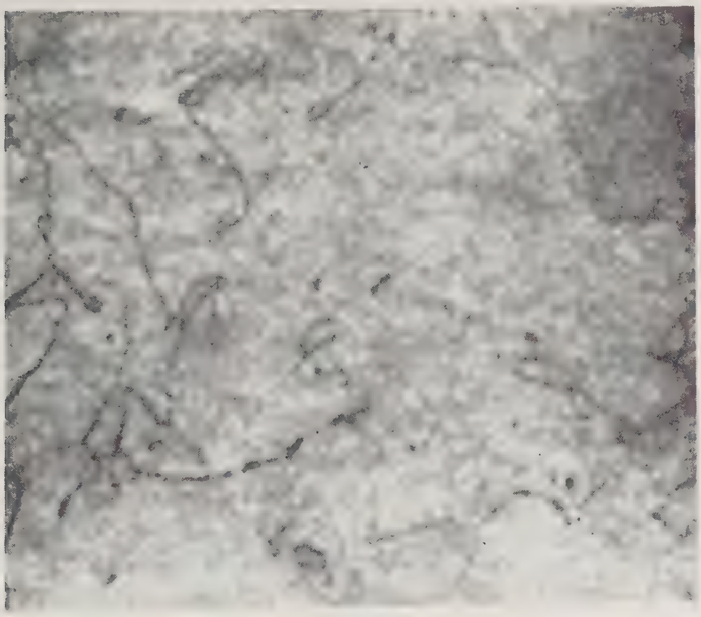

Al–5% Ag. Quenched from 580°c. Foil orientation [100]. There are fewer loops than in fig. 9. ×36 000.

Fig. 11

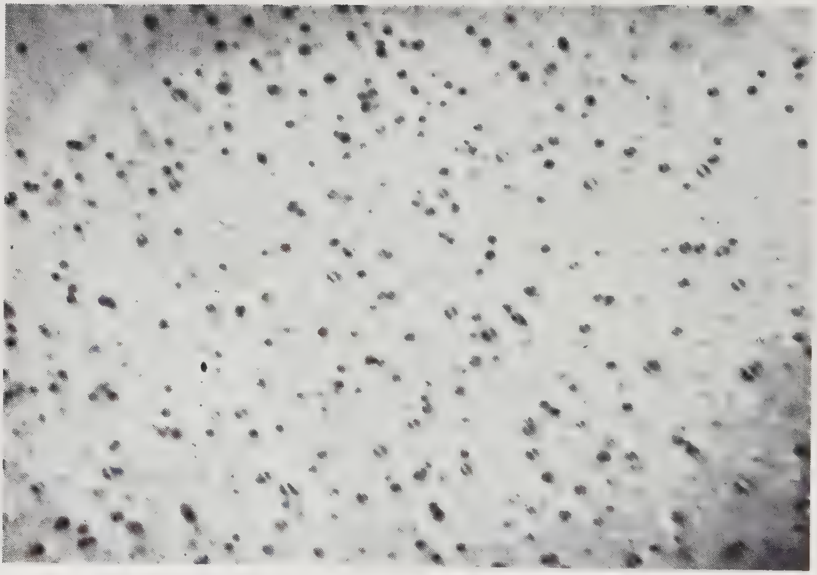

Al–10% Zn. Quenched from 540°c. Loops 100–200 Å diameter. ×60 000.

Fig. 12

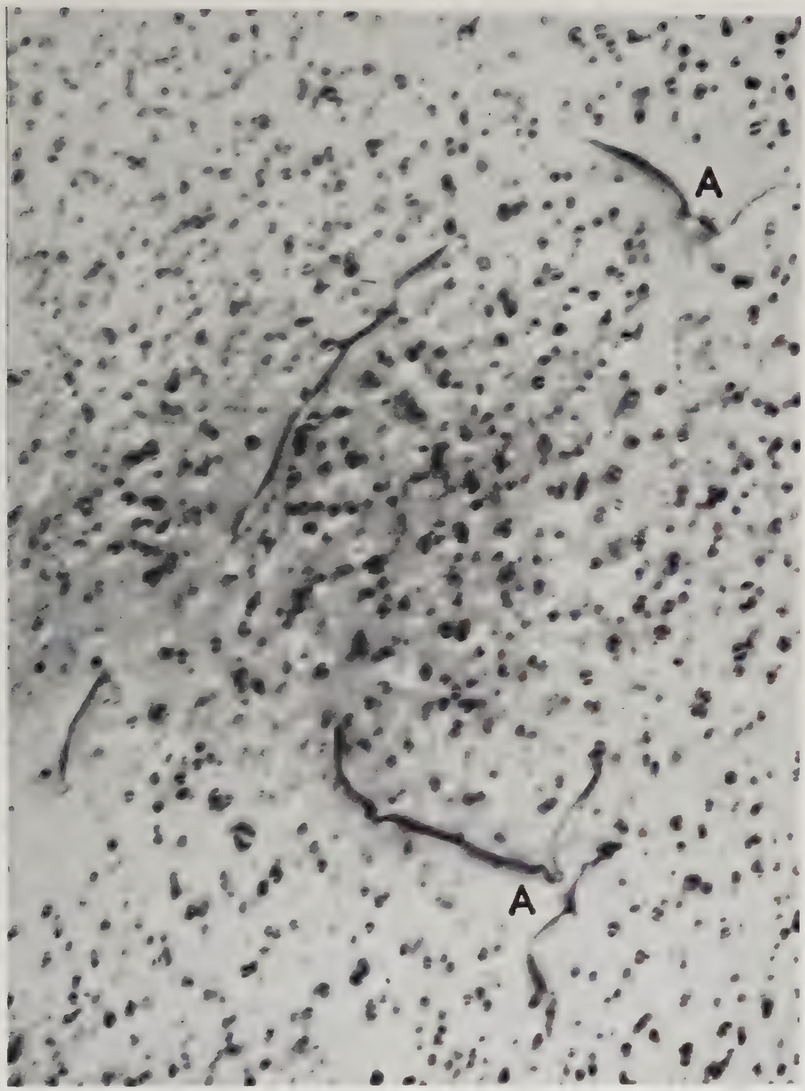

Al–10% Zn. Quenched from 580°c. Note that loops are absent near dislocation lines at A. × 64 000.

Fig. 13

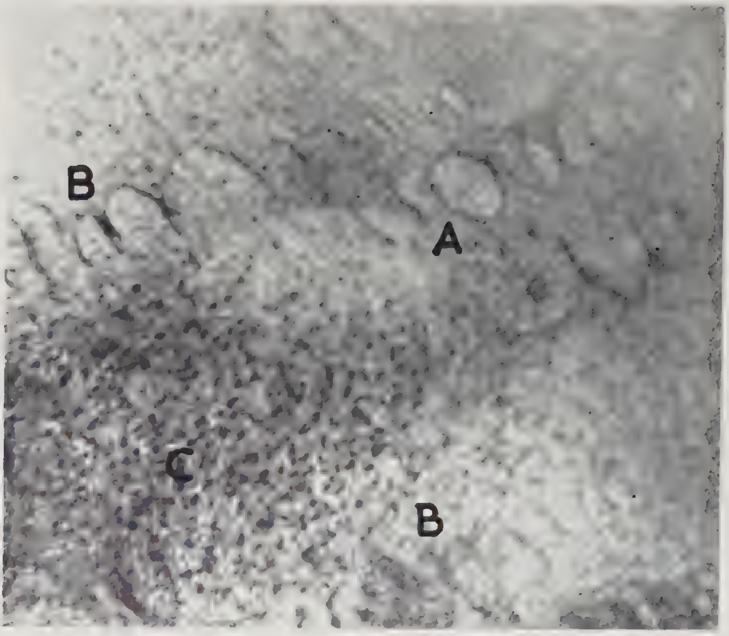

Al–30% Zn. Quenched from 510°c. Foil orientation [03̄1]. Helical dislocations at B, large loops at A. ×36 000.

Fig. 14

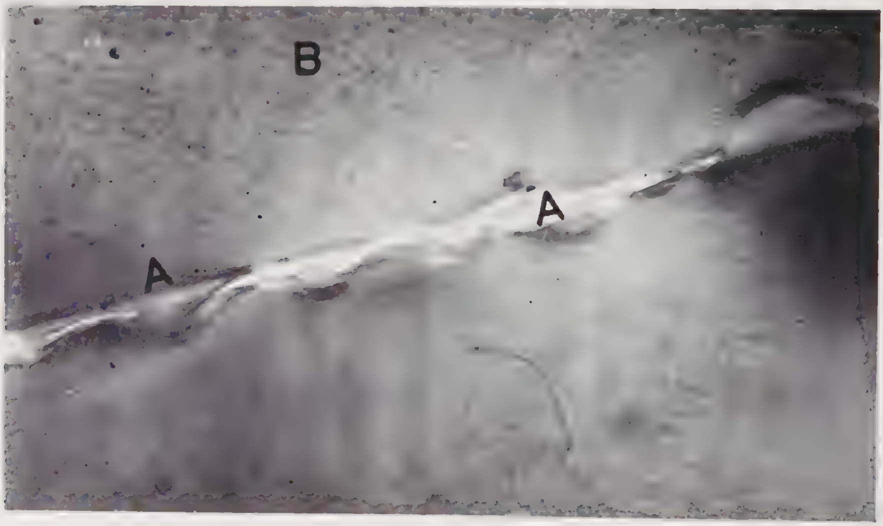

Al–30% Zn. Quenched from 510°c. Grain boundary at A previously contained zinc particles but are leached out in preparing the foil. Note loops at B and loop-free regions adjacent to A. Precipitation at A occurred during quenching. ×36 000.

Fig. 15

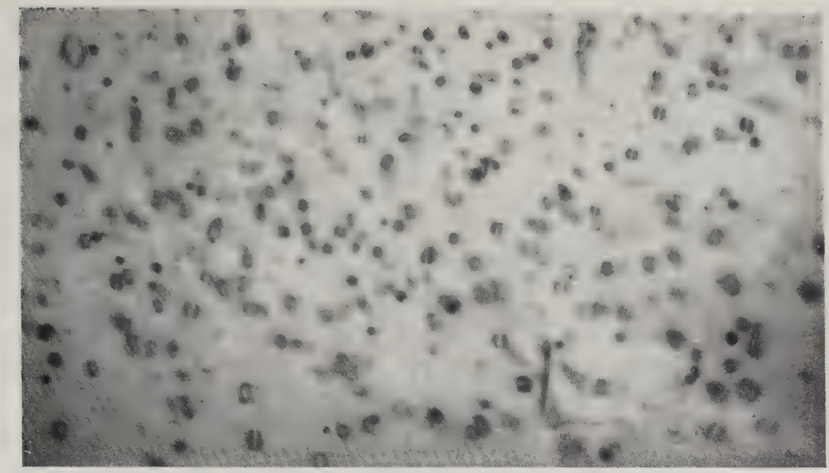

Al–1% Mg. Quenched from 550°c. Dislocation loops ~200 Å diameter. ×72 000.

Fig. 16

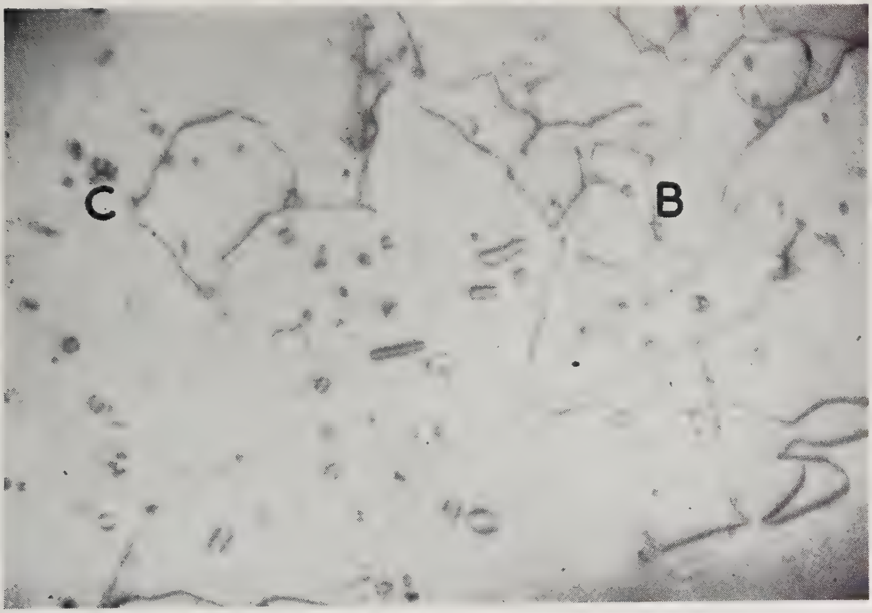

As fig. 15 but aged 2 hours at 100°c. Loops now up to 1000 Å diameter. The complex dislocation networks at B are thought to be due to climb. Coalescence of three loops may be taking place at C. ×36 000.

Fig. 17

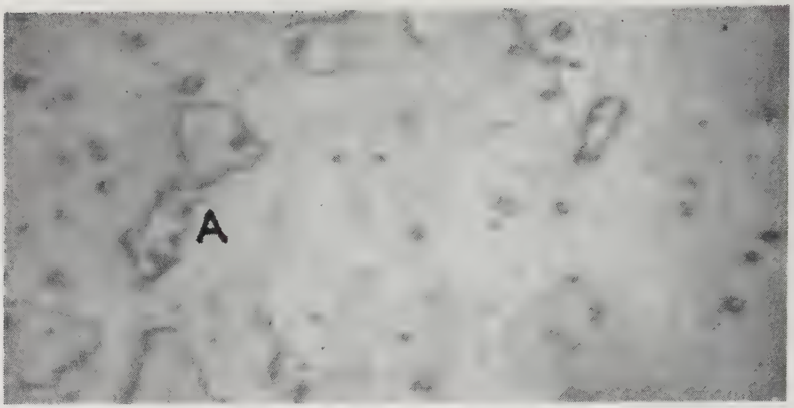

Al–3% Mg. Quenched from 550°c. Note there are fewer loops than in fig. 15. Foil orientation [110]. The two screw segments at A have climbed into helices. ×72 000.

Fig. 18

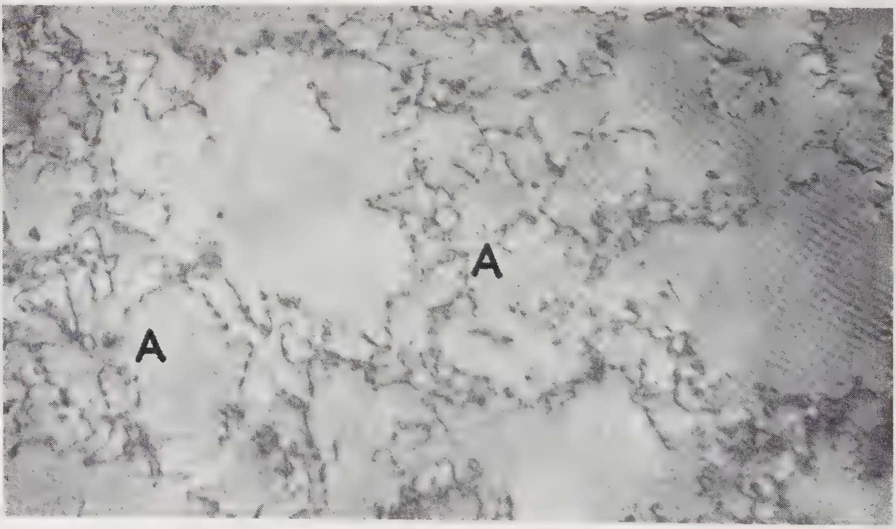

Al–7% Mg. Quenched from 550°c. There are very few loops for example at A. Dislocation networks always found in this alloy after quenching. ×36 000.

Fig. 2

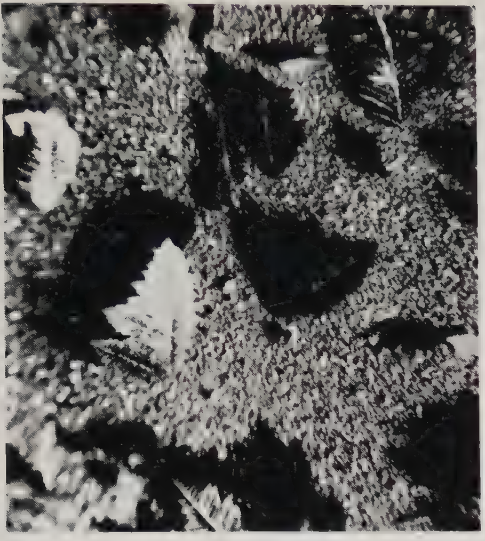

Part of the top surface of the cell after 15 hours of growth. ×7·5.

Fig. 4

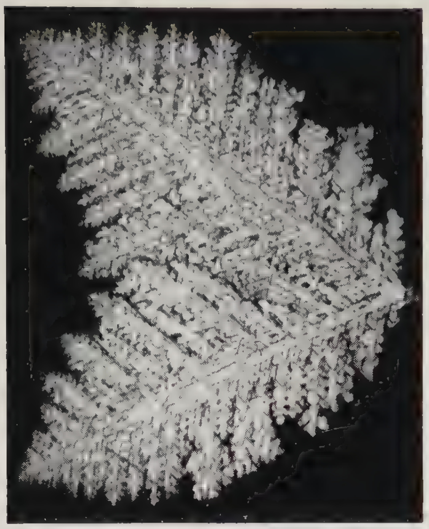

Type II or ‘ roof tile ’ dendrite with two arms at 60°. ×50.

Fig. 3

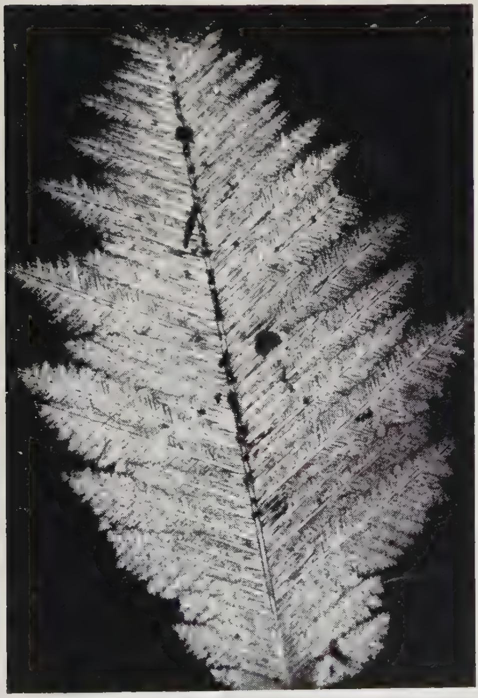

Type I or ‘ ribbed ’ dendrite with overgrowth. ×100.

Fig. 5

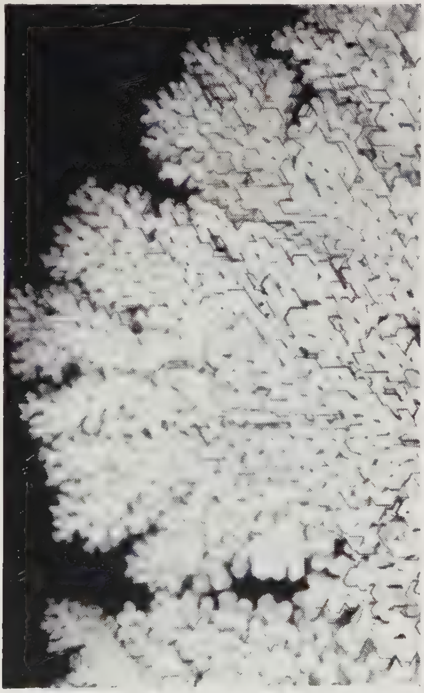

‘ Roof tile ’ growth layers on a Type II dendrite. ×250.

Fig. 6

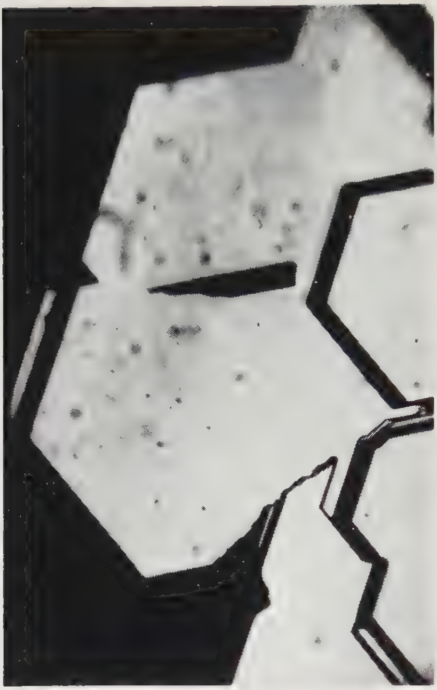

Junction of two ‘ roof tiles ’. ×1000.

Fig. 7

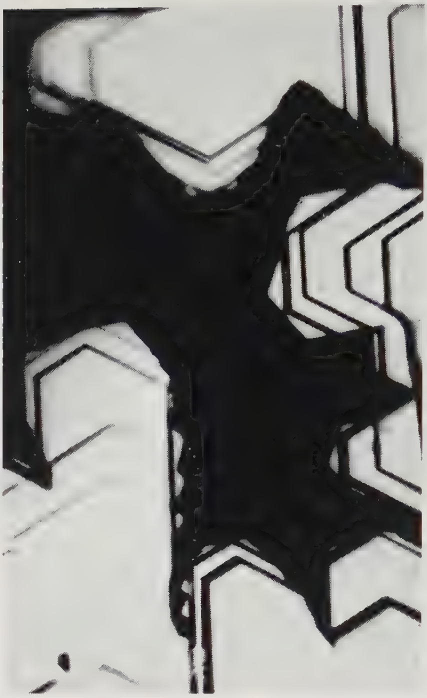

Region between two adjacent dendrite branches whose ‘ roof tiles ’ have not grown together yet. Under each set of tiles is a tile which appears to be rotated by 21·8°. ×1000.

Fig. 8

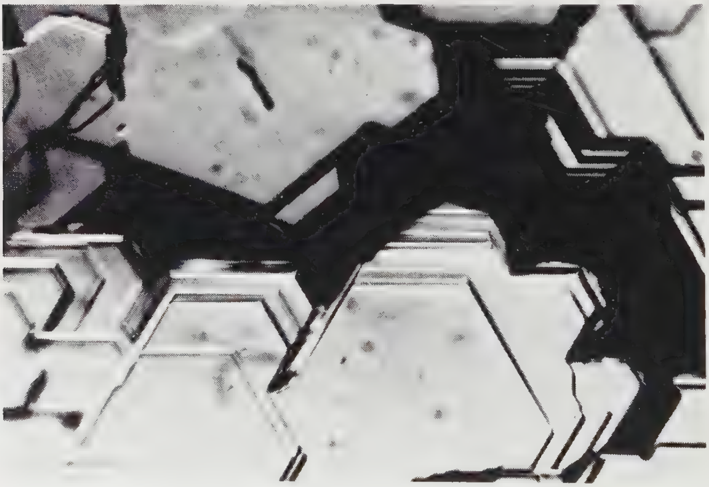

More growth layers rotated by 21·8° with respect to the main crystal. At the top left and centre is a large exposed block of ‘ misoriented ’ layers. ×1000.

Fig. 9

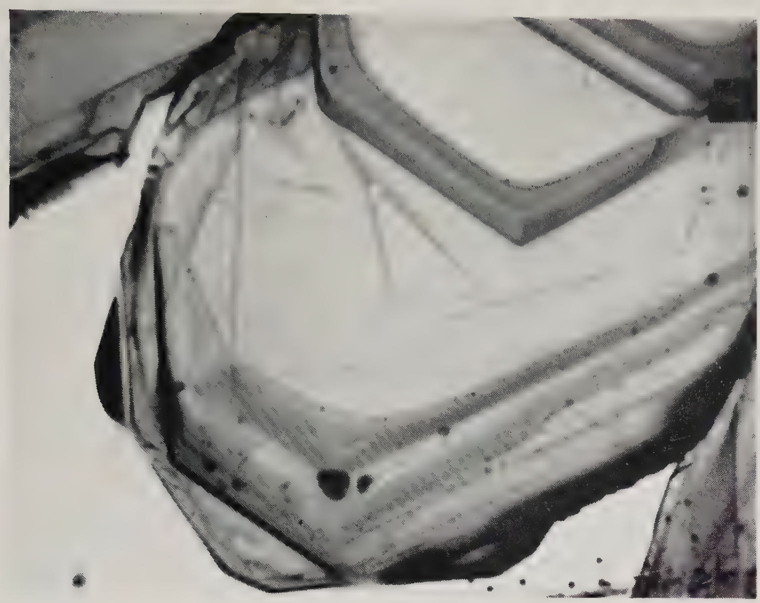

Electron micrograph of a carbon replica of a dendrite showing part of a ‘roof tile’ which is in the rotated or twin orientation. Two complete edges are visible, as well as parts of two others. ×4000.

Fig. 10

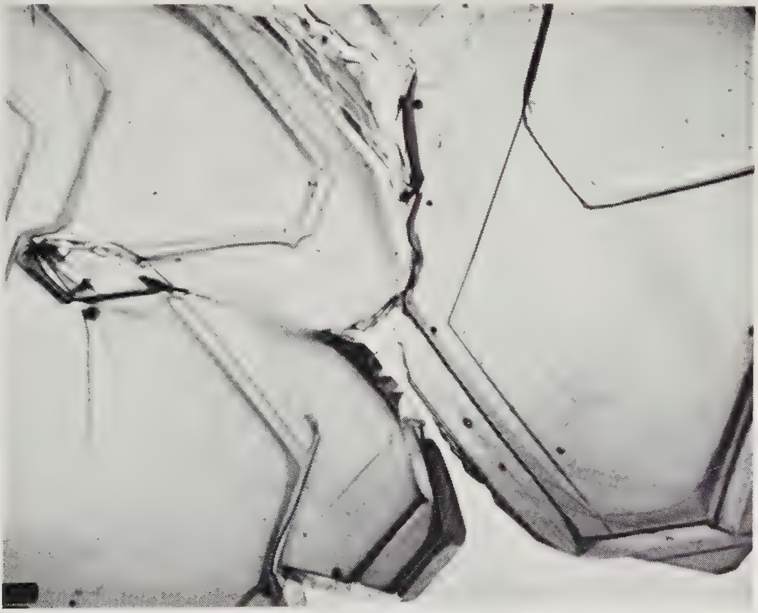

Electron micrograph showing growth layers from the bottom surface which are in the rotated or twin orientation. ×1500.

Fig. 11

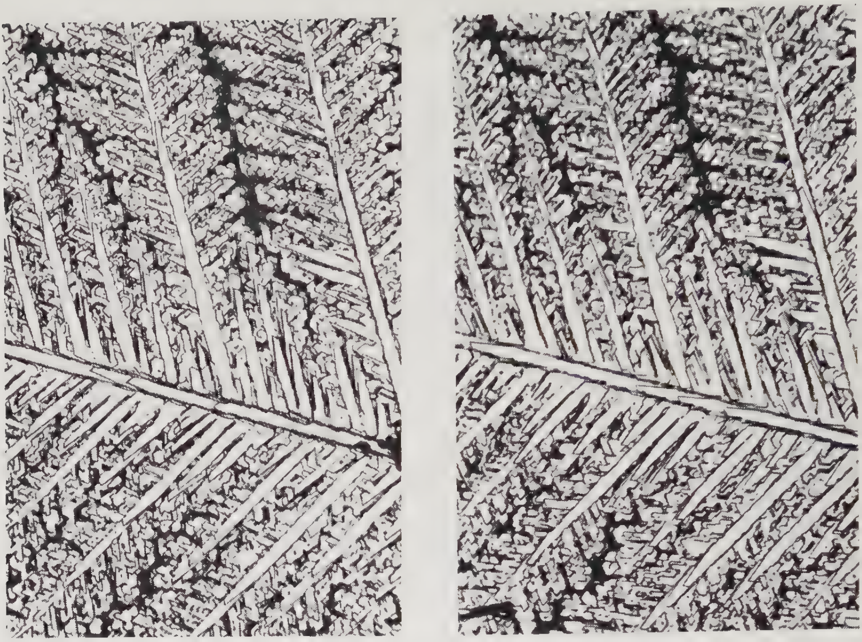

(*a*) (*b*)

(*a*) ' Front ' side of a Type I dendrite; (*b*) ' back ' side reversed in printing. ×100

Fig. 12

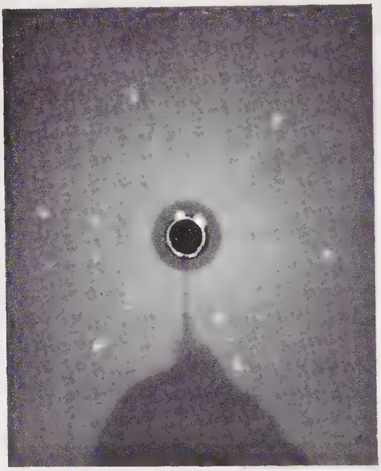

Laue back-reflection pattern of a [1230] twinned leaf dendrite.

Fig. 15

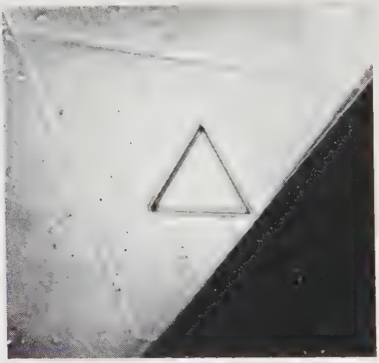

Rotational intercrystalline boundary on a cadmium ' ribbon ', with $\theta \simeq 7{\cdot}0°$. ×1000 and phase contrast.

Fig. 1

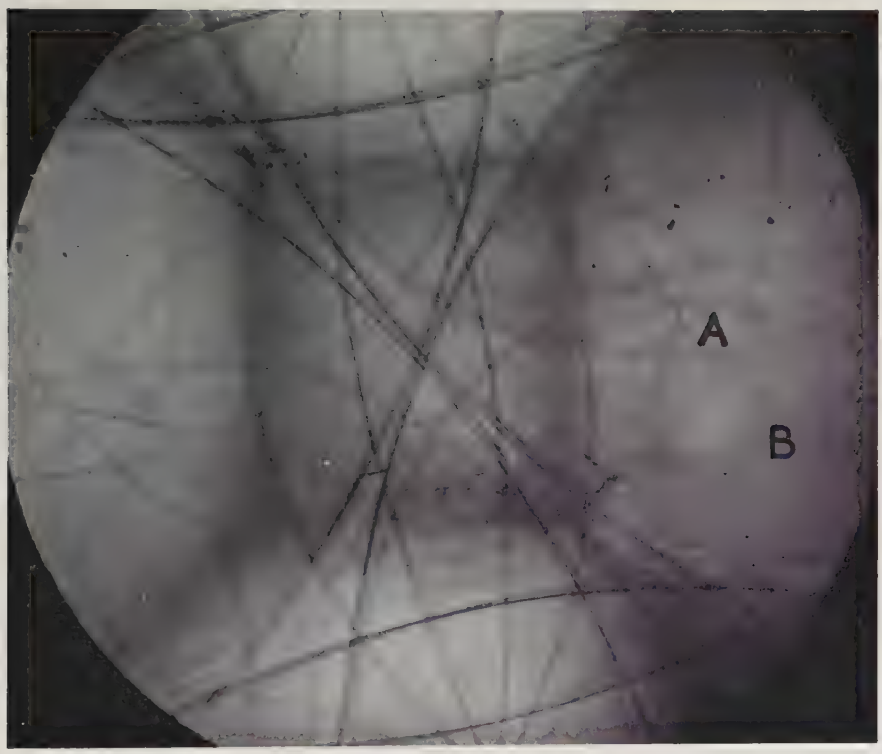

Photograph of a single crystal of beryllium in divergent Cu radiation, with the plate normal to (1010).

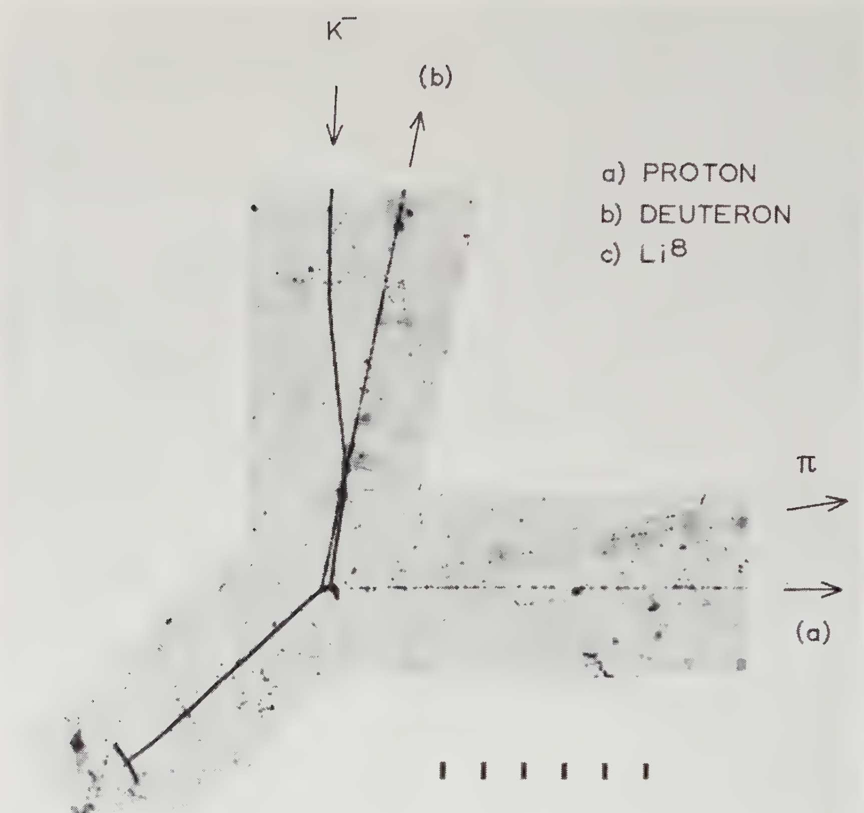

ORIGIN & DECAY OF $_\Lambda B^{11}$

$_\Lambda B^{11} \rightarrow Li^8 + d + p$

Fig. 4 (*a*)

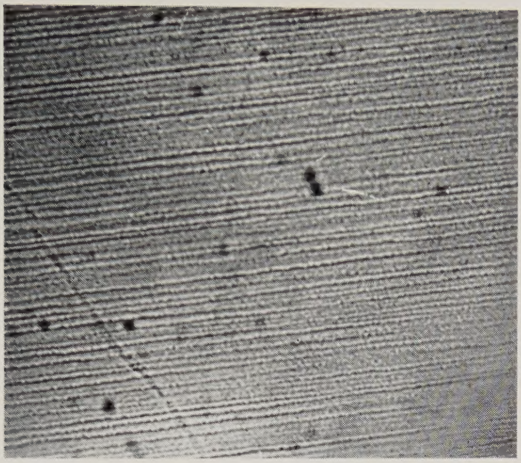

Slip lines on the side surface of crystal D3 deformed to 13% elongation at room temperature. ×1000.

Fig. 4 (*b*)

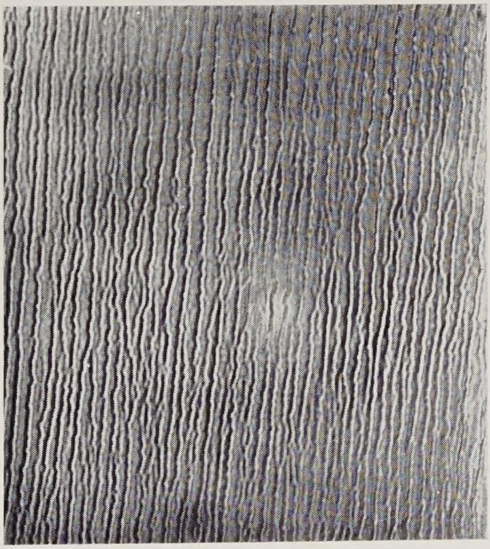

Slip lines on the top surface of crystal D3 deformed to 13% elongation at room temperature. ×1000.

Fig. 5

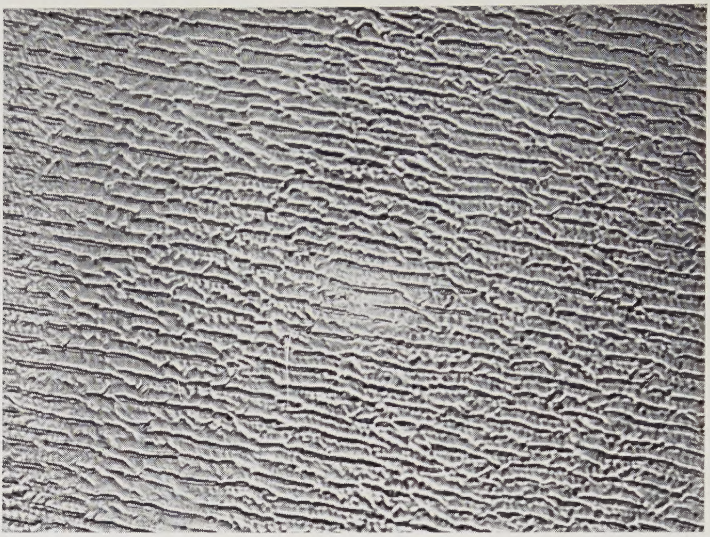

Slip lines on the top surface of crystal C5 deformed to 75% elongation at 77°K. ×1000.

Fig. 6

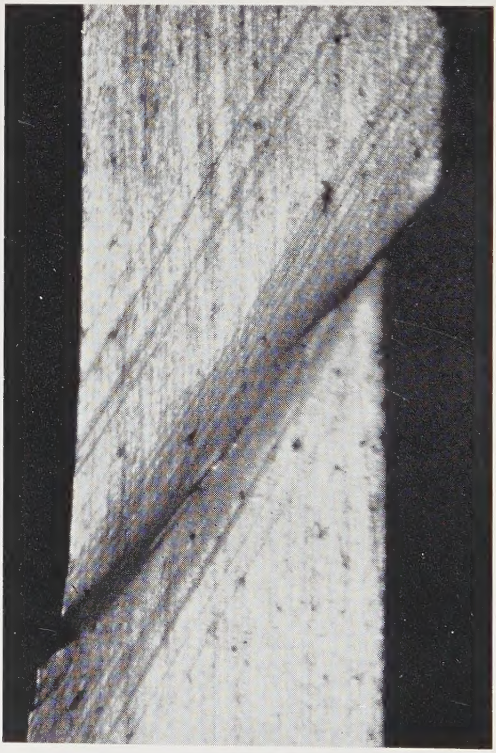

Illustrating the mode of fracture of crystal 14. ×16.

Fig. 1

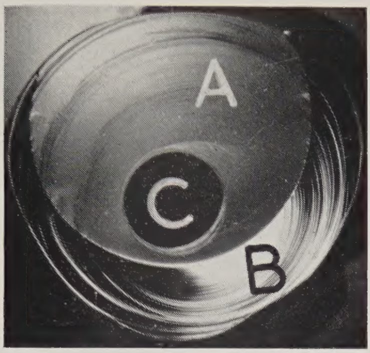

Photograph of crystal end. (×4.) *A*, facet ; *B*, rounded surface ; *C*, spike due to solidified droplet of melt.

Fig. 2

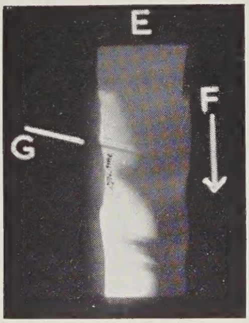

Auto-radiograph of radio-Te doped crystal. (×1.) *E*, seed end ; *F*, growth direction ; *G*, trace of {111} plane ; positive print, i.e. white = high Te conc.